COLLOIDAL GOLD NANOPARTICLES FOR CANCER THERAPY: EFFECTS OF PARTICLE SIZE ON TREATMENT EFFICACY, TOXICOLOGY, AND BIODISTRIBUTION

A Dissertation
Presented to
The Academic Faculty

By

Kate Y.J. Lee

In Partial Fulfillment
Of the Requirements for the Degree
Doctor of Philosophy in the
Wallace H. Coulter Department of Biomedical Engineering

Georgia Institute of Technology
Emory University

May 2011

COLLOIDAL GOLD NANOPARTICLES FOR CANCER THERAPY: EFFECTS OF PARTICLE SIZE ON TREATMENT EFFICACY, TOXICOLOGY, AND BIODISTRIBUTION

Approved by:

Dr. Shuming Nie, Advisor
School of Biomedical Engineering
Georgia Institute of Technology

Dr. Mark Prausnitz
School of Chemical and Biomolecular Engineering
Georgia Institute of Technology

Dr. Ravi Bellamkonda
School of Biomedical Engineering
Georgia Institute of Technology

Dr. Lily Yang
College of Medicine
Emory University

Dr. Niren Murthy
School of Biomedical Engineering
Georgia Institute of Technology

Date Approved: [January 19, 2011]

To Mom, Dad, King, and Mark

ACKNOWLEDGEMENTS

First of all, I would like to thank my advisor Dr. Shuming Nie, who has provided me tremendous support and continuous guidance throughout the years. I still remember his words when I first met him: “In our lab, you have the freedom to succeed, but also the freedom to fail.” These words have been my motto for the past five years, constantly challenging myself to be a better scientist. I greatly admire Dr. Nie’s passion for science, especially for nanotechnology. Through him, I learned no statement can be made without any scientific reasoning or proofs, allowing me to pursue false-proof and meticulous research studies. Also, through the numerous talks and conferences hosted by Dr. Nie, I got to meet world-class scientists, who further motivated my studies. Thank you very much for the invaluable insights and advice for my research. Thank you again for always motivating me and believing in me to prove myself to be the scientist as I am today.

I am also very fortunate to be surrounded by such kind, intellectual people in the Nie Lab. Without the help and support from Dr. Yiqing Wang, Dr. Ximei Qian, and Dr. Aaron Mohs, I could not have been here. Thank you Dr. Yiqing Wang for numerous research ideas and support-your encouragement and guidance has been invaluable for the success of my research. Also, thank you for always entertaining me with your wonderful stories. Thank you Dr. Ximei Qian for introducing me to the world of gold nanoparticles. I have learned so much about research in general from you, and you have been a great role model for me in the Nie lab. Thank you Dr. Aaron Mohs for your advice in research and life. Your life lessons always kept me motivated and focused on my research. I am also lucky to interact with other group members, especially Dr. Brad Kairdolf, Michael

Mancini, Anthony Nicolini, Christopher Shen, Dr. Andrew Smith, and Mary Wen. I would like to thank them for their friendship, collaboration, and support. Because of you, my days in the Nie lab have been more pleasant and enjoyable. I would like to thank our administrator Ms. Michelle Denney for her hardwork and friendship. Lastly, I also like to thank past Nie lab members Dr. Tushar Sathe, Dr. Matthew Rhyner, Dr. Gang Ruan, Dr. Jun Li, Dr. Min Kuang, Dr. Hongwei Duan, Dr. Tao Liu, Dr.Jian Liu, Dr. Gloria Kim, Dr. Dominic Ansari, Dr. Debatosh Majumdar, Dr. Xiaohua Huang, Ryan Jowers, and Shefaet Raman for all their support and friendship.

Next, I would like to convey my appreciation to Dr. Gee Young Lee. She has been a great collaborator, who helped me to overcome my fear of mice. I have learned so much about *in vivo* work, and without her, I couldn't have completed my *in vivo* studies. She is like an elder sister that I have never had. She has been of great help and influence in my professional and personal life.

I also like to thank my committee members. I was lucky to interact with each of my committee members personally. I first met Dr. Ravi Bellamkonda and Dr. Mark Prausnitz when I was an undergraduate. I visited Georgia Institute of Technology for Research Experience for Undergraduate program, and I had a great opportunity to work in Dr. Mark Prausnitz lab over the summer. Dr. Ravi Bellamkonda, who happened to be a close friend of my undergraduate research advisor Dr. Christine Schmidt, gave me invaluable advice for getting into Georgia Tech's prestigious Biomedical Engineering program. Dr. Lily Yang has been a great collaborator of our lab, and I got to personally interact with her through her research. Finally, I got to interact with Dr. Niren Murthy by working as a teaching assistant for his biotransport class.

A lifelong friendship that I made in Atlanta with Vivek Mukhatyar, Alyssa Ngangan, Brandon Kitchel, Adam Martinez, Marly Martinez, Fred Sieling, Steve Feng, Jaemin Shin, Jeeyun Yoon, Nick Willet, Kelly Brink, Stacie Chvatal, Hajira Ahmad, and Nola Li will be treasured forever.

I would like to thank my family for their tireless support and love. My parents have given me indefinite support and encouragement throughout my time here in Atlanta. Despite being thousands of miles apart, my parents always cared and wished the best for me. Without your nurture and patience, I would have not been here today. I also thank my parents for giving me a wonderful younger brother, King, who always rooted for me throughout my journey in Atlanta. Finishing PhD degree was one of my dad's top lists, since he had to stop at Masters due to birth of me and my brother in his graduate school years. Today, I am very proud to follow my dad's footsteps and pursue my PhD degree in biomedical engineering.

Last but not least, I would like to thank my charming and magnificent fiancé, Mark Aramwattananont, who has been patiently waiting for me to finish my degree in Seattle, WA. I first met Mark in college as a sophomore, and he has been my best fan and supporter for the past ten years. Without your love and support, I would have not been here. You mean so much to me and I am very excited to start a new chapter of our lives together. Seattle, here I come!

TABLE OF CONTENTS

LIST OF TABLES

LIST OF FIGURES

Page

Page

LIST OF SYMBOLS AND ABBREVIATIONS

ALT	Alanine Transaminase
Alk Phos	Alkaline Phosphatase
AST	Aspartate Aaminotransferas
Au-DOX	Gold nanoparticle coated with doxorubicin
Au-DOX-PEG	Gold nanoparticle coated with doxorubicin then with PEG
AuNP	Gold Nanoparticle
BSA	Bovine Serum Albumin
DAPI	4',6-diamidino-2-phenylindole (fluorescent dye)
DLS	Dynamic Light Scattering
DNA	Deoxyribonucleic acid
DOX	Doxorubicin
EPR	Enhanced Permeability and Retention
FDA	Food and Drug Administration
ICP-MS	Inductive-Coupled Plasma Mass Spectroscopy
LDH	Lactate dehydrogenase
MRI	Magnetic Resonance Imaging
MW	Molecular Weight
NaCl	Sodium Chloride
NIR	Near Infrared
PDPH	3-[2-Pyridyldithio] propionyl hydrazide
PEG	Poly (ethylene glycol)
PEGylation	Act of coating nanoparticle surface with PEG
PLGA-PEG	Poly(lactic-co-glycolic acid)-Poly(ethylene glycol)

RES	Reticuloendothelial system
SEM	Scanning Electron Microscopy
SERS	Surface-Enhanced Raman Scattering
TEM	Transmission Electron Microscopy
UV-vis	Ultraviolet-visible

SUMMARY

The complexity and heterogeneity nature of cancer makes it difficult to successfully diagnose and treat cancer. Advances in cancer research have been focused on studying the molecular level of the disease, and nanotechnology plays a critical role in overcoming the obstacles in cancer biology. The size-scale (1-100nm) of nanotechnology provides a powerful tool to easily manipulate the cancer environment by distinctively size-tuning the nanomaterial to interact with biological molecules in tumor.

Recently, gold nanoparticle has emerged as an attractive platform for drug delivery applications by complementing the existing drug delivery carriers. Gold nanoparticles confer several advantages such as biocompatibility, size-tunability, and easy surface modification methods. Furthermore, due to its unique optical properties, multiple analytical chemistry methods such as UV-vis spectrophotometry, SERS, TEM, ICP-MS, darkfield microscopy, fluorescence can be used. Currently, only a few gold nanoparticle-based anticancer drug delivery systems have been reported, compared to the polymer-based delivery systems. Additionally, there is still a lack of understanding for the behavior and fate of the gold-drug conjugate in the body that further attention is required. The *overall goal* of this thesis is to investigate the *in vivo* behavior of colloidal gold nanoparticle and its therapeutic efficacy in an animal model, especially in a drug delivery application. To achieve this goal, we investigated the feasibility of using colloidal gold nanoparticle as an anticancer agent delivery vehicle for treatment of cancer. Then, long-term clearance, toxicity, and biodistribution of colloidal gold nanoparticle were studied to further aid in understanding of using colloidal gold nanoparticle as a drug delivery platform. In particular, two representative sizes of gold

nanoparticles, 5nm and 60nm, were investigated for the size effect on therapeutic efficacy, toxicity, biodistribution, and clearance in cancer nanotherapy.

First, we report the development and characterization of multifunctional drug delivery system for *simultaneously* therapy and SERS spectroscopic detection of tumor. Doxorubicin, serving a *dual* function of chemotherapeutic agent and SERS reporter molecule, was chemically conjugated to 60nm gold nanoparticle via pH-sensitive hydrazone linker, and then PEG was added to develop multifunctional delivery system. The multifunctional delivery system demonstrated successful pH-dependent drug release profile, therapeutic effect on tumor cells, along with *in vitro* SERS spectroscopic detection. SERS spectra were detected for *non-aggregated* gold system at near-infrared wavelength. Thus, the development of multifunctional drug delivery system raises exciting opportunities for simultaneous spectroscopic detection and therapy for tumors.

Then, we report development of smaller-sized 5nm gold nanoparticle drug delivery system. Similar to 60nm gold system, 5nm gold nanoparticles were coated with doxorubicin, which was modified with pH-sensitive hydrazone linker, and then with PEG to give colloidal stability and biocompatibility. When tested in a tumor mouse model, 5nm gold drug delivery system resulted in therapeutic efficacy against tumor with no apparent systemic toxicity. In contrast, pure doxorubicin resulted in kidney, heart, and lung toxicity, along with insignificant therapeutic efficacy compared to other groups tested. The success of 5nm gold system resulted from (1) “high” accumulation at the tumor site compared to other non-tumor sites via EPR effect, (2) ideal spatial distribution and successful penetration at the tumor site, and (3) slow, controlled release of drug via pH-sensitive linker to result in no apparent systemic toxicity.

Finally, we demonstrated the size-dependent biodistribution and clearance of colloidal gold nanoparticles that (1) increased circulation time for 5nm gold system (due to size and PEG) resulted in biodistribution of gold in various organs compared to 60nm gold system, (2) larger 60nm gold system was mostly uptaken in the liver and the spleen, whereas smaller sized 5nm gold system was visible in the various organs in the system, especially resulting in pigmentation in the skin and the lymph nodes, and (3) size dependent clearance was observed where 5nm gold system gets excreted via renal (urine) and hepatobiliary (feces) pathways, whereas 60nm gold was mostly retained in the spleen and liver after 6 months. Thus, 5nm gold system is a potential candidate for biomedical applications, where 5nm gold core displays inherently different biodistribution and clearance characteristics than 60nm or larger nanoparticles.

In summary, we believe that nanoparticle size plays a critical role for not only delivering the drug to the target site but also determining the *in vivo* behavior such as biodistribution and clearance in the system. By choosing an appropriate size scale for the system, we were able to successfully use gold nanoparticles for drug delivery applications along with desirable clearance from the biological system. This work is *significant* by providing an insight on a potential ideal candidate for drug delivery carrier for cancer nanotherapy.

CHAPTER 1

CANCER AND NANOTECHNOLOGY

1.1 ABSTRACT

Nanotechnology is an interdisciplinary research field that combines chemistry, engineering, biology, and medicine that allows early detection, accurate diagnosis, and personalized treatment of cancer. Nanotechnology adopts a size scale that is equivalent to biological molecules of 5-100 nm in diameter. The complexity and heterogeneity nature of cancer makes it difficult to successfully diagnose and treat cancer. Advances in cancer research have been focused on studying molecular level of the disease, and nanotechnology plays a critical role in overcoming the obstacles in cancer biology. In this chapter we will look at general characteristics of cancer and emphasizes the role of nanotechnology, particularly in terms of size effect, for successful detection, diagnosis, and treatment of cancer.

1.2 INTRODUCTION

According to the American Cancer Society, cancer is defined as the following:

> "Cancer is a group of disease characterized by uncontrolled growth and spread of abnormal cells. If the spread is not controlled, it can result in death. Cancer is caused by both external factors (tobacco, infectious organisms, chemicals, and radiation) and internal factors (inherited mutations, hormones, immune conditions, and mutations that occur from metabolism). These causal factors may act together or in sequence to initiate or promote carcinogenesis."

Cancer has been the second leading cause of death worldwide, following heart diseases [1]. Cases of cancer doubled globally between 1975 and 2000, will double again

by 2020, and will nearly triple by 2030, according to the World Cancer Report by World Health Organization. There were an estimated 12 million new cancer diagnoses and more than 7 million deaths worldwide in 2009. The projected numbers for 2030 are 20 to 26 million new diagnoses and 13 to 17 million deaths. Looking at the United States alone, approximately 1.5 million new cancer cases are expected to be diagnosed in 2010 [2].

Over the past 50 years, the death rate due to top mortality causes (heart diseases, cerebrovascular diseases, and pneumonia/influenza) has declined dramatically in the US [2]. However, despite the vast knowledge and efforts made over the past decade to fight cancer, relatively little progress has been made to reduce the cancer death rate. Thus, the rapid increase in the global cancer burden represents a real challenge for health systems worldwide.

Table 1.1. Leading Causes of Death Worldwide in 2001 (thousands) [1]

	Worldwide		
	Rank	**Deaths**	**%**
Heart diseases	1	11,004	19.6
Malignant neoplasms	2	7,021	12.5
Cerebrovascular diseases	3	5,390	9.6
Lower respiratory infections	4	3,753	6.7
Chronic obstructive pulmonary disease	5	2,676	4.8
HIV/AIDS	6	2,574	4.6
Perinatal conditions	7	2,522	4.5
Diarrhoeal diseases	8	1,783	3.2
Tuberculosis	9	1,606	2.9
Road traffic accidents	10	1,108	2.0
Malaria	11	1,208	2.1
Diabetes mellitus	12	960	1.7
Suicide	13	875	1.6
Cirrhosis of the liver	14	771	1.4
Measles	15	763	1.4
All causes		56,242	100.0

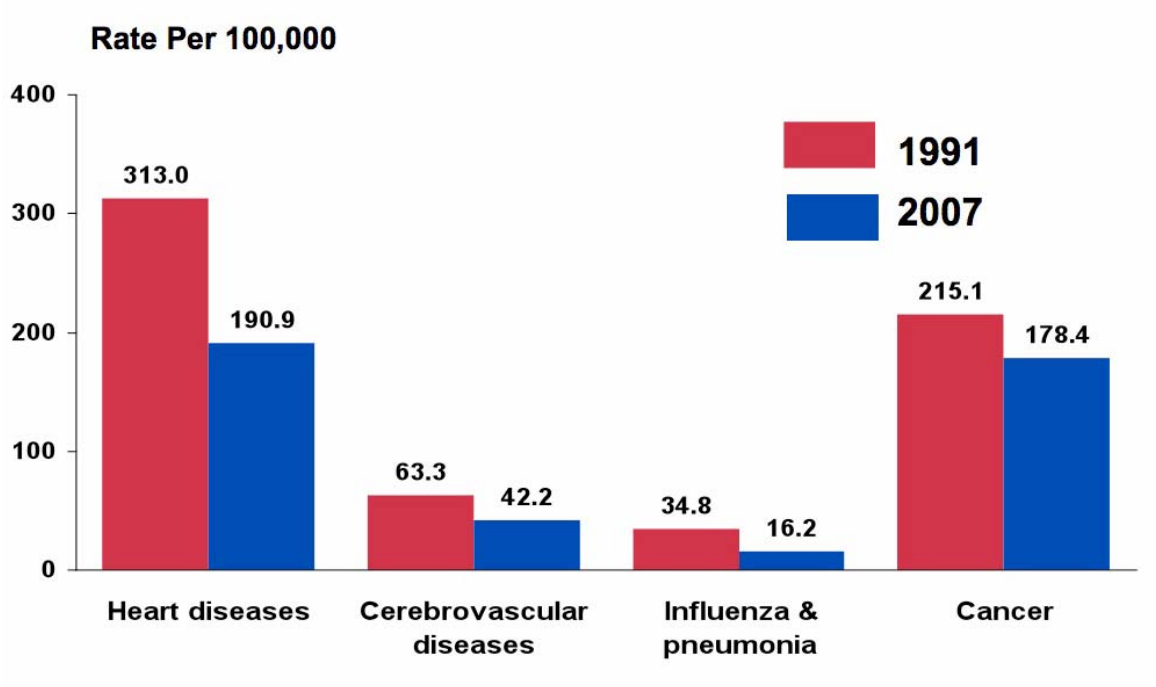

Figure 1.1. Comparison of Death Rates for Top Four Leading Causes of Mortality in the United States [2]

As seen in Figure 1.1, compared to the peak rate of 215.1 per 100,000 in 1991, the cancer death rate decreased 17% to 178.4 in 2007. Rates for other major chronic diseases decreased substantially during this period.

The complexity and heterogeneity nature of cancer makes it difficult to successfully diagnose and treat cancer. Advances in cancer research have been focused on studying molecular level of the disease, and "nanotechnology" plays a critical role in overcoming the obstacles in cancer biology. Nanotechnology is an interdisciplinary research field that combines chemistry, engineering, biology, and medicine that allows early detection, accurate diagnosis, and personalized treatment of cancer [3]. Nanotechnology adopts a size scale that is equivalent to biological molecules (i.e protein, DNA, etc.) of 5-100 nm in diameter. Due to its small size, nanoparticle improves the

availability of particular agent by increasing its interactions with biomolecules both inside and outside surface of the cells. The most well-studied nanoparticles include quantum dots [4-7], iron oxide [8-11], polymer-based nanoparticles [12-14], carbon nanotube [15], gold nanoparticle [16-19], and many others [20].

One of the most extensively studied subjects in nanotechnology is "size". In particular, the relationship between size and various aspects such as tumor accumulation/ targeting, cellular uptake, toxicity, biodistribution, and clearance has been the major focus for successful application of nanoparticles in detection, diagnosis, and treatment of cancer. In this chapter, we will closely look at the general characteristics of cancer and the role of nanotechnology in cancer biology, especially focusing on the "size effect".

1.3 CHARACTERISTICS OF CANCER

Research over the past decades have revealed that tumorigenesis in humans is a multi-step process that results in dynamic changes in the genome. The transformation of normal cells to malignant cells is an extremely complicated process that brings heterogeneity in cancer cells. To make the matter more complex, more than 100 distinctive types of human cancer have been identified, and multiple subtypes of tumors are found within a specific type of cancer. However, it has been reported that most and possibly all types of human cancer share common traits that are acquired during tumor development: 1) self-sufficiency in growth signals, 2) insensitivity to anti-growth signals, 3) evasion of programmed cell death or apoptosis, 4) limitless replicative potential, 5) sustained angiogenesis, 6) tissue invasion and metastasis [21].

Normal cells heavily depend on growth factors and signals from its environment to control proliferation. However, tumor cells provide their own growth factors and proliferate independently from external growth signals. Furthermore, tumor cells display

abnormal cell growth by disrupting the anti-growth signal pathway to result in uncontrollable growth.

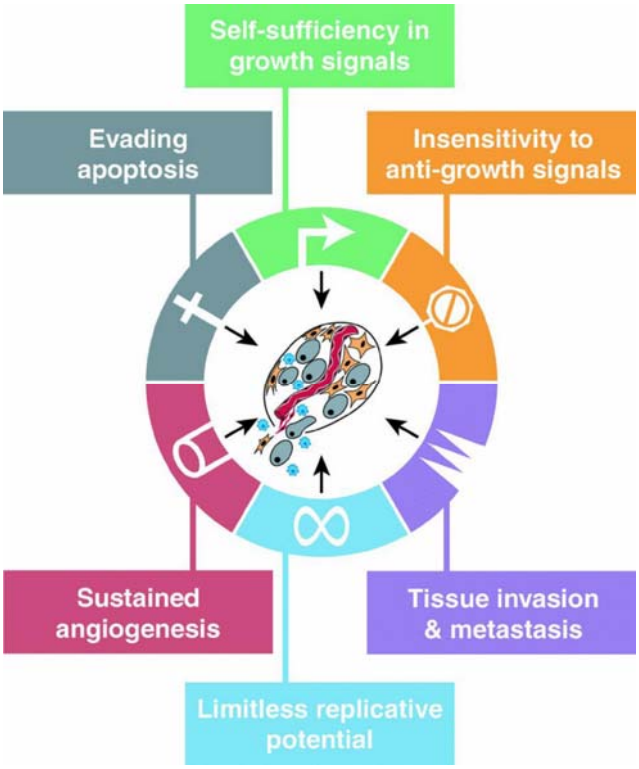

Figure 1.2. Six Acquired Traits of Human Cancer [21]

Apoptosis is body's defense mechanism where diseased cells are removed from the system through programmed cell death. Tumor cells avoid apoptosis by altering the cellular pathway for programmed cell death, which allows them to grow without any restriction or confinement. As the tumor cells proliferate, they provide their own nutrients via creating their own network of blood vessels to access oxygen and other required nutrients. Finally, tumor cells invade adjacent tissues and travel distant sites where nutrients and space is not limited initially. It is this metastasis of tumor cells that results in 90% of human cancer deaths.

1.4 ENHANCED PERMEABILITY AND RETENTION (EPR) EFFECT

Tumor vasculature is characterized as "leaky" due to its irregular-shaped, dilated, disorganized, and poorly-aligned endothelial cells [22-24]. Additionally, poor lymphatic drainage results in leakage of plasma components from the circulation into the interstitial space of the tumor. This phenomenon, originally described by Matsumura and Maeda, is called enhanced permeability and retention (EPR) effect [25].

As seen in Figure 1.3, normal, healthy vasculature displays continuous morphology where pores are 2-6 nm in size [26]. Tumor vasculature has larger pores than the normal vessels that size ranges from 100 to 2000 nm [27-29]. Increased cutoff pore size for tumor vasculature allows increased permeability of plasma proteins for tumor and lack of functional lymphatic vessels within tumor decreases the rate of clearance.

The EPR effect now has become the "gold standard" in anticancer drug delivery that takes advantage of the unique anatomical-pathophysiological nature of the tumor blood vessels. The EPR effect is a molecular weight dependent phenomenon that only occurs in the tumor tissue. Particles larger than 40 kDa selectively leak out from the tumor vessel to accumulate in the tumor tissue. The increased accumulation of >40 kDa are due to prolonged circulation time and decreased clearance rate from the body. In attempt to prolong the drug residence time and selectively trap the nanoparticle in the tumor cells, biocompatible poly (ethylene glycol) is commonly used to prevent rapid clearance of the nanoparticle by the reticuloendothelial system.

a)

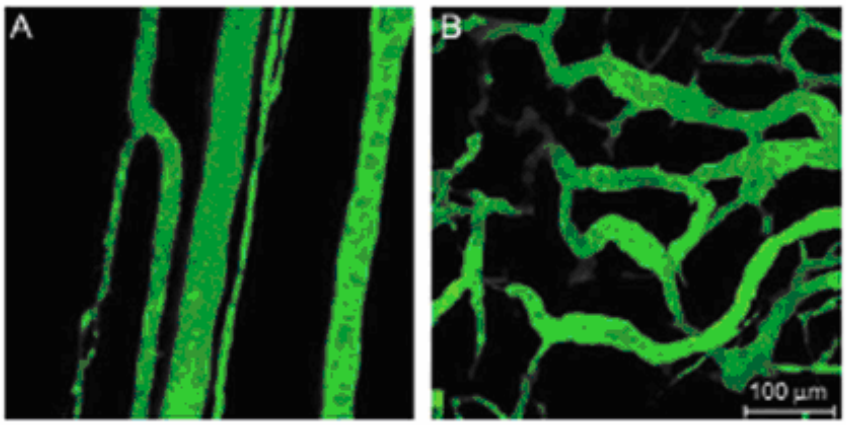

b)

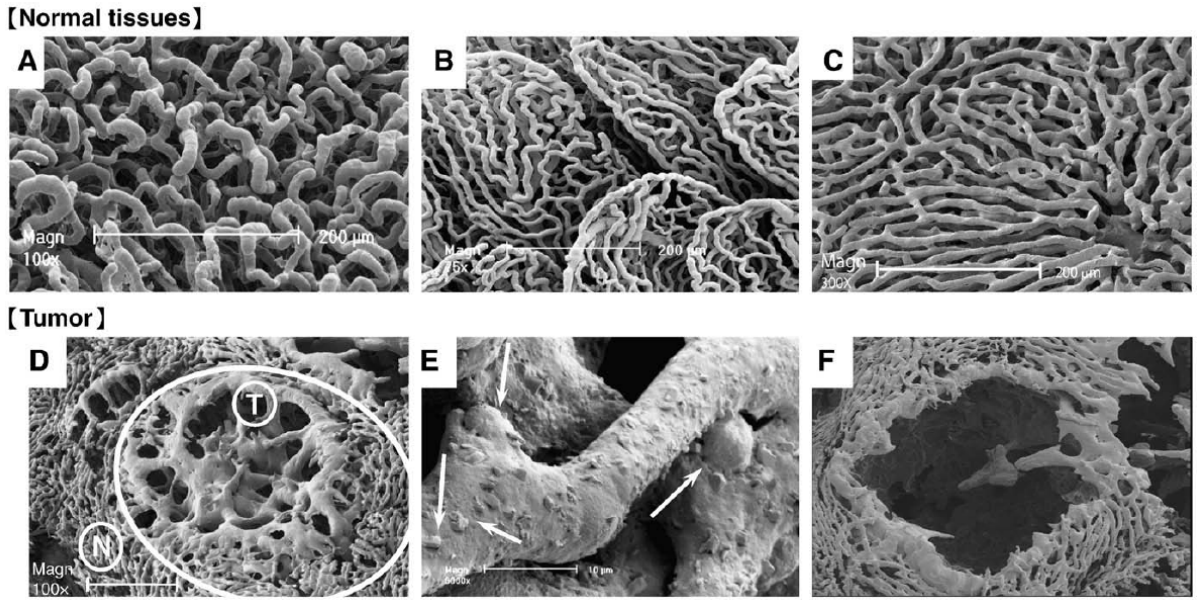

Figure 1.3. Normal and Tumor Vasculature. a) Normal vessels are aligned in parallel to one another (A), whereas tumor vessels have chaotic morphology with uneven diameters [23]; b) SEM images of normal blood vessels of pancreas (A), colon (B), and liver (C) compared to tumor vessels of liver (D, metastatic tumor nodule marked as "T" and normal liver tissue marked as "N"), tumor nodule (E), and empty void in tumor vascular bed (F) [24]

1.5 SIZE EFFECT

Various nanoparticles such as semiconductor quantum dots, iron oxide, polymer-based nanoparticles, and gold nanoparticles are present for *in vitro* and *in vivo* applications in nano-diagnostics and nano-therapy. Quantum dots are approximately 2-9 nm in size and are widely used in cell-tracking, solution-based detection, and *in vivo* imaging in whole animals [4, 7, 30]. Quantum dots display unique physical and chemical properties of narrow emission peaks, high photostability and brightness, broad absorption peaks, and size-tunable emission wavelengths throughout visible and infrared spectrum [30]. Paramagnetic iron oxides are widely used *in vivo* MRI contrast imaging agent [8, 9, 11, 31] and is also used as a carrier for targeted delivery of anticancer agent [32]. Polymer-based nanoparticles are commonly used for drug delivery applications and can be synthesized in various shapes and sizes that can carry multiple agents to the diseased cells [12-14]. Some of the polymer-based nanoparticles, such as PLGA-PEG, are biodegradable that can be cleared out from the body after the application over time [33]. Finally, gold nanoparticles are widely used for chemical sensing such as surface-enhanced Raman scattering (SERS), photo-thermal therapy, dark-field optical microscopy, and drug delivery applications due to its unique optical properties [34].

All of the above quantum dots, iron oxide, polymer-based nanoparticle, and gold nanoparticles can be synthesized in various sizes for biological applications. Not only each type of nanoparticle has unique chemical and physical characteristics but different sizes within each type of nanoparticle also results in unique property. Thus, size becomes an important factor for successful applications of these nanoparticles in cancer nanotechnology.

Size Effect on Tumor Targeting and Accumulation

Solid tumors are characterized by defective vascular architecture and impaired lymphatic drainage/ recovery system that lead to enhanced permeability and retention

(EPR) effect [35]. The key mechanism to this phenomenon is the retention of the macromolecules (MW > 40KDa, which is renal clearance cutoff) in solid tumors, where low-molecular weight particles are returned (instead of getting retained) back into the blood circulation by diffusion [36]. Many nanoparticle systems take advantage of EPR effect to increase the bioavailability of the delivered agent for successful cancer detection and treatment.

Recently, Perrault and coworkers have tested wide size ranges of gold nanoparticles (10-100nm) and found that accumulation of 40−100 nm particles is exclusively dependent on blood half-life, whereas the accumulation of particles in the 20 nm range depends on size and half-life [37]. They concluded that particles with hydrodynamic diameter of 60-100 nm with PEGylation (5 or 10kDa) would provide excellent candidate to utilized EPR effect for increased tumor accumulation. However, Perrault et al. found that larger particles (60-100nm) permeated less into the tumor and localized in the perivascular region. For 20nm particles, they permeated far from the vessel centers and may have cleared into the surrounding tissues that led to lower degree of accumulation.

Similarly, Dreher and coworkers used dextrans to study the tumor vascular permeability and accumulation of drug carriers [23]. They found that tumor accumulation increased with larger molecular weight dextrans (40−70 kDa or 11.2−14.6 nm). They accounted poor accumulation of low molecular weight dextrans (3.3-10kDa) is due to the increased permeation of rate and clearance of dextrans into interstitial space.
Thus, EPR effect is very sensitive to size and appropriate size needs to be selected for the successful accumulation and permeation of nanoparticle in solid tumor.

Size Effect on Cellular Uptake

Many studies in the past have demonstrated that size plays a critical role in cellular uptake of various nanoparticles such as liposomes, polymer nanoparticles, DNA-

coated glycocluster nanoparticles, and inorganic nanostructures [38-42]. Compared to other sizes (range of 14-100 nm), Chithrani et al. found that nanoparticles with a diameter of approximately 50nm were taken up by cells at a higher concentration with a faster rate. Particularly, Osaki et al. showed that 50nm quantum dot nanoparticles entered the cell more efficiently than smaller nanoparticles via receptor-mediated endocytosis.

Within the same size, additional factors such as surface charge can complicate the cellular uptake process of nanoparticles [38, 41-44]. Generally, cationic particles tend to bind to the cell surface more efficiently than the anionic particles due to electrostatic attraction to the negatively charged cellular membrane. Surface charge of the nanoparticle can be easily modified with various coatings. However, surface coatings with thiolated PEG (MW 1500) can increase the nanoparticle diameter up to ~6nm [38], which affects the overall size of the nanoparticle for cellular uptake.

Size Effect on Nanoparticle Toxicity

A concern for nanomaterial toxicity arises as the physical and chemical properties of the material changes dramatically at a nanoscopic scale. Various sizes of nanoparticles, especially gold nanoparticles, have been frequently been in the focus of interest for testing nanotoxicity. It has been reported that gold nanoparticles or clusters as small as 1.4nm in diameter lead to unusual cytotoxicity, where 1.4nm particles strongly interact with the major grooves of the DNA [45]. Similarly, Pan et al. found that 1.4 nm gold particles predominantly cause necrosis while 1.2nm gold particles mainly cause apoptosis in connective tissue fibroblast, epithelial cells, macrophage, and melanoma cells [46]. For a given concentration, Pan et al. reported that 15nm gold nanoparticle did not show toxicity compared to 1.4 nm gold particles.

Connor et al. reports gold nanoparticles with 4nm, 12nm, and 18nm in diameters did not display toxicity towards human leukemia cell lines [47]. Furthermore, Shukla et al. reported lysine and poly-lysine capped 35 ± 7 Å gold nanoparticle lacked toxicity towards macrophages but reactive oxygen and nitride species were observed [48]. Finally, 50nm gold nanoparticles were uptaken by HeLa cells without any toxicity [38]. Thus, for a given nanomaterial (gold in this case), size plays a critical role in exerting toxicity to cells.

Size Effect on Nanoparticle Biodistibution

The unique physico-chemical properties of nanoscale particles results in an increased reactivity with the biological systems that it renders different effects in the system compared to the larger, bulk materials. It is important to know the distribution and the effects of absorbed nanoparticle in various organs after an exposure. Generally, nanoparticles with size less than 10nm get distributed throughout the system, whereas larger particles like ~60nm is mostly confined to the liver and spleen after intravenous injection [49]. Furthermore, in detailed studies on various nanoparticle size and its distribution confirm that majority of nanoparticles accumulated in the "liver" and "spleen" regardless of size (1.9nm~250nm), shape (sphere or rod), type (carbon nanotube, quantum dots, iron oxide, gold nanoparticle), and dose of exposure (0.01~2700 mg/kg) after intravenous injection [18, 49-62].

Table 1.2. Biodistribution of Various Size, Shape, and Dosage of Gold Nanoparticles [52]

Reference	Model	Type of AuNPs	Study duration	Dose	Dose level normalized to this study	Organs/tissues examined
Hainfeld et al. 2004	Mice	1.9 nm	5 min	1350–2700 mg/kg	1.3×10^4–2.7×10^5	5 organs
Paciotti et al. 2004	Mice	33 nm (surface modified with PEG-thiol)	Up to 6 h	0.3–0.6 mg/kg	30–60	5 organs
Bergen et al. 2006	Mice	50, 80, 100 and 150 nm (Unmodified and surface modified with PEG_{5000}-thiol or gal-PEG-*O*-pyridyl disulfide)	2 h	0.5–0.6 mg/kg	45–56	3 organs
Hainfeld et al. 2006	Mice	1.9 nm	24 h	700, 70, 7 mg/kg	$700–7 \times 10^4$	5 organs
Niidome et al. 2006	Mice	nanorods (length: 65 nm; width: 11 nm)	0.5-, 3-, 6-, 12, 24- and 72-h	0.98–1.52 mg/kg	98–151	5 organs
Balogh et al. 2007	Mice	Au composite nanodevices (5- and 22-nm positive surface; 5- and 11-nm negative surface; 5 nm neutral surface)	5 min, 1 h, 1-, 4-, and 7-days	16 mg/kg	1591	10 organs
Sadauskas et al. 2007	Mice	2 and 40 nm	1-, 4- and 24-h	0.6–3.2 mg/kg	57–322	8 organs
De Jong et al. 2008	Rat	10, 50, 100 and 250 nm	24 h	77–120 μg	25–36	13 organs
Huang et al. 2008	Mice	Au–Au_2S NPs	7 days	10 mg/kg	995	10 organs
Sonavane et al. 2008	Mice	15, 50, 100 and 200 nm	24 h	1000 mg/kg	9.9×10^4	9 organs
Cho et al. 2009	Mice	13 nm (PEGylated)	5-, 30-min, 4-, 24-h and 7 days	0.17–4.26 mg/kg	17–424	7 organs
Sadauskas et al. 2009	Mice	40 nm	1 day, 1-, 3- and 6-months	1.4–1.6 mg/kg	138–161	Only in liver
Terentyuk et al. 2009	Rat	15, 50 and 160 nm (PEGylated)	24 h	57 μg	19	6 organs
Zhang et al. 2009	Mice	20, 40 and 80 nm (PEGylated and ^{111}In-labelled)	48 h	0.1–4.4 mg/kg	5–437	11 organs
Balasubramanian et al 2010	Rat	20 nm	1 day, 1 week, 1 and 2 months	0.01 mg/kg	1	28 organs; feces and urine

Size Effect on Nanoparticle Clearance

After delivering imaging or therapeutic agent with a nanocarrier to the target site, it is desirable to see the delivery vehicle to clear out from the body, minimizing any harm to the healthy, normal cells. It has been reported that larger particles such as 20nm gold nanoparticle is minimally excreted through feces and urine that there is a significant and persistent accumulation of gold nanoparticle in the liver and spleen through intravenous exposure [52]. Similarly, metal-based 13nm quantum dot showed accumulation in kidney but there was no urinary excretion up to 28 days after the injection in mice [63]. Recently, Perrault and coworkers found that PEGylated 20nm gold nanoparticle cleared out rapidly from the blood without corresponding accumulation in the spleen and liver. Also, 40nm gold nanoparticle was removed from the circulation primarily by Kupffer

cells in the liver and remained as clusters even after six months [58]. In contrast, particles with less than ~6nm (MW ~50,000**)** in diameter displayed clearance from the system. For example, 77% of the injected 1.9nm gold nanoparticle was rapidly cleared through the kidney and excreted 5 hours after the intravenous injection in the mouse [56]. Similarly, Choi et al showed rapid clearance of zwitterionic coated quantum dots (4.36-5.52nm) through kidney and urinary excretion within 4 hours after the intravenous injection [64]. Based on these findings, we believe that nanoparticle "size" plays a critical role for not only delivering the imaging or therapeutic agents to the target site but also determining the *in vivo* behavior such as clearance of the nanoparticle in the body.

Search for an Ideal Nanoparticle Size for Various Applications in Cancer Nanotechnology

Due to the complex nature of nanostructures, conflicting studies have led different views on various sizes of nanoparticles. Despite all the efforts in finding the optimal size to satisfy each category (relationship between size and 1) tumor accumulation, 2) cellular uptake, 3) toxicity, 4) biodistribution, and 5) clearance) listed above, there has not been a complete study that looks into a size that satisfies the majority of the categories at once. To make the matter worse, most of the studies conducted for each category were under *in vitro* conditions, which do not reflect the complexity of *in vivo* conditions.

To detect, diagnose, and treat cancer, one needs to be well aware of the unique cancer environment. It is the size-scale of nanotechnology that provides a powerful tool to easily manipulate the complex cancer environment by distinctively size-tuning the nanomaterial to interact with biological molecules in tumor. Furthermore, increased surface-to volume ratio in nanoparticles allows attaching various agents to further strengthen the unique properties of each nanomaterial.

Here, biocompatible and inert nanomaterial, gold nanoparticle, will be chosen as a model system to test the size effect *in vivo.* Gold nanoparticles have been widely used in cell imaging [65, 66], targeted drug delivery [67], and cancer diagnostics and therapeutic applications [16, 68-70]. Furthermore, gold nanoparticle is an appropriate candidate for our study since various sizes (and shapes) can be easily synthesized. Since gold is not an intrinsic element in biological system, it is easily characterized by various analytical chemistry techniques such as UV-absorption spectroscopy, SERS, ICP-MS, TEM, dark-field microscopy, etc. Thus, gold nanoparticle seems to be a logical choice to represent nanoparticles used in biomedical applications. In particular, we will focus on PEGylated small-sized gold nanoparticle (5nm) system in order to establish a universal size scheme that could be applied to satisfy tumor accumulation, cellular uptake, toxicity, biodistribution, and clearance issues *simultaneously* in biomedical application.

1.6 DISSERTATION STRUCTURE

This dissertation focuses on the size effect in cancer nanotechnology, particularly focusing on the smaller-sized nanoparticle (5nm) that can be applied universally for various applications to detect, diagnose, and treat cancer. Gold nanoparticle will be used as a model system to test the size effect, comparing the smaller-sized gold nanoparticle (5nm) with the larger nanoparticle (60nm) *in vivo*. Each chapter will discuss the details and results for the development and applications of gold nanoparticle in cancer nanotechnology. The following briefly summarizes each chapter.

Chapter 1 – This chapter looks at the general characteristics of cancer and emphasizes the role of nanotechnology, particularly in terms of size effect, for successful detection, diagnosis, and treatment of cancer.

Chapter 2 – This chapter focuses on the general background for gold nanoparticles, which is used as a model nanoparticle system for the thesis.

Chapter 3 – This chapter looks at design and development of a multifunctional drug delivery system that consist of large (60nm) gold nanoparticle system. The limitation seen in 60nm gold nanoparticle will set the motivation to look into smaller-sized gold nanoparticle for cancer nanotechnology.

Chapter 4 – We discuss using smaller-sized gold nanoparticle (5nm) to overcome short-comings of larger-sized gold nanoparticle in drug delivery application. The study focuses on treatment of breast cancer in mice model and looks at the effectiveness of the small-sized gold nanoparticle system and its toxicity (if any).

Chapter 5 – Here, we use mice model to investigate the unique characteristics of small-sized gold nanoparticle (5nm) compared to larger-sized gold nanoparticle (60nm) in terms of biodistibution and clearance. The results from this chapter suggest "5nm" as a potential universal size candidate that can be used successfully for various applications in cancer nanotechnology.

Chapter 6 – Finally, we present several suggestions for further development of the system discussed in this dissertation as well as future directions of cancer nanotechnology in general.

1.7 CONCLUSION

The complexity and heterogeneity nature of cancer makes it difficult to successfully diagnose and treat cancer. Advances in cancer research have been focused on studying molecular level of the disease, and nanotechnology plays a critical role in overcoming the obstacles in cancer biology. It is the size-scale of nanotechnology that provides a powerful tool to easily manipulate the complex cancer environment by distinctively size-tuning the nanomaterial to interact with the biological molecules in tumor. In particular, the relationship between size and various aspects such as tumor accumulation/ targeting, cellular uptake, toxicity, biodistribution, and clearance has been the major focus for successful application of nanoparticles in detection, diagnosis, and

treatment of cancer. Thus, searching for the optimal size that can be universally applied for various applications in cancer nanotechnology will be useful. We will focus on using biocompatible, inert gold nanoparticle as a model system to find that "universal size" in this thesis.

CHAPTER 2

BIOMEDICAL APPLICATIONS OF GOLD NANOPARTICLES IN CANCER NANOTECHNOLOY

2.1 ABSTRACT

Gold nanoparticles are widely used in biomedical applications such as imaging, diagnostics, targeted drug delivery, and photo-thermal therapeutic applications. Due to its unique optical properties, multiple analytical chemistry methods such as UV-vis spectrophotometry, SERS, TEM, ICP-MS, darkfield microscopy, fluorescence exist. Also, gold nanoparticle renders several advantages of size-shape tunability, biocompatibility, and easy surface modification method that are useful for studying size effect in biomedical applications. Here, we will closely look at the general background and characteristics of gold nanoparticle and the rational behind choosing gold nanoparticle as a model system for studying size effect in cancer nanotechnology.

2.2 INTRODUCTION

Gold nanoparticles have a long history of medical usage. Red colloidal gold has been used by the Chinese since 2500 B.C. as a drug for longevity [71], whereas colloidal gold has been used for rejuvenation medicine in India [72]. Furthermore, colloidal gold has been used to treat rheumatoid arthritis for half a century [73, 74]. Colloidal gold also has ornamental usage that red colloidal gold was widely used in stained glasses during medieval period [75, 76].

Currently, gold nanoparticles are widely used in industrial and biomedical applications. For biomedical applications, a lot of the effort has been dedicated to "chemical sensing" such as SERS or particle aggregation sensing (Figure 2.1). The

unique optical property of gold nanoparticle allows "tracking" and imaging via dark field optical microscopy or two-photon luminescence microscopy for diagnostic purposes [34]. For therapeutic application, gold nanoparticle has been mainly used for "photothermal therapy", where irradiated gold nanoparticle releases heat to their local environment for destruction of cancer cells or tumor tissue [16, 77, 78]. Using small gold nanoparticle as a drug carrier in "drug delivery" is recent that further attention and study is required [20].

In this chapter, we will closely look at the physical and chemical characteristics of gold nanoparticle and the rational behind choosing gold nanoparticle as a model system to study the size effect for this thesis.

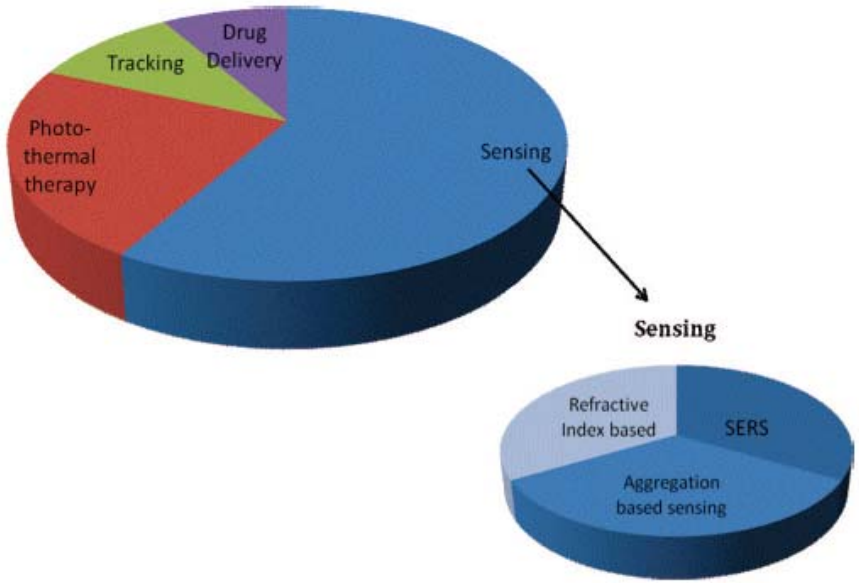

Figure 2.1. Pie Chart Depicting Different Biomedical Applications of Colloidal Gold: pie slices roughly estimate the proportions of collidal gold applications in four representative fields [34]

2.3 CHARACTERISTICS OF GOLD NANOPARTICLE

New properties are introduced when the material is reduced to a nanometer size scale. In particular, the nanometer size scale brings dramatic changes in the electronic and chemical properties of the material as seen in semiconductor quantum dots and gold nanoparticles [79, 80]. Furthermore, the surface-to-volume ratio becomes larger as the size is reduced that the surface dominates the particle and brings new properties to the material. Gold nanoparticles confer several attractive physical and chemical properties. Due to its unique optical property arising from surface plasmon absorption and scattering of light from the surface, various characterization methods are available for biomedical applications.

Surface Plasmon Absorption of Gold Nanoparticle

For noble metals such as gold, decrease in size below the electron mean free path (i.e. the distance the electron travels between scattering collisions with the lattice centers) leads to intense absorption in the visible-near UV wavelength [81]. This phenomenon or "surface plasmon absorption" is a result of the coherent oscillation of the free conduction band electrons from one surface of the particle to the other, which interact with an electromagnetic field [82]. As seen in Figure 2.2, the electric field of an incoming light wave induces a polarization of the electrons with respect to the much heavier ionic core of a spherical nanoparticle where net charge difference is only found at the surface of the nanoparticle [83].

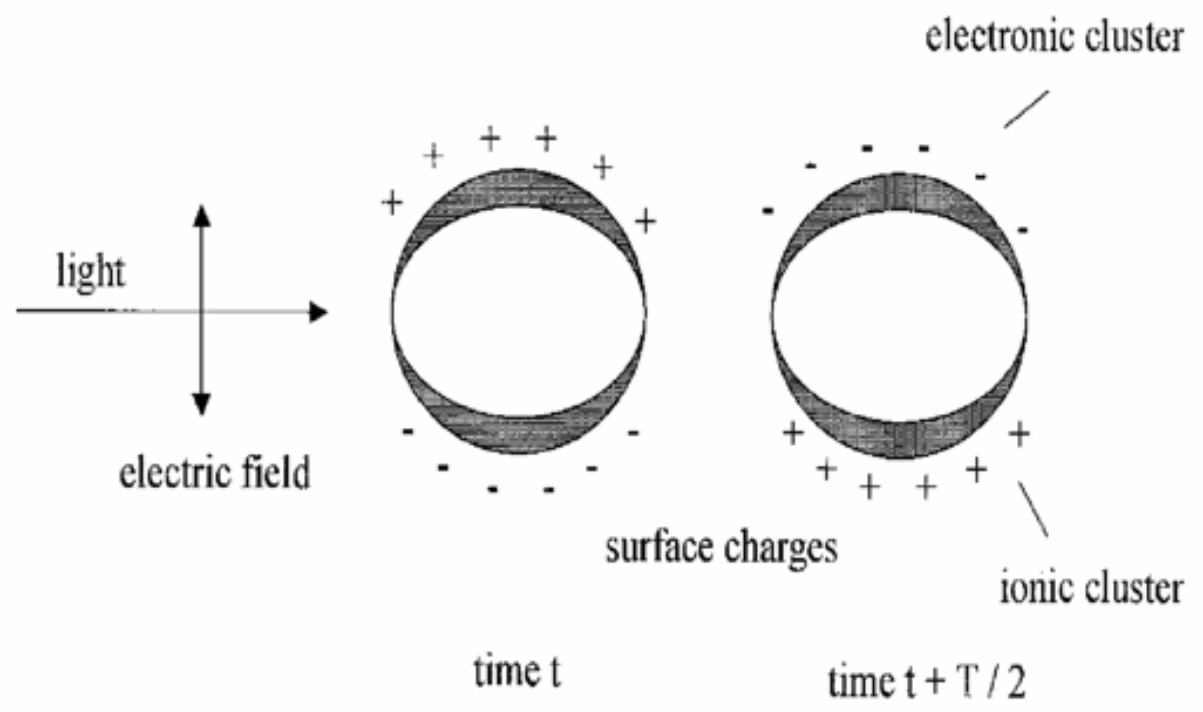

Figure 2.2. Classical Illustration of the Excitation of the Dipole Surface Plasmon Oscillation for Spherical Nanoparticle [80]

The brilliant colors observed in gold colloidal solutions (Figure 2.3) are the consequence of surface plasmon absorption where strong absorption induced strong coupling of the nanoparticles to the electromagnetic radiation of light. In other words, when the frequency of the electromagnetic field becomes resonant with the coherent election motion, a strong absorption in the spectrum is observed. The size, shape, dielectric constant of the metal nanoparticles as well as the dielectric constant of the medium surroundings affect the frequency and the width of the surface plasmon absorption.

a) b)

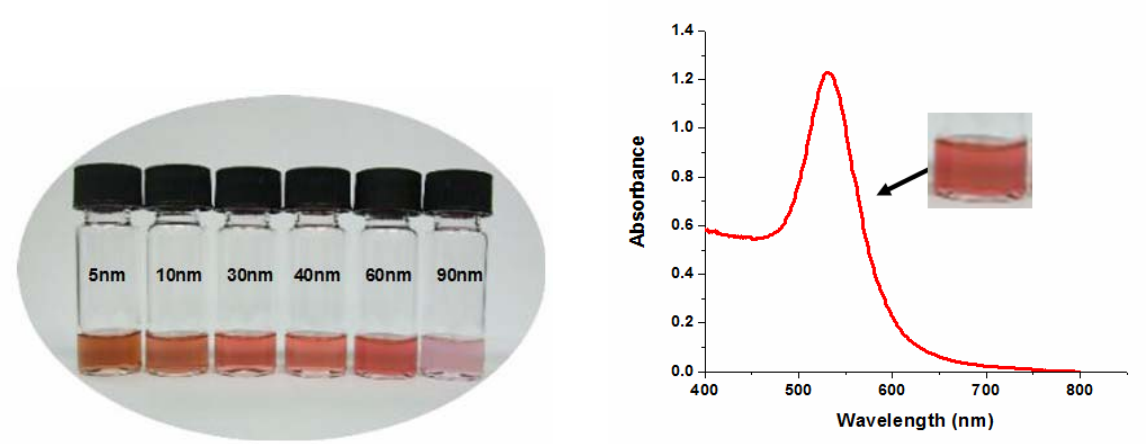

Figure 2.3 Surface Plasmon Absorption seen in Spherical Gold Colloidal Solution (a) Various colors are visible due to surface plasmon absorption of different size gold colloids (b) Typical surface plasmon absorption spectrum of spherical nanoparticle that absorption peak is around ~532nm for deep pink color solution of 60nm spherical gold nanoparticle.

In 1908, Mie was the first person to theoretically explain the surface plasmon resonance of small spherical metal particles [84]. Mie solved the Maxwell's equation for an electromagnetic light wave interacting with a small sphere having the same macroscopic, frequency-dependent material dielectric constant as the bulk metal. For particles < 20nm, Mie theory explains that the dipole oscillation contributes significantly to the extinction cross section. Mie's theory is expressed as the following:

$$\sigma_{ext} = \frac{9V\epsilon_m^{3/2}}{c} \cdot \frac{\omega\epsilon_2(\omega)}{[\epsilon_1(\omega) + 2\epsilon_m]^2 + \epsilon_2(\omega)^2}$$

EQN 2-1

Where V is the particle volume, ω is the angular frequency of the exciting light, and c is the speed of light. ε_m and $\varepsilon(\omega) = \varepsilon_1(\omega) + i\varepsilon_2(\omega)$ are the dielectric functions of the surrounding medium and the metal, respectively. For the metal, the dielectric function is complex and depends on the frequency. The resonance condition is fulfilled roughly when $\varepsilon_1(\omega) = -2\,\varepsilon_m$ if ε_2 is small or weakly dependent on ω [85].

For larger particles (>20nm), the absorption spectrum is combination of absorption and scattering modes. Higher order modes become more dominant with increasing particle size, causing the plasmon absorption band to red shift and resulting in increased bandwidth. Thus, the optical absorption spectra depend directly on the size of the nanoparticle (i.e. extrinsic size effect).

Surface Plasmon Light Scattering of Gold Nanoparticle

Gold nanoparticles have the ability to resonantly scatter visible and near-infrared light upon the excitation of their surface plasmon oscillation. The scattering light intensity is extremely sensitive to the size, shape, and aggregation state of the particles that determines the wavelength distribution of the light [86, 87]. Gold nanoparticles scatter light of many colors when illuminated with white light at appropriate angles that this color scattering property offers the potential for labeling studies.

It has been reported that the optical properties of nanoparticle (i.e. the optical resonance wavelength, the extinction cross-section, and the relative contribution of scattering to the extinction) are strongly dependent on the nanoparticle dimensions, allowing tunability for specific applications [88]. The increase in the nanoparticle size

results in an increase in the extinction as well as the relative contribution of scattering. This phenomenon is also described by Yguerabide et al. by the following equation [86].

$$C_{\mathrm{sca}}(\lambda_0) = \frac{128\pi^5 n_{\mathrm{med}}^4 a^6}{\lambda_0^4} \left| \frac{m^2 - 1}{m^2 + 2} \right|^2 \qquad \text{EQN 2-2}$$

Where C_{sca} is light scattering cross section, a is particle radius, n_{med} is the refractive index of the medium surrounding the particle, m is the relative refractive index of the bulk particle material, and λ_0 is the wavelength of the incident beam.

As seen in Equation 2-2, the scattering cross-section increases by 6 power of the particle radius in which increase in particle radius results in higher cross-section for stronger light scattering. Furthermore, gold nanoparticles provide high-scattering cross-section compared to the conventionally used fluorescent dyes by 4-5 orders in magnitude [88]. Thus, surface plasmon oscillation of electrons of the gold nanoparticle result in strongly enhanced scattering that is useful for various biomedical applications.

Advantages in Using Gold Nanoparticle

Size and Shape Tunability

Gold nanoparticles are easily synthesized in various shapes and sizes that it confers size and shape tunability[89]. In general, metal salts are reduced by reducing agents in a controlled manner to produce spherical nanoparticles. The ratio between the metal salt and the reducing agent determine the size of the nanoparticle. Some of the frequently used methods to synthesize spherical gold nanoparticles are 1) the Turkevich

method (1951) that reduces the gold chloride by citrate in boiling water, 2) the related Frens method (1973), 3) the Brust method (1994) for smaller (~2nm) gold nanoparticles, where aqueous gold ion solution is transferred to an organic phase, mediated by phase transfer agent, followed by reduction with borohydride, 4) microemulsion method, and 5) seeding method in which gold seed particles are used to grow more gold in the presence of of a weak reducing agent [90]. Spherical shapes are the easiest to synthesize since spheres are the lowest-energy shape.

Gold nanorods are synthesized in various methods such as seed-mediated growth methods [81, 85]. Nanoshells are synthesized by having spherical dielectric nanoparticle (i.e. silica nanoparticle) surrounded by an ultrathin, conductive, metallic layer (i.e. gold) [68]. Most recently, Xia group of the University of Washington have created gold nanocages sizes ranging from 10 to 150nm, which are porous gold nanoparticles. Gold nanocages are created by reacting silver nanoparticles with chloroauric acid in boiling water [91].

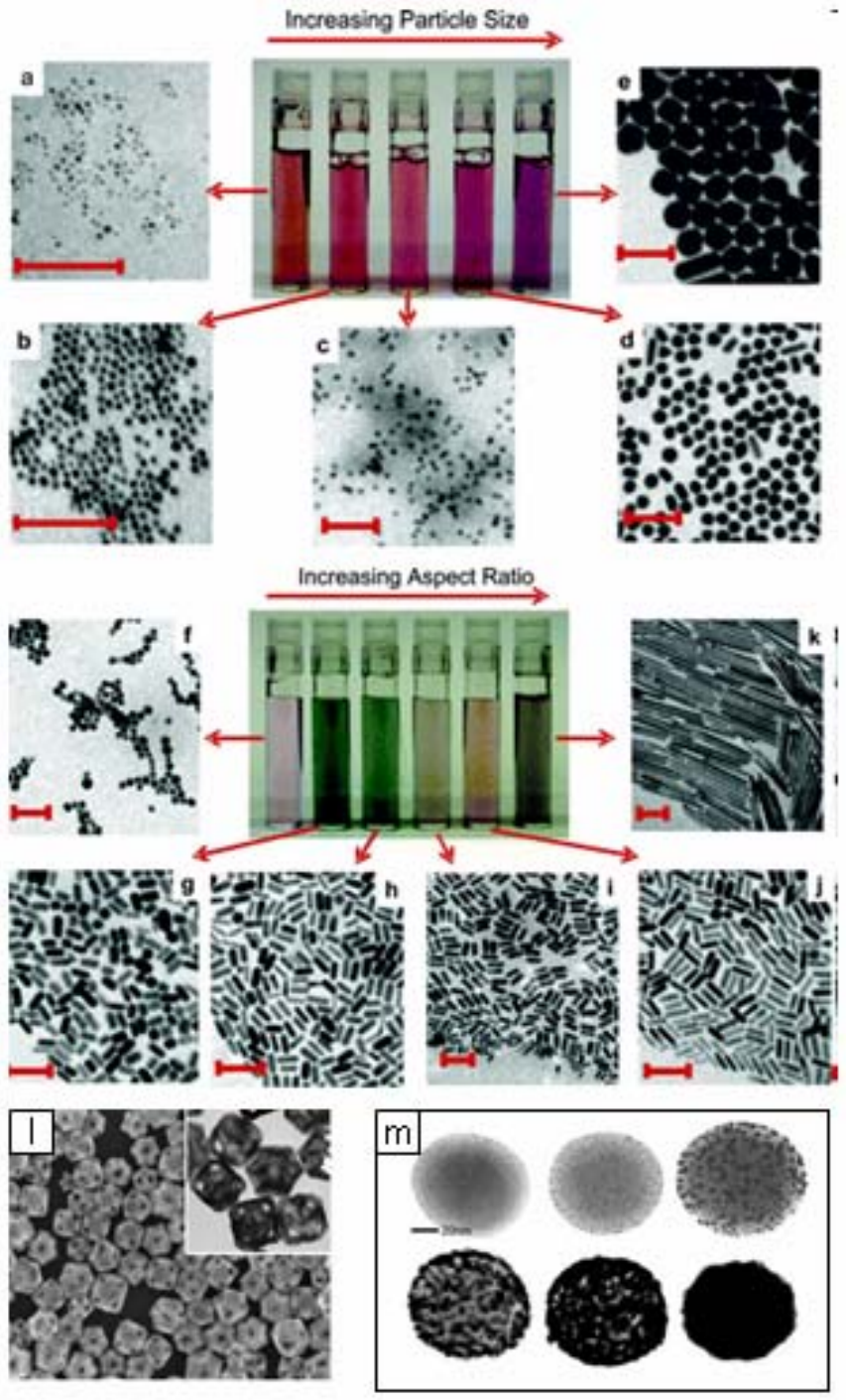

Figure 2.4. TEM Images of Various Shapes and Sizes of Gold Nanoparticles: a-d represent spherical gold nanoparticle, f-k represent gold nanrods, l represents gold nanocage, and m represent gold nanoshells [a-j: [34]; l: [91]; m: [92]].

Biocompatibility

Gold nanoparticles are inert and have low *in vivo* toxicity compared to the other metallic materials [93, 94]. Several groups have examined the cellular toxicity of gold nanoparticles (Table 2.1). It was found that gold nanoparticles show little or no cytotoxicity in several studies. The biocompatibility of gold nanoparticle suggests that biological effect of gold nanoparticle is unlikely due to the intrinsic toxicity of the metal.

Table 2.1. Summary of Selected Cytotoxicity for Gold Nanoparticles [34]

author	size (nm)	shape	surface group	cell line	toxicity results
Shukla	3.5 ± 0.7	sphere	lysine, poly(L-lysine)	RAW264.7 mouse macrophage cells	85% cell viability after being exposed to 100 μM gold nanoparticles for 72 h
Connor	4, 12, 18	sphere	citrate, cysteine, glucose, biotin, CTAB	K562 human leukemia	none of the spherical nanoparticles were toxic at the micromolar ranges used
Goodman	2	sphere	quaternary ammonium, carboxylic acid	COS-1 mammalian cells, mammalian red blood cells, *Escherichia coli*	cationic nanoparticles were found to be much more toxic than anionic particles of the same size
Niidome	65 ± 5 × 11 ± 1	rod	CTAB, PEG	HeLa cells	80% cell death with 0.05 mM CTAB-coated nanorods, only 10% cell death at 0.5 mM PEG-coated nanorods
Huff		rod	CTAB	human tumor KB cells	gold nanoparticles were rapidly taken into the cells and formed permanent aggregates, but the cells remained healthy
Patra	33	sphere	CTAB, citrate	BHK21 baby hamster kidney cells, Hep2G human liver carcinoma cells, A549 human carcinoma lung cells	nontoxic to BHK21 and HepG2 cells, but toxic to A549 cells
Takahashi	65 × 11	rod	phosphatidyl-choline	HeLa cells	phosphatidylcholine-modified gold nanorods were much less toxic than CTAB-coated nanorods
Khan	18	sphere	citrate	HeLa cells	gold nanoparticles did not cause significant gene-expression patterns or cyotoxicity even though they were internalized in the cells.

Easy Detection by Using Various Analytical Methods

Ultraviolet-Visible Spectroscopy

The absorption spectra for spherical nanoparticle depend directly on the size of the nanoparticle (i.e. extrinsic size effect) due to the surface plasmon resonance [95]. Particularly for gold nanoparticles, they have a strong visible-light plasmon resonance

that Ultraviolet-Visible (UV-Vis) Spectroscopy is useful for characterization. As the particle size gets larger, we can observe red shift and increase in bandwidth in the absorption spectra obtained from the UV-Vis Spectroscopy (Figure 2.5). Red shift (and/or broadening of the bandwidth of the absorption peak) is also observed when the nanoparticle is coated with different ligands or aggregation occurs within the gold nanoparticles in the solution. Thus, UV-Vis Spectroscopy is also useful to check the stability of the colloidal gold in solution.

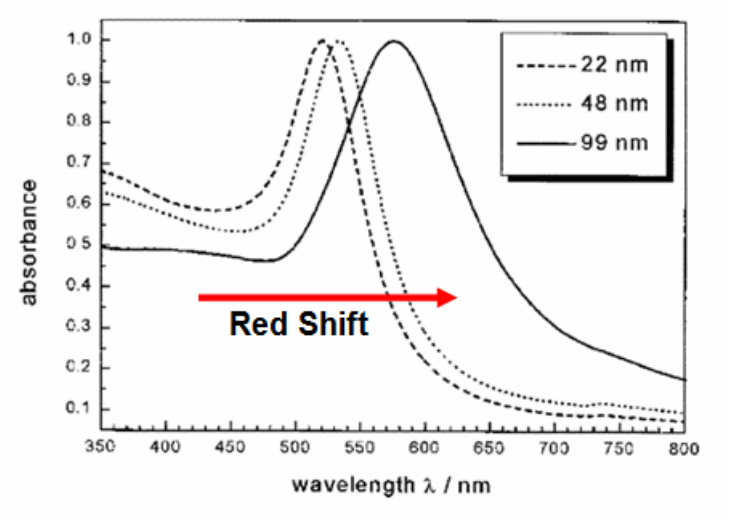

Figure 2.5. Increase in Particle size results in red shift and increased bandwidth in absorption spectra [85]

The Beer-Lambert law can be used to calculate the concentration of the solution.

$$A = \log_{10}(I_0/I) = \epsilon \cdot c \cdot L \qquad \text{EQN 2-3}$$

Where A is the measures absorbance, I_0 is the intensity of the incident light at a given wavelength, I is the transmitted intensity, L the pathlength through the sample, c is the

concentration of the absorbing species, and ε is a constant known as molar absorptivity or extinction coefficient.

The Beer-Lambert law states that the absorbance of the solution is directly proportional to the concentration of the absorbing species and the path length. Thus, for a fixed path length with known extinction coefficient, UV-Vis Spectroscopy can be used to determine the concentration of the absorbing species in the solution.

Darkfield Light-Scattering Imaging

Colloidal gold nanoparticle has become an important alternative as imaging agents due to their biocompatibility and nonsusceptibility to photo-bleaching or chemical/thermal denaturation, a common problem observed with organic dyes [96]. Recently, El-Sayed et al. demonstrated differentiation of cancerous cells from healthy cells by darkfield light –scattering imaging with 35nm gold nanoparticle [97].

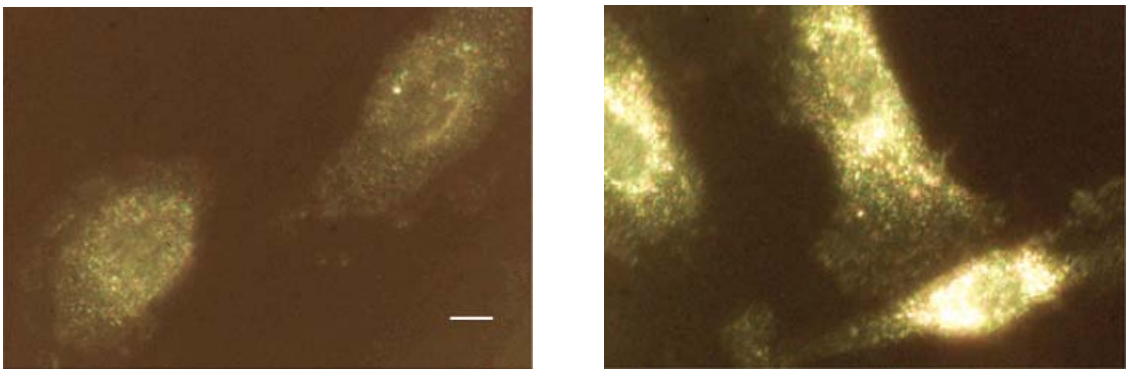

Figure 2.6 Darkfield Light-Scattering Images of HSC Cancer Cell: HSC cancerous cells without (left column) gold nanoparticles and HSC cancerous cells with (right column) gold nanoparticles that scatter light to display bright yellow glow (scale bar: 10 μm) [97]

Darkfield light-scattering imaging utilizes microscopy techniques. The darkfield imaging microscopy requires a condenser that has numerical aperture higher than the objective. The condenser delivers a very narrow beam of white light from the light source. Then the objective collects the only scattered light (not transmitted light from the samples) that the center of the illuminating beam is blocked from the entering light collection cone of the microscope objective and only the scattered light of the side beam is collected. As a result, a bright image with a dark background is created (Figure 2.7).

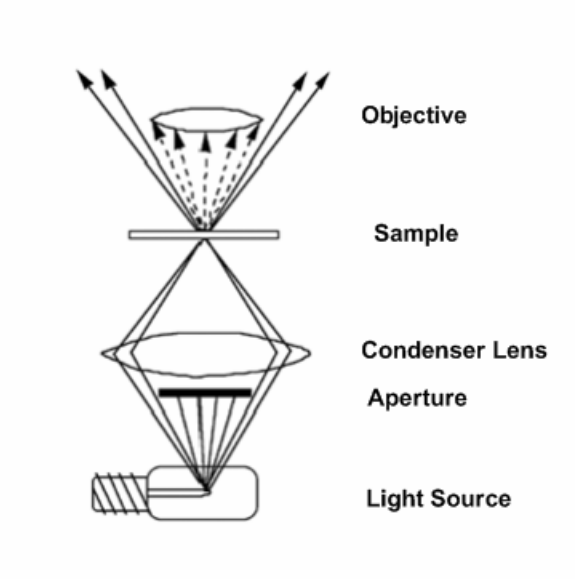

Figure 2.7. Diagram of Darkfield Light-Scattering Microscopy Setup

A high-scattering cross-section is essential for imaging applications based on darkfield light-scattering microscopy. Gold nanoparticles provide cross-sections of 4-5 orders higher in magnitude than that of the conventional organic dyes. Darkfield allows label-free detection that does not require staining of the sample. It also creates a distinctive image that reflects the true-color of the gold nanoparticle, which depends on the size and shape of the particle.

Fluorescence

Resonant energy-transfer is observed in fluorescent ligand-capped gold nanoparticles. For most of chemisorbed chromophores on gold surface, quenching of the fluorescence is observed. Quenching is generally due to increased non-radiative relaxation of the excited state due to energy and/or electron transfer [98]. Also, quenching is partly due to a decrease in the rate of radiative relaxation related to changes in the photonic mode density near the metal cluster surface (plasmonic effect) [99]. Both radiative and non-radiative rates critically depend on the size and shape of the nanoparticle, the distance between the dye molecules, the orientation of the dipole with respect to the dye-nanoparticle axis, and the overlap of the molecule's emission with the nanoparticle's absorption spectrum [100]. Also, enhancement of fluorescence by metal nanoparticles is reported, mostly occurring in aggregated metal colloids [101].

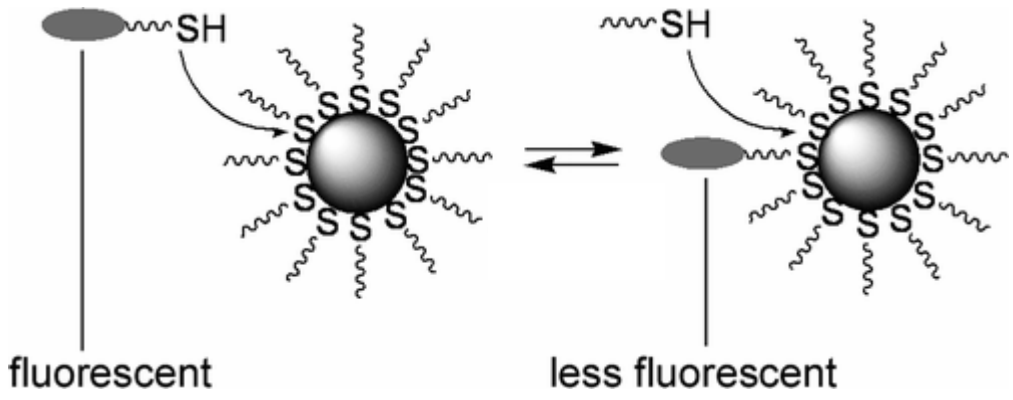

Figure 2.8. Fluorescence Quenching of Chemisorbed Chromophore on Gold Nanoparticle [98]

Fluorescence quenching phenomenon can be used to check successful ligand exchange process. When thiolated chromophore, such as doxorubicin, is added to the gold colloid solution, the fluorescence of doxorubicin is quenched by successful coating or chemisorption of thiolated doxorubicin onto gold nanoparticle surface, where quenching is mediated by the thiol group.

Transmission Electron Microscopy

High Resolution Transmission electron microscopy (TEM) is the most common characterization technique used to photograph the gold core of the gold nanoparticle. TEM can be used to verify the morphology and size of the gold nanoparticle. Due to the electro-dense surface of the gold nanoparticle, gold core is visible as dark spots in the TEM images.

Surface Enhanced Raman Scattering (SERS)

SERS is a spectroscopic technique that results from strongly increased Raman signals when molecules are attached to nanometer-sized gold nanostructures. Gold nanoparticle has unique optical properties that Raman signal from adsorbed reporter molecules can be increased up to 10^{14}~10^{15} orders in magnitude, allowing "single" molecular level spectroscopic detection through SERS [102-104]. SERS, an analytical technique, can give information on any small chemical changes occurring at the surface and interfaces of gold nanoparticle [103, 105].

SERS has generated considerable interest, particularly in molecular diagnosis and *in vivo* Raman spectroscopy and imaging. SERS nanoparticle tags, gold nanoparticle with

embedded reporter molecules, are capable of providing detailed spectroscopic information and results in signals that are much brighter than semiconductor quantum dots in near-infrared spectral window [106]. Recently, Qian et al. has demonstrated *in vivo* spectral imaging of cancer in a mouse model (Figure 2.9) [19].

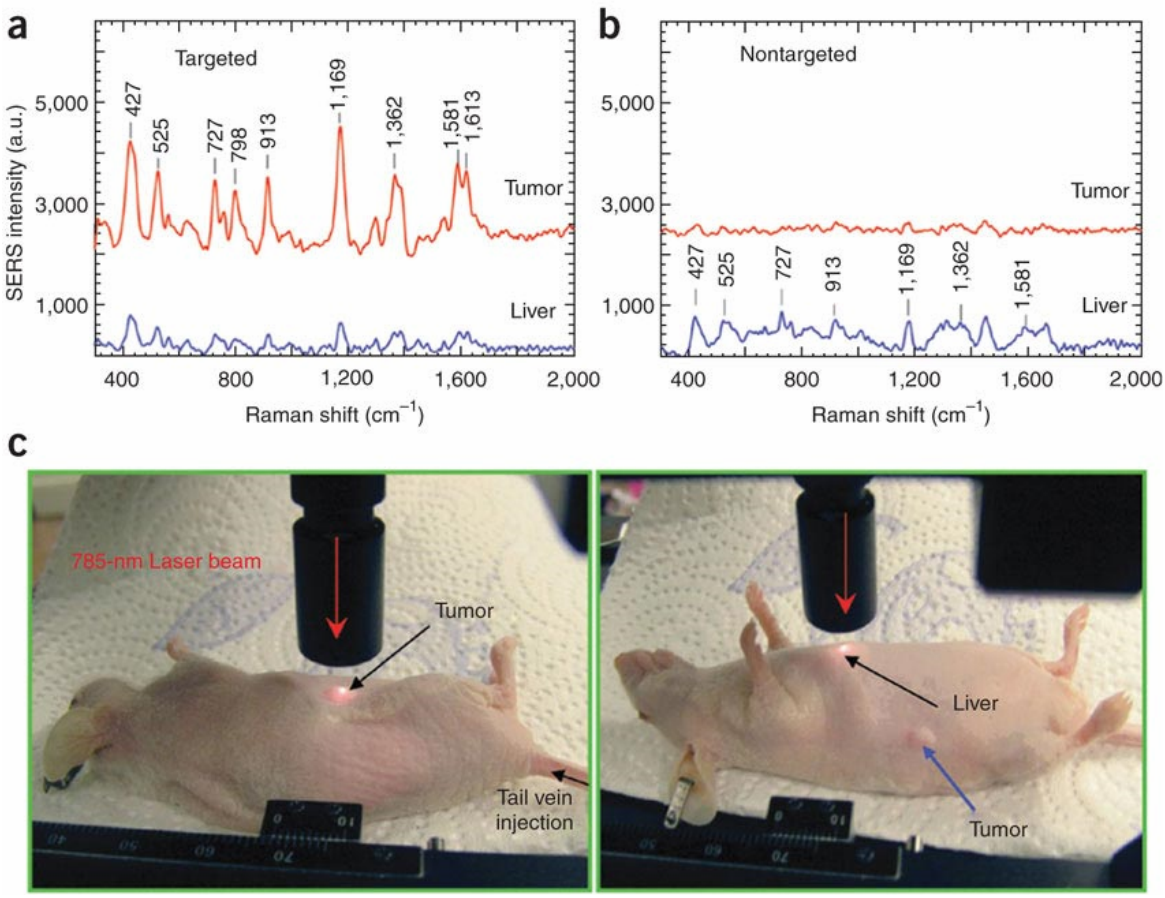

Figure 2.9. *In vivo* Cancer Targeting and Surface-Enhanced Raman Detection by Using Antibody-Conjugated Gold Nanoparticle: SERS spectra obtained from the tumor and liver locations by using (a) targeted and (b) non-targeted nanoparticles. (c) is pictures showing a laser beam focusing to the tumor site or the liver to obtain SERS spectroscopic signal [19]

Inductive-Coupled Plasma Mass Spectroscopy

Due to lack of presence of elemental gold in animals, the major advantage of using gold in biological application is to use it as a "tracer" to quantitatively detect the accumulated gold in various organs or tumor by elemental mass spectroscopy [17]. Gold nanoparticle is generally insoluble and rarely present in the biological tissues that it makes easy to detect even at low concentrations using methods such as inductive coupled plasma-mass spectroscopy (ICP-MS). Unlike the "qualitative" approach to detect the presence/absence of the molecule of interest by immunohistochemical staining, ICP-MS allows to directly "quantify" the exact amount of atom/particle of interest at the location of interest. ICP-MS also allows comparing of relative amount of atom/ particle of interest at different organs in a single or multiple subjects.

Dynamic Light Scattering and Zeta Potential

In conjunction with the TEM images, dynamic light scattering (DLS) can be used to characterize the size of the gold nanoparticle. Furthermore, successful ligand exchange process can be verified via dynamic light scattering and zeta potential measurements. As the gold nanoparticle is coated with surface ligands, the hydrodynamic diameter increases with the addition of the surface ligands, seen in the DLS measurements. Similarly, with the addition of surface ligands, the surface charge or the zeta potential of the gold nanoparticle becomes more positive.

Easy Surface Modification

The surface of gold nanoparticle can be easily modified via place exchange reaction to introduce new physical and chemical properties. Surface capping ligand can provide 1) functionality (i.e. targeting ligand for cellular detection, delivery of therapeutic or imaging agent) [56, 97, 107], 2) colloidal stability to prevent aggregation [19], 3) non-fouling surfaces to prevent opsonization by RES (i.e PEGylation) [108], 4) positively, neutrally, or negatively charged hydrophilic monolayer [109-111], or 5) hydrophobic monolayer [112, 113]. Gold surface is usually coated via thiol-gold bond interactions, where chemisorbed thiol onto gold surface has high bond energy of 47kcal/mol, compared to weak 6 kcal/mol of amine-gold bond, for strong covalent bonding [114].

(a) (b)

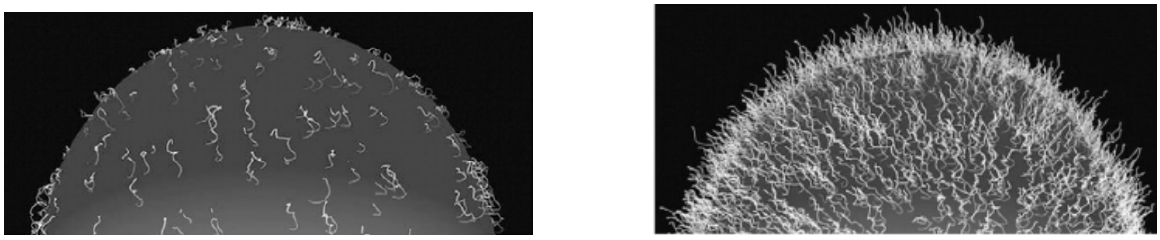

Figure 2.10. Different PEG Configurations on Gold Surface: Low surface coverage of PEG chains lead to mushroom (a) configuration and chains are located closer to the gold surface. A high surface coverage of PEG chain leads to brush (b) configuration that PEG chains are extending away from the surface [115]

The place exchange reaction occurs when clean metal is immersed in a dilute solution of thiols or disulfides to produce well-defined, organized, self-assembled structures at the metal/liquid surface. The place exchange reaction starts with initial rapid

(kinetically driven) adsorption of a monolayer, followed by slower processes which results in the formation of the thermodynamically favored layer [116]. It has been speculated that longer thiolated ligands displaces the shorter thiolated ligands, which are bound onto gold surface [117]. Also, the exchange occurs preferentially at minority sites such as defects on the gold surface that 1) the incoming ligand penetrates less crowded site of the monolayer in order to undergo place-exchange or 2) bound ligands undergo desorption (preferentially at the defect sites), followed by incoming thiol attachment to the newly created surface vacancy [118].

Depending on the concentration of ligands added to the gold colloid solution, various configurations of polymer monolayers can form. The two representative configurations are "mushroom" and "brush" configurations (Figure 2.10). Brush configuration tends to give full surface coverage of the gold surface that result in better colloidal stability in high salt *in vivo* conditions.

Numerous types of ligands with thiolated terminals can be used to for place exchange reaction on a single gold nanoparticle. Thus, the capability to coat gold surface with various ligands has brought gold nanoparticle as a promising "multifunctional" agent for biomedical applications.

Rationale for Using AuNP in this study

Model System for Biomedical Applications in Nanotechnology

There are several reasons why gold nanoparticle is suitable for study of size effect in nanotechnology. First, gold nanoparticles are widely used in biomedical research such as cancer diagnostics, cellular imaging, photothermal therapy, and targeted drug delivery

applications [56, 65-70, 119], which are representative fields of nanotechnology. Second, gold nanoparticle can represent the other hard surface metallic nanoparticles such as quantum dots and iron oxide nanoparticles inside the biological system. Third, unlike the liposomes or polymeric particles, gold nanoparticles can be synthesized with greater size (1-100nm) and shape variabilities (rods, cages, spheres, shells) in a controlled manner. Fourth, due to its unique optical properties, various analytical methods such as UV-vis spectrophotometry, TEM, SERS, darkfield microscopy, fluorescence, ICP-MS, etc. can be used. Polymeric nanoparticles are difficult to trace within the biological system that usually fluorescence tags are applied for detection, whereas gold nanoparticle itself can be used as a tag for detection due to its unique optical property. Fifth, unlike the other metallic nanoparticles such as quantum dots, gold is biocompatible that there is minimal toxicity. Sixth, gold nanoparticle is inert and does not degrade inside the biological system that it can be easily identified with various analytical techniques. Polymeric nanoparticles used for size studies can change its property (via interactions with biological molecules) when applied to the biological system and it can further degrade over time, making it difficult to trace them for size study. Seventh, chemical and physical properties of gold nanoparticle can be easily modified via surface coatings with various ligands that it does not require complicated chemical synthesis steps as seen for polymeric nanoparticles. Finally, the biggest strength of using gold nanoparticle for size effect study is that the amount of gold in the biological system can be easily "quantified", rather than qualitatively referring to the presence and absence of the nanoparticle in various organs, by ICP-MS since it is not a readily available element in the biological systems. Other biocompatible metallic particle such as iron oxide nanoparticle exists, but

this nanoparticle degrades over time and iron (Fe) is prevalent in biological system that can lead to false results for ICP-MS-based size effect studies. Similarly, it is difficult to quantify the different amount of polymer in various organs since polymer nanoparticle or polymer-fluorescence tag nanoparticle can degrade over time and change its property.

Gold Nanoparticle Design In This Study

Figure 2.11 illustrates the general design of the gold nanoparticle system used in this thesis. There are four types of gold nanoparticle systems used in this thesis (in order of appearance): 1) 60nm gold core-drug-PEG system, 2) 5nm gold core-drug-PEG system, 3) 5nm gold core-PEG system, and 4) 60nm gold core-PEG system. For the size effect study for drug delivery applications, pro-drug approach was taken where chemotherapeutic agent (i.e. doxorubicin) was modified with acid-sensitive hydrazone linker. It was designed in a such way that drug will be intact during circulation and will be released in an appropriate condition (pH< 5.5) for efficient delivery of the chemotherapeutic agent. PEG layer was added to give colloidal stability and non-fouling surface for longer circulation time and biocompatibility in the biological system.

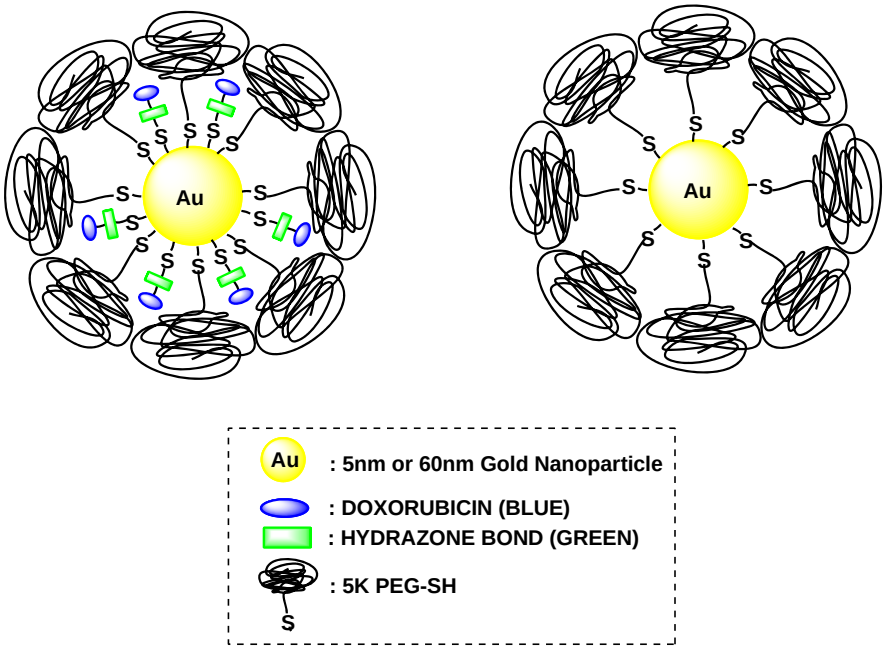

Figure 2.11. Schematic Design of Gold Nanoparticle Used In This Thesis

2.4 CONCLUSION

In conclusion, gold nanoparticle is an ideal candidate for studying the size effect in cancer nanotechnology. Gold nanoparticle represents many research fields in the cancer nanotechnology, and its unique optical properties render multiple analytical methods for characterization. By applying different sizes of gold nanoparticle (5nm versus 60nm) in various studies in this thesis, we can find the ideal size candidate that can be applied universally in many research fields in cancer nanotechnology. Here, we will particularly focus on the drug delivery application of gold nanoparticle and the size effect on therapeutic efficacy, toxicity, biodistribution, and clearance.

CHAPTER 3

SURFACE-ENHANCED RAMAN SCATTERING (SERS)-ACTIVE GOLD NANOPARTICLE

3.1 ABSTRACT

We report development and characterization of multifunctional drug delivery system (Au-dox-PEG) for treatment and SERS spectroscopic detection of tumor. Doxorubicin, a therapeutic agent and a SERS tag, was chemically conjugated to gold nanoparticle via pH-sensitive hydrazone linker then PEG was added to develop Au-dox-PEG. Doxorubicin occupied maximum of 20% of total surface area of gold nanoparticle to result in colloidal stability. SERS spectra were detected for non-aggregated Au-dox-PEG at near-infrared wavelength, and doxorubicin release was time and pH dependent. Consistency in release profile and *in vitro* cell viability results supports the efficacy of Au-dox-PEG system. Thus, the development of Au-dox-PEG multifunctional system raises exciting opportunities for simultaneous spectroscopic detection and therapy for tumors in the future.

3.2 INTRODUCTION

Cancer nanotechnology has gained great interest during recent years [4, 12, 13, 19, 20, 104, 120, 121]. Adopting a size scale equivalent to biological molecules, nanometer-scale particles (1~100 nm in diameter) contain large surface area for modification with targeting ligands, anticancer agents, imaging agents, and other small molecules. Due to its small size, there is an increased uptake of nanoparticles by cells [122], ultimately improving the availability of particular agent. Recently, semiconductor quantum dots [4-7] and iron oxides [9-11] have been used to detect and image tumor cells

for diagnostics, whereas polymer based nanoparticles [12-14] have been used for treatment of cancer. Normally, tumor cells are characterized by leaky vasculature and defective lymphatic drainage that results in enhanced permeability and retention (EPR) effect [35] . EPR effect prolongs nanoparticle residence time and also selectively "traps" nanoparticles for improved efficacy of therapeutic or imaging agents.

Here, we report development and characterization of a multifunctional nanoparticle consist of PEGylated colloidal gold and anticancer agent. The multifunctional delivery system demonstrated therapeutic effect on tumor cells along with *in vitro* spectroscopic detection based on surface enhanced Raman scattering (SERS). The idea of using gold nanoparticle as a carrier for drug delivery is recent [50, 123, 124]. Gold nanoparticles confer several advantages such as biocompatibility [47] and size-tunability (synthesizing various sizes) [125]. Furthermore, chemical properties are easily altered by attaching various ligands for surface modification. Finally, due to its unique optical properties, Raman signal from adsorbed reporter molecules can be increased up to 10^{14}~10^{15} orders in magnitude, allowing single molecular level spectroscopic detection [102-104]. This phenomenon, well known as SERS, is an ultra-sensitive analytical method. SERS provides characterization and spectroscopic detection of reporter molecules and further allows dynamic monitoring of small chemical changes occurring at the interfaces of gold nanoparticles [103, 105].

Recently, Qian, X. *et al*. reported successful *in vivo* tumor detection through SERS obtained from targeted PEGylated gold nanoparticle with raman tag (malachite green isothiocyanate). For our system, raman tag was replaced by doxorubicin, serving a *dual* function of chemotherapeutic agent and SERS reporter molecule. Eliminating the

possibility of adding any other SERS tag, sole presence of doxorubicin increases the loading efficiency of chemotherapeutic agent onto gold surface.

Doxorubicin, an anthracycline derivative, is commonly used chemotherapeutic agent for various malignancies such as solid tumors of breast, esophagus, liver, and soft-tissue sarcoma [126]. Despite its high anti-tumor activity, doxorubicin presents side effects by not only inducing tumor cell death but also affecting normal, healthy cells, especially leading to irreversible cardiotoxicity [127, 128]. Furthermore, doxorubicin exhibits poor water solubility and narrow therapeutic index that it is difficult to significantly increase the dosage at target sites [129]. To overcome these side effects along with addition of SERS spectroscopic detective function, doxorubicin conjugate systems has been developed: doxorubicin was modified with pH-sensitive hydrazone linker and attached to gold nanoparticle. Hydrazone linker, PDPH, was also chosen due to its pH sensitivity. Hydrazone bond is stable under neutral pH conditions, but it is cleaved under mild acidic conditions of less than pH 5 [130], resembling the endosomal and lysosomal environment. Furthermore, hydrazone linker provides thiol bond for adsorption of doxorubicin onto gold nanoparticle surface. To increase biocompatibility and stability of gold colloids, resulting doxorubicin-gold conjugates were coated with PEG. This self-assembled, biocompatible model system was characterized by various techniques and SERS signal was measured. PEGylated drug-gold system was stable in salt solutions (0.5M NaCl solution and 1X phosphate buffered saline) and released doxorubicin in pH and time dependent manner. Also, the resulting drug-gold model system not only demonstrated SERS signal but also had similar cytotoxicity effect on tumor cells compared to equivalent concentrations of free doxorubicin. Thus, this multifunctional system raises exciting opportunities for simultaneous spectroscopic detection and therapy for tumors in the future.

3.3 MATERIALS AND METHODS

Materials

Chemical Reagents

Doxorubicin hydrochloride was purchased from Polymed Science (Houston, TX). Citrate-stabilized gold colloid, 60nm in size, was obtained from Ted Pella, Inc. (Redding, CA). Hydrazone linker, 3-[2-Pyridyldithio]propionyl hydrazide (PDPH), was acquired from Pierce (Rockford, IL). Poly(ethylene glycol) (CH_3O-PEG-SH) of molecular weight 5000 was purchased from Rapp Polymere (Germany). Methanol, acetonitrile, dimethyl sulfoxide, citric acid, and MTT based *in vitro* toxicology assay kit were all obtained from Sigma (St. Louis, MO). Mili-Q deionized water (Millipore, 18.2 MΩ cm^{-1}) was used throughout the experiments. All of the products were used without modification or purification unless as noted.

Instrumentation

Nanoparticle surface charge (zeta potential) and size were measured by ZetaSizer Nano-ZS90 (Malvern Instrument). Adsorption spectra were obtained through ultraviolet-visible spectrophotometer (Beckman Coulter DU530). Fluorescence of nanoparticle was evaluated by Fluoromax-2 (Jobin Yvon-Spex, Horiba Group), equipped with xenon arc lamp. SERS spectra were obtained from HoloLab Series 5000 VPT sytem (Kaiser Optical Systems, Inc.) with the excitation wavelength at 785nm. NMR spectra were obtained from INOVA 600. Finally, scanning multiwell spectrometer, Synergy 2 (Biotek), was used to read absorption of blue formazan crystals for MTT assay.

Cell Line

Tu686 (human head and neck carcinoma cell line) was a gift from Dr. Xiang-Hong Peng (Emory University). Tu686 cells were cultured in DMEM/F-12 (Mediatech, Inc.; Manassas, VA) containing 10% fetal bovine serum (American Type Culture Collection; Manassas, VA) and penicillin-streptomycin solution (Mediatech, Inc.; Manassas, VA). Cells were grown in a 37°C humidified incubator containing 5% CO_2. 1X phosphate buffered saline (1X PBS) was purchased from Mediatech, Inc.

Synthesis of doxorubicin-PDPH

Doxorubicin was conjugated to hydrazone linker, PDPH, in a similar method reported previously by Greenfield, R. *et al.* with slight modifications [130]. Briefly, doxorubicin-HCl (11.340 mg, 0.017 mmol) and excess PDPH (10.340 mg, 0.045 mmol) were dissolved in methanol (7 mL) and stirred at room temperature in the dark for 6 days. Methanol from reaction mixture was evaporated by rotary evaporator and acetonitrile was added to obtain a precipitate. Precipitate was collected through centrifugation and reprecipitated twice with the same procedure indicated above to remove excess PDPH. Final product of 9.450 mg (71 %) was dissolved in dimethyl sulfoxide and stored at 4°C. Obtained ^{1}H NMR spectrum was consistent with the values reported in literature [130].

Maximum Loading of doxorubicin-PDPH onto gold nanoparticle

Maximum loading of doxorubicin-PDPH was governed by colloidal stability and surface area coverage of gold nanoparticle. Initially, total surface area of 60nm gold nanoparticle was calculated (4*pi* radius^2). Then, doxorubicin-PDPH footprint (~1.08

nm^2) was estimated based on chemical structure and known chemical bond lengths. Various concentrations of doxorubicin-PDPH solution (corresponding to 20, 25, and 33% surface coverage; diluted in deionized water) were added drop-by-drop manner into 300uL of stirring gold nanoparticle solution (2.6E10 particles/mL). UV-vis absorption spectra were used to verify the colloidal stability of resulting doxorubicin-PDPH-gold nanoparticle complex.

PEGylation of doxorubicin-PDPH-gold nanoparticle complex

Level of PEGylation for doxorubicin-PDPH-gold nanoparticle complex was determined based on surface area coverage and salt stability of resulting complex. Based on the results from maximum doxorubicin-PDPH loading onto gold surface, available surface area for binding can be calculated. For example, when 20% of gold nanoparticle surface area was covered by doxorubicin-PDPH, then there is 80% surface area available for other molecules to bind onto gold surface. 25, 50, 75, 100, 150, and 175 percent of the *remaining* (80%) gold surface area was coated with 5K CH_3O-PEG-SH. PEG solution (12.1 μM) was added very slowly drop-by-drop into stirring doxorubicin-PDPH-gold nanoparticle complex solution. PEG-doxorubicin-PDPH-gold nanoparticle (Au-DOX-PEG) complex was centrifuged at 2000g for 20 minutes to remove any unbound CH_3O-PEG-SH. Finally, Au-DOX-PEG complex was incubated in 1X PBS and 0.5M sodium chloride solutions to test salt stability. Au-DOX-PEG colloidal stability in salt solutions was determined by absorption spectra from UV-vis spectrometer.

Characterization of Overall doxorubicin-PDPH-PEG Coating

Complete adsorption of doxorubicin-PDPH onto gold nanoparticle

After verifying maximum loading of doxorubicin-PDPH onto gold nanoparticle with UV-vis absorption spectra, fluorescence of resulting complex was measured. The emission wavelength ranges 500-800nm with excitation wavelength at 471nm. Background noise was subtracted from the original spectra to result in doxorubicin signal. Then, for further verification of complete adsorption of doxorubicin-PDPH onto gold nanoparticle, supernatant was collected after centrifugation at 2000g for 20minutes and fluorescence of any unbound doxorubicin was measured. As a control, equal concentration of pure doxorubicin was mixed with equivalent amount of gold nanoparticles. Then, fluorescence of pure doxorubicin-gold nanoparticle and its supernatant was measured as above.

Full coverage of doxorubicin-PDPH-gold nanoparticle with PEG without replacing bound doxorubicin-PDPH

To confirm any replacement of bound doxorubicin-PDPH by addition of CH_3O-PEG-SH, fluorescence of Au-DOX-PEG with various percentages of PEG coating was compared to fluorescence of free doxorubicin-PDPH and doxorubicin-PDPH-gold nanoparticle (Au-DOX) complex. Furthermore, optimum concentration for full coverage of Au-DOX by PEG was determined by zeta-potential and Dynamic Light Scattering (DLS) measurements. Gradually, increasing amount of PEG was added to Au-DOX then zeta-potential and size of the resulting complex were measured at each adding step. Various concentrations of PEG were added to Au-DOX until saturation point was

reached that there was no more changes in numerical values for both zeta-potential and size.

SERS Measurements

SERS spectra were measured on HoloLab Raman microscopy. The excitation wavelength was at 785 nm from a diode laser. Laser power was 20 mW with the focus area of 15 μm in diameter. SERS spectra of pure gold nanoparticle, pure doxorubicin, pure doxorubicin-PDPH, AU-DOX, Au-DOX-PEG, and gold with free doxorubicin were measured. Each sample was placed on a glass slide and laser beam was focused 300 s for each sample. Resulting SERS spectra was corrected by subtracting the background.

pH-dependent drug release test

Au-DOX and Au-DOX-PEG, synthesized from the same batch according to the method listed above, was divided equally in volume for each time point and placed in pH 4 citric acid or pH 7.4 PBS buffer. All release study was carried out at 37°C. At each time point of 24, 48, 72, 96 hr, Au-DOX and Au-DOX-PEG were centrifuged at 2000g for 20 minutes and supernatant was collected. Comparing to concentration (equivalent to 100% doxorubicin release) of pure doxorubicin-PDPH in each buffer, concentration of released doxorubicin (from collected supernatant) was quantified against pure doxorubicin-PDPH fluorescence spectra.

In vitro drug delivery study

Tu686 cells were cultured on four different 96 well plates designated for 24, 48, 72, and 96 hour time points. For each time point, triplicates of Au-DOX-PEG (0.3 μg

DOX/ mL and 0.2nM of gold nanoparticle), pure doxorubicin (0.3 μg DOX/ mL), and Au-PEG (0.2 nM), synthesized from the same batch, were added to cells and incubated at 37°C accordingly with time. At each designated time point, MTT assay kit (Sigma) was used to measure cell viability. MTT assay measures the cellular reduction of MTT by the mitochondrial dehydrogenase of viable cells to form blue formazan crystals as product. These crystals can be measured spectrophotometrically by obtaining absorbance with a scanning multiwell spectrophotometer. Detailed procedure was followed from information sheet provided by Sigma. Briefly, MTT powder was reconstituted with 1X PBS and added to 10% of culture medium volume. 150uL of reconstituted MTT solution was added to each well and continued to culture for 2 hours in the incubator. After incubation, 150uL of MTT solubilization solution was added to the original culture to dissolve crystals. Dissolved blue formazan crystals were detected at a wavelength of 570nm, and background absorbance of 96 well plates at 690nm was subtracted from the original 570nm readings.

3.4 RESULTS AND DISCUSSION

Characterization of doxorubicin-gold nanoparticle system

Doxorubicin-PDPH conjugate (dox-PDPH) was synthesized in methanol (Figure 3.1(a)). PDPH acts as a linker and introduces thiol functional group to ensure adsorption of doxorubicin onto gold surface. Doxorubicin itself contains an amine group, but it has been reported that bonds between gold and sulfur group (~50 kcal/mol) [131-133] is much stronger than bonds between gold and amine group (3-6 kcal/mol) [133]. PDPH linker also contains acid-sensitive hydrazone bond that chemically bound doxorubicin is released under slightly acidic conditions of pH ~ 5 [130, 134], which resembles

intracellular endosomal and lysosomal pH conditions. The doxorubicin-PDPH conjugate was water-soluble and was stable when stored at 4°C in dimethyl sulfoxide.

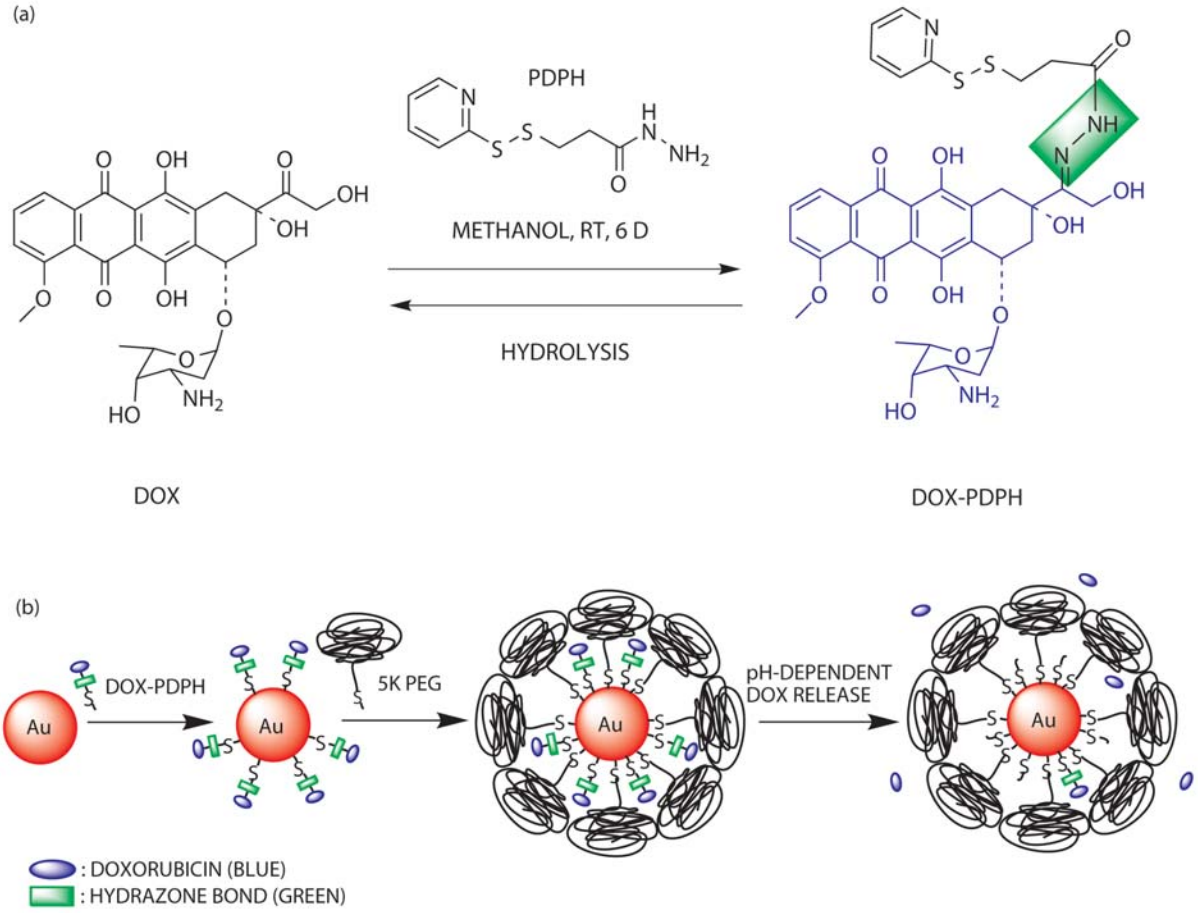

Figure 3.1. Chemical Synthesis and Self Assembly of Gold Nanoparticle System (a) Chemical synthesis of doxorubicin-hydrazone linker conjugate (DOX-PDPH); (b) Schematic illustration for synthesis of multifunctional drug delivery system and its pH-dependent doxorubicin release

Concentrations of dox-PDPH and gold nanoparticle were quantified by UV-vis spectroscopy. For dox-PDPH, standard curve at 495nm was created. The 60nm gold nanoparticle had the maximum absorption peak at 531nm and Beer-Lambert law was

used to calculate the concentration of gold nanoparticles (extinction coefficient of 3.531 x 10^{10} M^{-1} cm^{-1}). The UV-vis spectra of dox-PDPH-gold nanoparticle resembled the spectra of pure gold nanoparticle that fluorescence spectra was used to further assist in analysis.

Adsorption of dox-PDPH onto gold nanoparticle was studied via UV-vis and fluorescence spectra. Similar to the method used by Cheng, Y. *et al*., considering planar geometry for dox-PDPH on gold surface and inherent chemical bond lengths of the system, it was found that single dox-PDPH molecule has a theoretical footprint of ~1.08nm^2. Thus, a single 60nm gold nanoparticle can hold 10513 dox-PDPH molecules for complete surface coverage. However, experimental findings indicate that a single 60nm gold nanoparticle holds maximum of ~2147 dox-PDPH molecules and be colloidally stable. This is equivalent to coating 20% of available surface area (~0.1 wt-%) for 60nm gold nanoparticle. It was found that increasing the surface area coverage to 25% and furthermore to 33% resulted in aggregation of gold nanoparticles, as indicated by slight bump in red-wavelength region of UV-vis spectra (Figure 3.2(a)). Thus, there is a concentration dependence of doxorubicin coating that dox-PDPH can occupy maximum 20% of total surface area of 60nm gold nanoparticle. The resulting dox-PDPH-gold nanoparticle system (Au-DOX) was soluble in water and was stable without any aggregation.

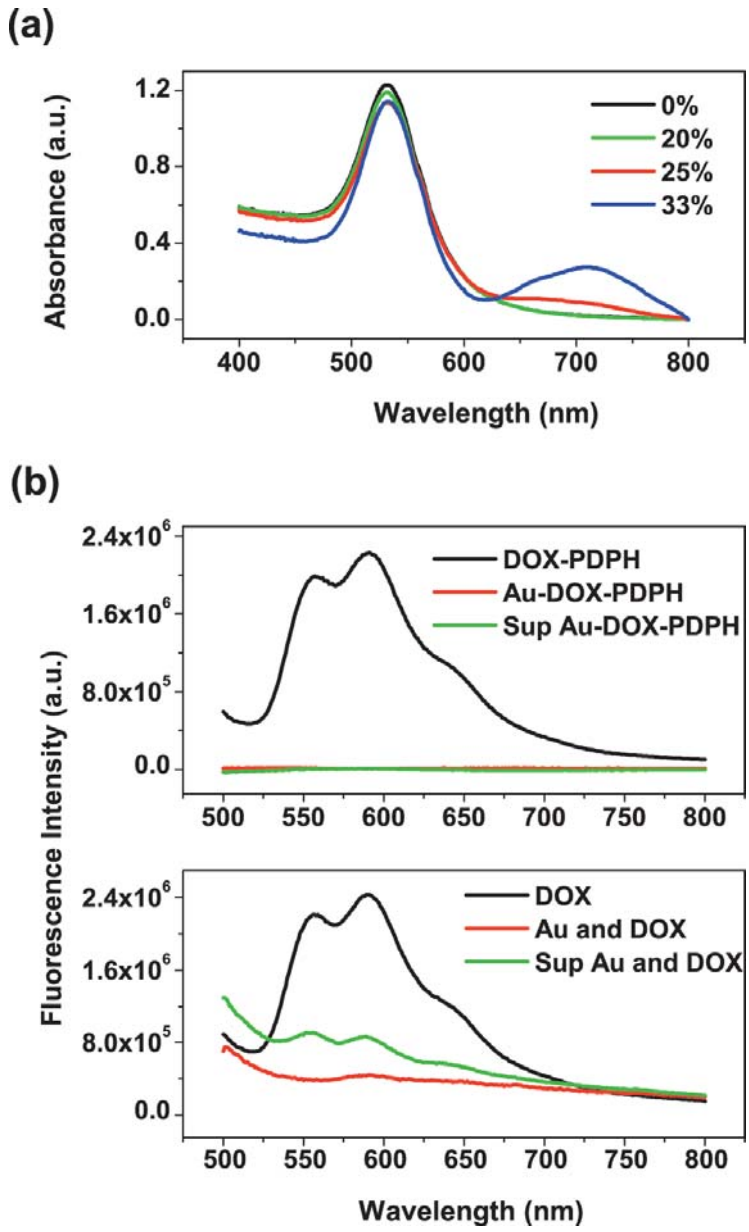

Figure 3.2. Characterization of Dox-PDPH Loading (a) UV-vis spectra indicate that maximum of 20% of gold surface can be coated with dox-PDPH for colloidal stability; (b) Fluorescence spectra indicate quenching of dox-PDPH on gold surface compared to partial quenching of pure doxorubicin with gold nanoparticles

Fluorescence spectra were used to further verify adsorption of dox-PDPH onto gold. When dox-PDPH was conjugated to gold nanoparticles in water, it was quenched on gold surface (Figure 3.2(b)). Previous studies also report quenching of fluorescent dyes on metallic particles when they are chemisorbed onto the surface [135-137].

Furthermore, fluorescence quenching on metallic surface is observed for distance of few nanometers [138, 139], which suggests proximity of doxorubicin onto gold surface linked via short PDPH linker.

When Au-dox was centrifuged, the supernatant did not contain any free doxorubicin (Figure 3.2(b)). In contrast, when equal concentrations of pure doxorubicin was added to the same amount of gold nanoparticles in water, fluorescence spectra (Figure 3.2(b)) indicate that doxorubicin was partially quenched and free doxorubicin was detected in the supernatant. Thus, this indicates that dox-PDPH is completely bound onto gold surface. A measurable change in fluorescence intensity resulted from dynamic displacement of adsorbed citrate on gold nanoparticle by dox-PDPH. We believe that dox-PDPH has formed a covalent bond, or chemisorbed, with gold surface via thiols from PDPH linker, whereas pure doxorubicin was loosely bound onto gold surface through weak electrostatic interactions, or physisorbed, between positively-charged amine group of doxorubicin and negatively-charged gold nanoparticle [140].

Characterization of PEGylated doxorubicin-PDPH-gold nanoparticle system

PEG is commonly used in biomedical applications to increase solubility in water and enhance biocompatibility of nanoparticles. PEG provides colloidal stability for Au-dox system that PEG protects gold nanoparticles from physiological conditions and prevents aggregation [141, 142]. PEG also serves as a protective barrier for bound dox-PDPH on gold surface. Furthermore, PEG reduces adsorption of cellular proteins and increases the circulation time of nanoparticles [143].

To find the optimum PEG density for colloidal gold stability, DLS and zeta potential measurements were used. After subtracting the gold surface area (20%) occupied by dox-PDPH, the free, available surface area was coated with various concentrations of PEG. As we increased the PEG concentration, saturation point was reached for both DLS and zeta potential measurements (Table 3.1).

Table 3.1. Change in Surface Charge (ζ-potential) and Size of Au-dox as More PEG is Added to Result in Au-dox-PEG System

% PEG[†]	*ζ-potential (mV)*	**Size (nm)**
0	-36.5 ± 4.4	61.0 ± 3.9
50	-27.4 ± 0.6	71.5 ± 0.8
100	-15.3 ± 4.8	75.0 ± 0.8
150	-15.0 ± 1.1	75.2 ± 1.2
175	-14.9 ± 1.4	75.8 ± 0.3

[†]Indicates the amount of excess PEG added to free, available surface area on gold surface after adsorbing dox-PDPH

For DLS measurements, Au-dox-PEG kept increasing in size until it reached ~75nm. As more PEG is added to Au-dox, PEG initially binds in a mushroom conformation then changes its conformation to brush mode for full coverage [144, 145]. Mushroom mode is characterized by low surface grafting density and polymer tends to "lie" close to the surface that multiple points of a single polymer is covering the surface. On the other hand, brush conformation is characterized by high surface grafting density and polymer tends to "stand up" that polymer is attached by a single point on the surface. Thus, as the conformation changes from mushroom to brush modes, nanoparticle size will increase and the size will stop increasing until all the anchoring sites on the gold

surface are saturated. For zeta potential measurements, Au-dox-PEG became more positive in charge as more PEG was added to the system. PEG has neutral charge and gold nanoparticle has negative charge. As more PEG is added to Au-dox, negative charge of gold nanoparticle is shielded and offset by more neutral charge of PEG. Both DLS and zeta potential measurements agreed in saturation PEG value to be between 100% and 150% coverage of the free, available surface area. This saturation PEG value resulted in PEG footprint of ~ 0.35 nm^2, which is consistent with the literature footprint value [146]. Thus, this also supports our dox-PDPH footprint to be a good approximation on 60nm gold nanoparticle. Centrifuging Au-dox-PEG did not affect the values for DLS and zeta potential. Findings in DLS and zeta potential measurements were supported with salt stability test that fully PEGylated Au-dox-PEG was stable in 1X PBS and 0.5M NaCl solution (data not shown).

Besides Au-dox-PEG colloidal stability, we wanted to ensure that bound dox-PDPH is not affected by addition of PEG. After conjugating dox-PDPH onto gold, various concentrations of PEG were added to Au-dox then fluorescence measurements were taken. Fluorescence spectra (Figure 3.3) indicate that addition of PEG, especially excess amount of PEG, did not affect bound dox-PDPH and there was no detectable replacement of bound dox-PDPH. Au-dox-PEG fluorescence spectra overlapped with Au-dox fluorescence spectrum.

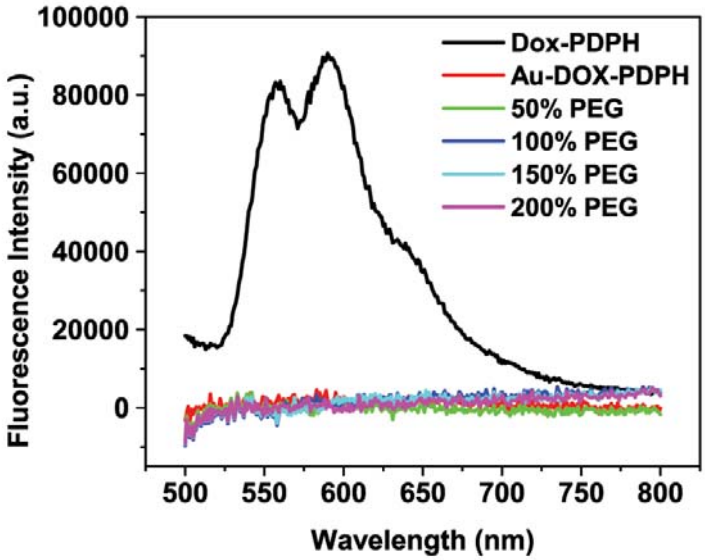

Figure 3.3. Fluorescence Spectra of Au-dox-PEG with Various Concentrations of PEG Indicate No Detectable Replacement of Bound Doxorubicin-PDPH on Gold Surface Compared to Au-dox and Pure Dox-PDPH

If there was replacement of bound dox-PDPH, there should be an increase in fluorescence intensity due to presence of free doxorubicin in Au-dox-PEG solution. As seen in Figure 3.2(b), when free doxorubicin is present in the mixture of gold nanoparticle, fluorescence of free doxorubicin is not completely quenched by the gold. Thus, increase in concentration of free doxorubicin in solution will result in increase in overall fluorescence intensity.

Surface Enhanced Raman Scattering (SERS) and Doxorubicin

When 20% of gold surface was covered by dox-PDPH, SERS signal was present in both Au-dox and Au-dox-PEG (Figure 4.4). 60nm gold nanoparticle is an appropriate size for SERS at near-infrared excitation as previous research reports 60-80nm in diameter gold nanaoparticles exhibit most efficient SERS at red (630-650nm) and near

infrared (785nm) excitations [147]. Doxorubicin SERS spectrum was characterized by major peaks at 1242, 1261, 1438, and 1603 cm^{-1} for Au-DOX-PEG system, where the Raman shift (cm^{-1}) values were consistent to those in previous studies [148, 149]. However, when equivalent concentration of free doxorubicin was added to gold nanoparticles, no SERS signal was present. Thus, in contrast to physisorbed free doxorubicin, only covalently tethered dox-PDPH induces SERS for *non-aggregated* gold nanoparticles. SERS is also distance dependent that SERS is only present when SERS tag is placed within few nanometer of metallic surface [150, 151]. For Au-dox, doxorubicin is conjugated to PDPH linker (< 1nm) to gold surface, which is well within the specification to induce SERS.

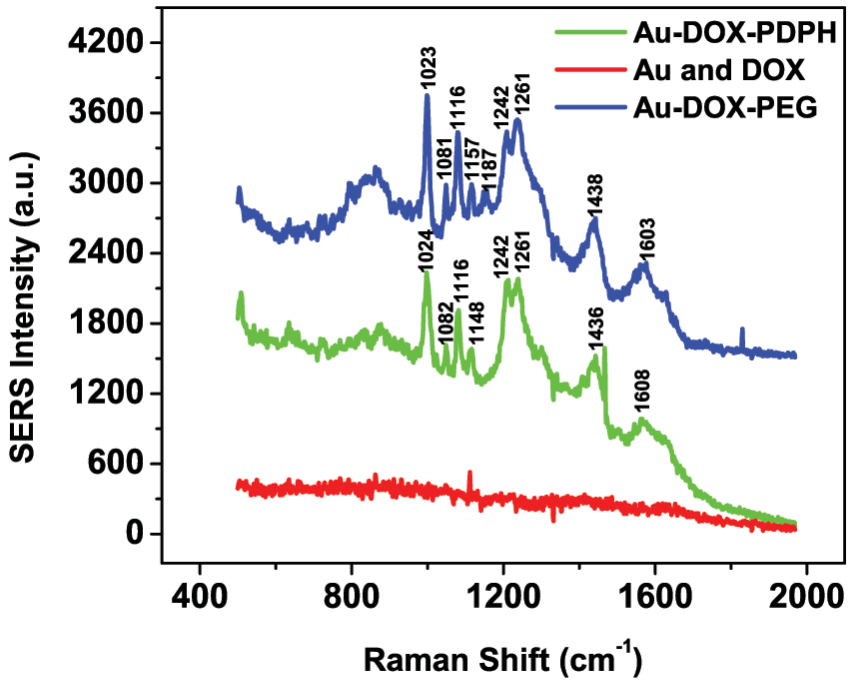

Figure 3.4. Surface Enhanced Raman Scattering (SERS) Spectra of Doxorubicin-PDPH on Non-Aggregated Gold Nanoparticle (Au-DOX and Au-DOX-PEG) Compared to SERS for Pure Doxorubicin and Gold Nanoparticle Mixture (spectra are shifted on purpose for better visualization).

It is important to note that doxorubicin SERS spectrum (Figure 3.4) resulted from colloidally stable *singlets* of Au-dox and Au-dox-PEG. Furthermore, doxorubicin was covalently bound to gold surface via an acid-sensitive linker, thus resulting in fluorescence quench. Previous research demonstrated SERS spectrum for mixture of free, unmodified doxorubicin and aggregated metallic sols or films. [148, 152-154] Metallic sols were aggregated by salts or DNA complexation and metallic surface was modified to trap doxorubicin to induce SERS.

The ability to induce SERS for Au-dox-PEG provides several advantages. First, doxorubicin itself can serve as SERS tag for spectroscopic detection of tumor. SERS utilizes the intrinsic SERS of the bound molecule, mostly with delocalized pi electrons, onto metallic particle and it does not require any labeling [105]. Au-dox-PEG SERS spectrum was measured with 785nm laser, allowing near-infrared (NIR) window detection of SERS tag for reduced *in vivo* background noise [155]. Combining the enhanced permeability and retention (EPR) effect of tumor cells and NIR window detection, Au-dox-PEG provides the potential to spectroscopically locate tumor cells. Second, in conjunction with UV-vis and fluorescence spectra, SERS spectra of Au-dox-PEG provides additional piece of evidence to support chemisorption of dox-PDPH onto gold surface. Third, SERS spectra of Au-dox-PEG can be used for real-time monitoring of doxorubicin release. As shown in Figure 3.4, non-covalently bound free doxorubicin does not induce SERS. This indicates that when hydrazone bond from PDPH is cleaved to release doxorubicin to the surroundings, there will be decrease in SERS intensity over time.

pH dependent release study of doxorubicin

Figure 3.5 shows pH-dependent release profile of doxorubicin linked to hydrazone bond of PDPH. For Au-dox, ~80% and ~20% of bound doxorubicin were released at pH 4 and pH 7.4 in 24 hours, respectively. More doxorubicin was released over time, especially for pH 4 condition, which led to four times more doxorubicin release at the end of 96 hours for pH 4 condition compared to that of neutral condition. Previous studies also reported increased hydrolysis of hydrazone bond and rapid release of doxorubicin in acidic conditions compared to neutral conditions [130, 156].

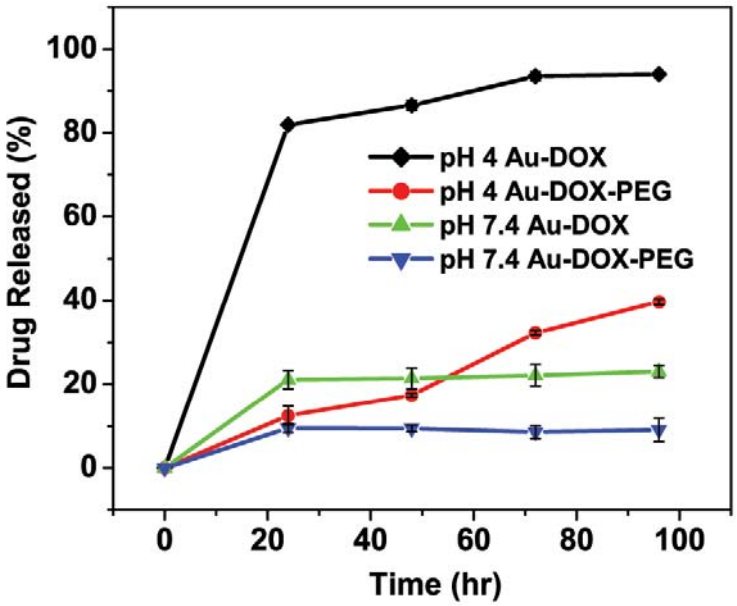

Figure 3.5. pH-Dependent Doxorubicin Release Over Time

Au-dox-PEG system also demonstrated pH-triggered release of doxorubicin, but there was a delayed release kinetics compared to Au-dox. Release profile for pH 4 and pH 7.4 conditions were similar up to 24 hrs; however, at 48 hr, there was a difference in

release profile that ~17% and ~9% of bound doxorubicin were released at pH 4 and pH 7.4, respectively. At the end of 96 hr, approximately four times more doxorubicin was released at acidic pH compared to neutral pH for Au-dox-PEG. There are two possible reasons for the delayed release of doxorubicin: (1) is due to diffusion barrier created by PEG coating and (2) is due to interactions between the polymer and the drug. PEG chains interact with one another that complex is formed amongst PEG chains by hydrogen bonding [157]. As polymer chain length increases and more inter-polymer complexes are formed, the release rate of the drug is decreased. Also, complexation affects PEG conformation that polymer coils provide additional diffusion barrier for more tortuous path for drug release [157, 158]. Because PEG is a hydrophilic polymer, as the hydrophobicity of the drug increases, the diffusion rate of the drug decreases.

There are several reasons why hydrolysis of hydrazone bond under acidic condition was responsible for doxorubicin release. First, dox-PDPH was completely bound onto gold surface (Figure 3.2(b) and Figure3. 3) unlike pure doxorubicin mixed with gold nanoparticles. In order to observe fluorescence in the supernatant, quenched doxorubicin on gold surface must be cleaved away from the gold surface. Bound doxorubicin could be released via cleavage of hydrazone bond or Au-S bond of PDPH linker. However, latter is highly unlikely due to strong Au-S bond energy [131-133]. Second, there was a high pH-dependent drug release that doxorubicin was released at a faster rate (four fold increase) in pH 4 buffer than in pH 7.4 buffer. Although increased aqueous solubility of doxorubicin in acidic pH may contribute to doxorubicin release, change in pH from neutral to acidic for a pH-insensitive system (micelle containing only pure doxorubicin) did not significantly increase the release rate of the drug [159-161].

Thus, hydrolysis of hydrazone bond is responsible for release of doxorubicin into surroundings.

The pH-dependent Au-dox-PEG is an optimal system for minimizing the drug release during circulation and maximizing the drug release under mildly acidic conditions of endosomal or lysosomal vesicles.

In vitro drug delivery study

MTT assay with Tu686 cell line was used to study the anticancer efficacy of Au-dox-PEG system. Cell viability was inversely related to doxorubicin activity that absence or minimal efficacy of doxorubicin resulted in increased cell survival. Cell viability for each group (pure doxorubicin, Au-PEG, and Au-dox-PEG) was compared to the control group which was free of doxorubicin. Initially, pure doxorubicin had higher anticancer efficacy compared to Au-dox-PEG. Figure 6 shows that pure doxorubicin had an immediate effect during 24 hour period where ~74% of cells were alive compared to the control. There was a gradual cell viability decrease for pure doxorubicin treated cells that about 21 % of cells survived at the end of 96 hour period.

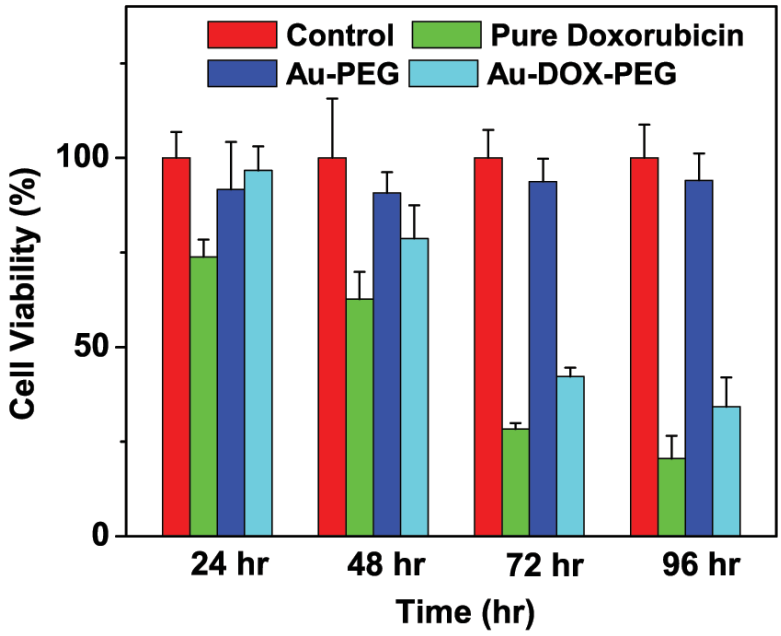

Figure 3.6. *In vitro* Drug Release Study on TU 686 Cells via MTT Assay [0.3 μg DOX/ mL]

According to Figure 3.6, Au-dox-PEG had minimal efficacy until 48 hour that approximately 80% of cells survived. Beyond 48 hours, there was a significant decrease in cell viability for Au-dox-PEG treated cells. Interestingly, *In vitro* cell viability results were consistent with the data obtained from the release profile (Figure 3.5), indicating 48 hour is a critical time point for doxorubicin release from Au-dox-PEG. This time delay is advantageous to elongate *in vivo* circulation time of drug delivery system in the future. Furthermore, compared to the control, cell rounding and decrease in cell density were apparent under the microscope (data not shown) at 48 hour time point. At the end of 96 hour period, ~34% cells survived with Au-dox-PEG treatment.

Compared to the pure doxorubicin 96 hour toxicity (~21% cell viability), the slight lower toxicity of Au-dox-PEG could have resulted from slow release of

doxorubicin within PEG shell and different cellular localization of Au-dox-PEG system compared to pure drug. However, Au-dox-PEG provides potential to significantly increase the accumulation and dosage at target sites by EPR effect and eventually increase the anticancer efficacy compared to pure drug.

To eliminate any uncertainty stemming from gold nanoparticle toxicity itself, we used PEGylated gold nanoparticle (Au-PEG), free of doxorubicin, as another control. When equivalent gold concentration for Au-PEG was used to treat cells, Au-PEG had minimal toxicity on Tu686 cells and had average of 93% cell viability throughout the 96 hour incubation period.

Overall, Au-dox-PEG is an effective drug delivery system. Even though Au-dox-PEG has slower release rate of doxorubicin, gold nanoparticle successfully delivered doxorubicin to cells to release it under acidic conditions. Au-dox-PEG's anticancer efficacy caught up with that of pure doxorubicin after 48 hours and we observed sustained release of doxorubicin over time.

3.5 CONCLUSION

Here, we have shown the feasibility of developing and characterizing a pH-sensitive multifunctional drug-gold delivery system for treatment and SERS spectroscopic detection of tumor. Multifunctional delivery system, comprising of poly(ethylene glycol), doxorubicin, pH-sensitive linker, and gold nanoparticle (Au-dox-PEG), successfully delivered anticancer agent to tumor cells and displayed surface enhanced raman scattering (SERS) for spectroscopic detection. Doxorubicin, modified with pH-sensitive hydrazone linker and attached to gold nanoparticle, served as therapeutic agent *and* spectroscopic detection agent. There was a concentration dependence of doxorubicin binding to the gold surface that doxorubicin can occupy

maximum 20% of total surface area of gold nanoparticle. SERS spectra were detected for non-aggregated Au-dox-PEG at near-infrared wavelength. Also, Au-dox-PEG displayed pH and time dependent release of doxorubicin. Decrease in pH to acidic condition resulted in increased release of doxorubicin compared to neutral condition. It took approximately 48 hours to see significant anticancer efficacy of Au-dox-PEG. Consistency in release profile and *in vitro* cell viability results supports the therapeutic efficacy of Au-dox-PEG. Anticancer efficacy of Au-dox-PEG caught up with that of pure doxorubicin after 48 hours that we observed controlled release of doxorubicin over time. Thus, the development of Au-dox-PEG multifunctional nanoparticle raises exciting opportunities for simultaneous spectroscopic detection and therapy of tumors in the future.

CHAPTER 4

DRUG DELIVERY APPLICATION OF SMALL-SIZED GOLD NANOPARTICLE

4.1 ABSTRACT

Our results demonstrated that functionalized 5nm gold nanoparticle-based drug delivery system represents a highly attractive candidate as a potential drug delivery carrier for cancer nanotherapy. Our smart design of combining prodrug approach (drug-hydrazone linker) with PEGylation renders controlled release of anticancer agent and colloidal stability characteristics to the system, thus making gold nanoparticle-anticancer agent-PEG (Au-DOX-PEG) system a promising drug delivery platform for *in vivo* applications. Due to its size, Au-DOX-PEG accumulated at a high concentration at the tumor site via enhanced permeability and retention (EPR) effect and displayed therapeutic efficacy against tumor. In contrast to pure doxorubicin which resulted in heart, kidney, and lung toxicities, passively targeted Au-DOX-PEG system did not display any apparent toxicity in vital organs.

4.2 INTRODUCTION

The ultimate goal of drug delivery is 1) to increase the bioavailability of the drug and 2) to reduce the toxicity to healthy cells. Nanoscopic systems, such as gold nanoparticles, can alter the pharmacological and therapeutic properties of the drugs being incorporated and overcome any intrinsic toxicity or poor bioavailability of the drug.

Normally, tumor cells are characterized by leaky vasculature and defective lymphatic drainage that results in enhanced permeability and retention (EPR) effect [35].

EPR effect prolongs nanoparticle residence time and also selectively "traps" nanoparticles for improved efficacy of therapeutic agents. By taking advantage of these size and EPR effect, one can increase the efficacy of drug at the tumor site.

The idea of using gold nanoparticle as a carrier for drug delivery is recent [50, 123, 124, 143]. Previously, gold nanoparticles have been mainly used for chemical sensing, photothermal therapy, and diagnostic purposes[34]. Gold nanoparticle makes an ideal candidate as a drug delivery platform for cancer therapy due to its several attractive physical and chemical properties. Gold nanoparticles are inert and have low *in vivo* toxicity compared to the other metallic materials [93, 94]. Gold nanoparticles are easily synthesized with various shapes and sizes that it confers size and shape-tunability [89]. Furthermore, chemical properties are easily altered by attaching various ligands via covalent thiol-gold bond interactions for surface modification. Also, gold nanoparticle is generally insoluble and rarely present in the biological tissues that it makes easy to detect even at low concentrations using methods such as ICP-MS [17]. Finally, its unique optical property allows spectroscopic detection (SERS) [102-104] and microscopic visualization (transmission electron and darkfield microscopy) [97, 162].

Currently, only a few gold nanoparticle-based anticancer drug delivery systems have been studied, compared to the polymer-based delivery systems [124, 143, 163-165]. Few cases are reported for delivery of small molecule therapeutic agents by gold nanoparticles for cancer therapy, which relies on passive (EPR effect) and active targeting [50, 78, 166]. For example, 13nm gold nanoparticle was coated with methotrexate (MTX) for treatment of lung cancer [166]. Similarly, 26nm gold nanoparticle was coated with TNFα, thiolated poly (ethylene glycol), and paclitaxel and

resulted in 10-fold more delivery of TNFα and paclitaxel to the tumor site for effective treatment [143]. When anticancer agent gemcitabine was conjugated to gold nanoparticle with VEGF antiangiogenic molecule, it also showed therapeutic efficacy [164]. Finally, 30nm gold nanoparticle coated with PEG, arginine-glycine-aspartic acid (RGD) peptide, and nuclear localization signal peptide resulted in nuclear-targeting gold nanoparticles that causes apoptosis of cancer cells [167].

To this date, most of the gold nanoparticle-based drug delivery system utilizes gold nanoparticles that are larger than 10nm, with an exception of recent study on 2nm gold nanoparticle loaded with paclitaxel [124]. However, this 2nm gold nanoparticle-paclitaxel system study only focuses on characterization and loading efficiency, omitting any biological effects of the system. Moreover, it has been reported that gold nanoparticles of 1-2nm are highly toxic to both healthy and cancerous cells [45, 46].

This work is *significant* by providing an insight on a potential ideal candidate for gold nanoparticle-based drug delivery system that uses small (5nm) gold nanoparticle to study therapeutic efficacy on solid tumor. To our knowledge, we are the first team to investigate in detail for 5nm gold nanoparticle drug delivery system *in vivo* and its behavior for better understanding of the gold nanoparticle-based drug delivery. To date, most of the gold nanoparticle-based drug delivery systems have been focusing on a size scale of 20~35nm. 5nm gold nanoparticle is an ideal size scale that renders the following characteristics that is attractive for usage in gold nanoparticle-based drug delivery: (1) it has been reported that gold nanoparticle with a size of 4nm~18nm were taken up by human cells without any cytotoxicity [93], (2) particles that are smaller than 5.5nm can be cleared out from the body through rapid and efficient renal filtration and urinary

excretion [64], (3) 5nm particles are big enough to be visualized under various microscopy methods and allow application of various characterization techniques such as UV-vis spectroscopy, SERS, dynamic light scattering, etc., (4) it confers higher drug loading efficiency than larger particles, (4) it is small enough for extravasation from the blood vessel to be delivered to the target site [37], (5) it fits the size range that is effective for EPR effect for tumor passive targeting [24], and (6) the ease of surface modification such as PEG allows prolonged circulation time of the particle and delays the RES uptake of the system.

Here, the application of small-sized 5nm gold nanoparticle as a drug delivery system (Au-DOX-PEG) demonstrated 1) successful accumulation of Au-DOX-PEG at the tumor site via passive targeting by taking advantage of the EPR effect for therapeutic efficacy and 2) resulted in no apparent toxicity to vital organs.

4.3 MATERIALS AND METHODS

Materials

Chemical Reagents

Doxorubicin hydrochloride was purchased from Polymed Science (Houston, TX). Citrate-stabilized gold colloid, 5 nm in size, was obtained from Ted Pella, Inc. (Redding, CA). Hydrazone linker, 3-[2-Pyridyldithio]propionyl hydrazide (PDPH), was acquired from Pierce (Rockford, IL). Poly(ethylene glycol) (CH_3O-PEG-SH) of molecular weight 5000 was purchased from Rapp Polymere (Germany). Methanol, acetonitrile, dimethyl sulfoxide, citric acid, and MTT based *in vitro* toxicology assay kit were all obtained from Sigma (St. Louis, MO). Mili-Q deionized water (Millipore, 18.2 MΩ cm^{-1}) was used

throughout the experiments. All of the products were used without modification or purification unless as noted.

Instrumentation

Nanoparticle surface charge (zeta potential) and size were measured by ZetaSizer Nano-ZS90 (Malvern Instrument). Adsorption spectra were obtained through ultraviolet-visible spectrophotometer (Beckman Coulter DU530). Fluorescence of nanoparticle was evaluated by Fluoromax-2 (Jobin Yvon-Spex, Horiba Group), equipped with xenon arc lamp. Scanning multiwell spectrometer, Synergy 2 (Biotek), was used to read absorption of blue formazan crystals for MTT assay. Gold content was analyzed by ICP-MS (HP 4500, Agilent Technologies). TEM were taken by using Hitachi H7500 high-magnification electron microscope. Finally, Olympus IX71 inverted microscope was used to take brightfield and darkfield images.

Cell Line and Mouse Model

Murine breast cancer cell line 4T1 was a gift from Dr. Lily Yang (Emory University). 4T1 cells were cultured in RPMI-1640 (Mediatech, Inc.; Manassas, VA) containing 10% fetal bovine serum (American Type Culture Collection; Manassas, VA) and penicillin-streptomycin solution (Mediatech, Inc.; Manassas, VA). Cells were grown in a 37°C humidified incubator containing 5% CO_2. 1X phosphate buffered saline (1X PBS) was purchased from Mediatech, Inc. 6-7 week old female Balb/C mice were obtained from commercial vendor (Jackson Laboratories). The protocols were approved by the Institutional Animal Care and Use Committee (IACUC) of Emory University.

Statistical Analysis

Statistical analysis was performed using one-way ANOVA followed by multiple comparison Bonferroni's test. Data were collected from at least three different animals and $P<0.05$ was considered statistically significant.

Synthesis of doxorubicin-PDPH

Doxorubicin was conjugated to hydrazone linker, PDPH, in a similar method reported previously by Greenfield, R. *et al.* with slight modifications [130]. Briefly, doxorubicin-HCl (11.340 mg, 0.017 mmol) and excess PDPH (10.340 mg, 0.045 mmol) were dissolved in methanol (7 mL) and stirred at room temperature in the dark for 6 days. Methanol from reaction mixture was evaporated by rotary evaporator and acetonitrile was added to obtain a precipitate. Precipitate was collected through centrifugation and reprecipitated twice with the same procedure indicated above to remove excess PDPH. Final product of 9.450 mg (71 %) was dissolved in dimethyl sulfoxide and stored at 4°C. Obtained ^{1}H NMR spectrum was consistent with the values reported in literature [130].

Drug Loading Efficiency

Adsorption of DOX-PDPH onto gold nanoparticle was studied via UV-vis and fluorescence spectra. Concentrations of DOX-PDPH and gold nanoparticle were quantified by UV-vis spectroscopy. For DOX-PDPH, standard curve at 495nm was created. The 5nm gold nanoparticle had the maximum absorption peak at 514 nm and Beer-Lambert law was used to calculate the concentration of gold nanoparticles (extinction coefficient of 9.696×10^{6} M^{-1} cm^{-1}). Similar to the method used by Cheng, Y.

et al., considering planar geometry for DOX-PDPH on gold surface and inherent chemical bond lengths of the system, it was found that single DOX-PDPH molecule has a theoretical footprint of ~1.08nm^2. When surface coverage per 5nm gold nanoparticle was increased from 25, 100, 150, and 200 %, the corresponding loaded doxorubicin weight percents (wt-%) were 1.42, 5.58, 8.35, 11.12 wt-%, respectively. UV-vis absorption spectra and fluorescence were used to verify the colloidal stability of resulting doxorubicin-PDPH-gold nanoparticle complex.

PEGylation of Gold Nanoparticle-Anticancer Agent System

To find the optimum PEG density for colloidal gold stability, dynamic light scattering measurement was used for size change. After subtracting the gold surface area occupied by modified doxirubicin, available surface area was coated with various concentrations of PEG. As we increased the PEG concentration, saturation point was reached for gold-drug-PEG size measurement (Table 1). PEG-doxorubicin-PDPH-gold nanoparticle (Au-DOX-PEG) complex was ultra-centrifuged at 100,000g for 1 hour to remove any unbound CH_3O-PEG-SH. Then the resulting gold system was freezed-dried to a powder form. Finally, Au-DOX-PEG complex was incubated in 1X PBS and 0.5M sodium chloride solutions to test salt stability. Au-DOX-PEG colloidal stability in salt solutions was determined by absorption spectra from UV-vis spectrometer.

pH-dependent drug release test

Colloidal gold system, Au-DOX-PEG, synthesized from the same batch according to the method listed above, was divided equally in volume for each time point and placed

in pH 5 citric acid or pH 7.4 PBS buffer. All release study was carried out at 37°C. At each time point of 24, 48, 72, 96 hr, Au-DOX-PEG were ultra-centrifuged at 100,000g for 1 hour and supernatant was collected. Comparing to concentration (equivalent to 100% doxorubicin release) of pure doxorubicin-PDPH in each buffer, concentration of released doxorubicin (from collected supernatant) was quantified against pure doxorubicin-PDPH fluorescence spectra.

***In vitro* cytotoxicity study**

4T1 cells were cultured on four different 96 well plates designated for 24, 48, 72, and 96 hour time points. For each time point, triplicates of Au-DOX-PEG (7 μg DOX/ mL equivalent), pure doxorubicin (7μg DOX/ mL), and Au-PEG, synthesized from the same batch, were added to cells and incubated at 37°C accordingly with time. At each designated time point, MTT assay kit (Sigma) was used to measure cell viability. MTT assay measures the cellular reduction of MTT by the mitochondrial dehydrogenase of viable cells to form blue formazan crystals as product. These crystals can be measured spectrophotometrically by obtaining absorbance with a scanning multiwell spectrophotometer. Detailed procedure was followed from information sheet provided by Sigma. Briefly, MTT powder was reconstituted with 1X PBS and added to 10% of culture medium volume. 150μL of reconstituted MTT solution was added to each well and continued to culture for 2 hours in the incubator. After incubation, 150uL of MTT solubilization solution was added to the original culture to dissolve crystals. Dissolved blue formazan crystals were detected at a wavelength of 570nm, and background absorbance of 96 well plates at 690nm was subtracted from the original 570nm readings.

Cellular Uptake of Colloidal Gold Study

4T1 cellular uptake of doxorubicin, gold-drug-PEG, and gold-PEG will be determined by fluorescence and darkfield microscopy. Control, doxorubicin, gold-drug-PEG, and gold-PEG groups will be created. Equal concentration of doxorubicin (5 μg DOX/ mL) will be used for doxorubicin and gold-drug-PEG groups, whereas same amount of gold will be used for gold-drug-PEG and gold-PEG groups. Control group will be left untreated. Cells will be treated with according groups and incubated at 37°C for 2.5 hours. Then, cells will be fixed with 3.7% formaldehyde and stained with DAPI for nucleus detection. Cover-slipped cell slide will be then imaged with fluorescence microscope to confirm the uptake of drug and particles by cells.

***In vivo* study of gold system**

Murine breast cancer cell line 4T1 will be injected into Balb/c mouse at mammary fat pad, subcutaneously with 2 X 10^6 tumor cells. When tumor size was approximately 100mm^3, mice were divided randomly into group of four (n=5) of control (untreated), pure doxorubicin, polymer-drug-gold conjugate, and polymer-gold conjugate groups. Drug will be administered through tail-vein injection (2mg DOX/kg and 0.04g Au/kg) and all groups will be treated four times total (every 3 days) except for the control group, which is left untreated. Tumor size and body weight will be measured every 2 days. In addition to tumor size and body weight changes, effect of polymer-drug-gold conjugate on tumor treatment is further evaluated by weighing the harvested tumor and comparing the "actual" size of the tumor amongst various groups. After the sacrifice, various organs including heart, kidney, lung, liver, spleen, brain, and tumor will be collected for various

analyses. To verify the uptake of polymer-drug-gold conjugate via EPR effect, concentration and location of gold nanoparticle within tumor tissue will be studied by ICP-MS, histology, TEM, and dark-field microscopy. Evaluations of any toxicity exerted by polymer-drug-gold conjugate on healthy, normal tissue will be mainly investigated by histological analysis. For serum biochemical analysis, whole blood was centrifuged twice at 3000 rpm for 10 minutes in order to separate serum. Using a biochemical analyzer (Type 7170, Hitachi), serum biochemical analysis was carried out to determine the serum level of various proteins. A certified pathologist will compare the stained tissue section from all four groups for any morphological changes occurring in various organs harvested from the mouse.

4.4 RESULTS AND DISCUSSION

Chemical Synthesis and Characterization of Au-DOX-PEG

Doxorubicin, an anthracycline derivative, is commonly used chemotherapeutic agent for various malignancies such as solid tumors of breast, esophagus, liver, and soft-tissue sarcoma [130]. Despite its high anti-tumor activity, doxorubicin presents side effects by not only inducing tumor cell death but also affecting normal, healthy cells, especially leading to irreversible cardiotoxicity. Furthermore, doxorubicin exhibits poor water solubility and narrow therapeutic index that it is difficult to significantly increase the dosage at the target sites. To overcome these side effects, doxorubicin conjugate system has been developed: doxorubicin was modified with pH-sensitive hydrazone linker (PDPH) and attached to gold nanoparticle. Hydrazone bond is stable under neutral pH conditions, but it is cleaved under mild acidic conditions of pH less than 5.5 [168],

resembling the endosomal and lysosomal environment. In addition to providing pH sensitivity, hydrazone linker PDPH provides thiol bond for adsorption of modified doxorubicin onto gold nanoparticle surface.

Gold nanoparticle-anticancer agent-PEG (Au-DOX-PEG) drug delivery system was synthesized by first coating the gold nanoparticle with modified doxorubicin (DOX-PDPH) then with thiolated methoxy-PEG (Figure 4.1(a)). PEG provides colloidal stability for gold-doxorubicin conjugate (Au-dox) system that PEG protects gold nanoparticles from physiological conditions and prevents aggregation. Furthermore, PEG reduces adsorption of cellular proteins and increases the circulation time of nanoparticles [169]. The self-assembly of gold nanoparticle-anticancer agent-PEG system is a spontaneous process, which resulted in water-soluble, colloidally stable Au-DOX-PEG system with a size of ~17.8 ± 1.3 nm and -2.16 ± 0.217 mV for zeta potential.

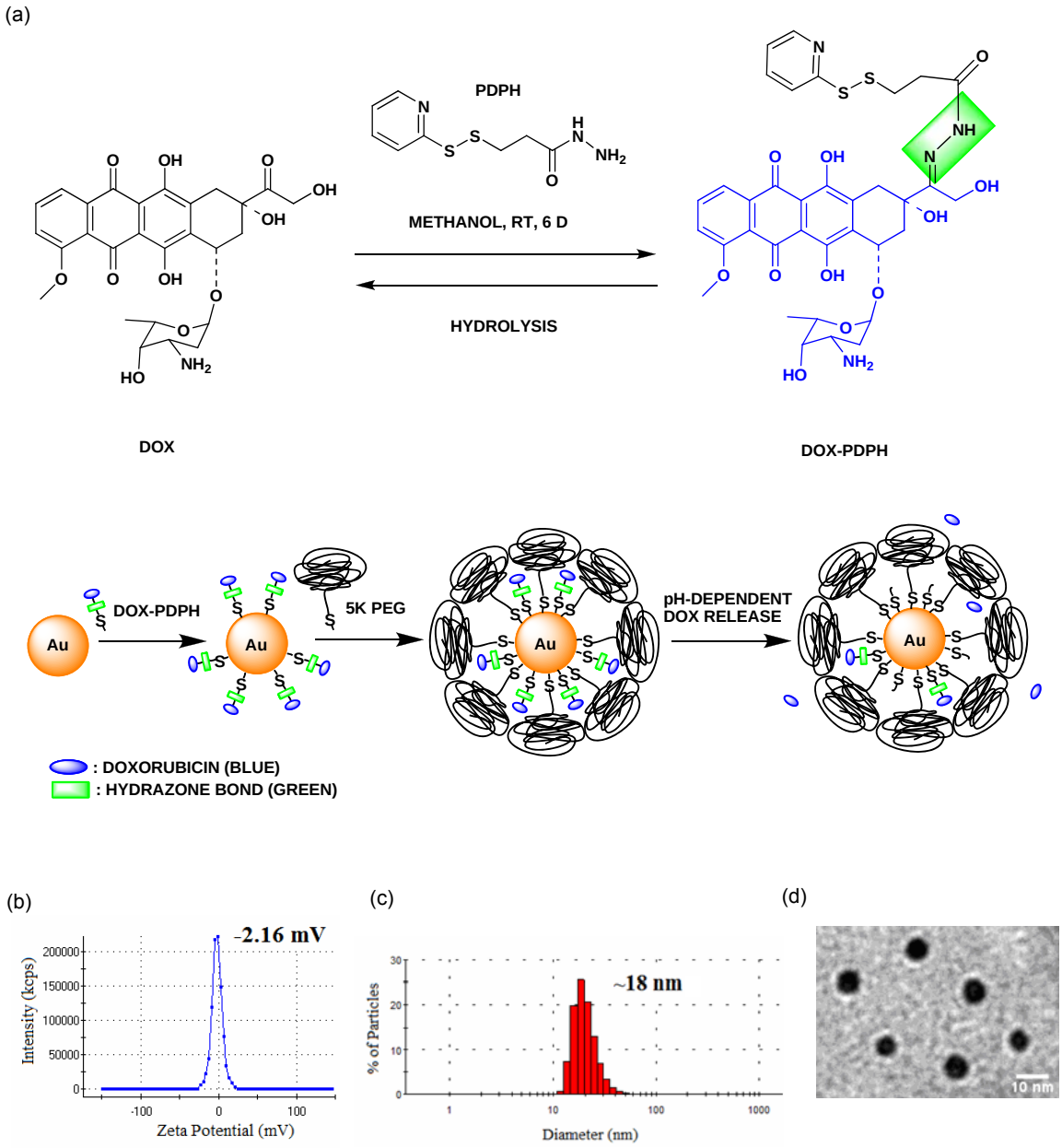

Figure 4.1. Chemical Synthesis and Self Assembly of AU-DOX-PEG

To find the maximum drug loading capacity of 5nm gold nanoparticle while maintaining the colloidal stability of gold nanoparticle, UV-vis spectroscopy and fluorescence spectra were used to test the adsorption of series of different concentrations of DOX-PDPH onto gold. When DOX-PDPH was conjugated to gold nanoparticles in

water, the fluorescence of doxorubicin was quenched on gold surface (Figure 4.2 "Before Centrifuge"). Previous studies also report quenching of fluorescent dyes on metallic particles when they are chemisorbed onto the surface [135-137]. Furthermore, fluorescence quenching on metallic surface is observed for distance of few nanometers [138, 139], which suggests proximity of doxorubicin onto gold surface linked via short PDPH linker. When gold nanoparticle-anticancer agent-PEG system was centrifuged for purification, the supernatant did not contain any detectable amount of unbound doxorubicin up to 5.58 wt-%. However, when excess amount of DOX-PDPH was added to the gold nanoparticle solution, we observed fluorescence of unbound DOX-PDPDH in the supernatant (Figure 4.2 (c)). Thus, the maximum drug loading capacity of 5nm gold nanoparticle was ~5.5 wt-%.

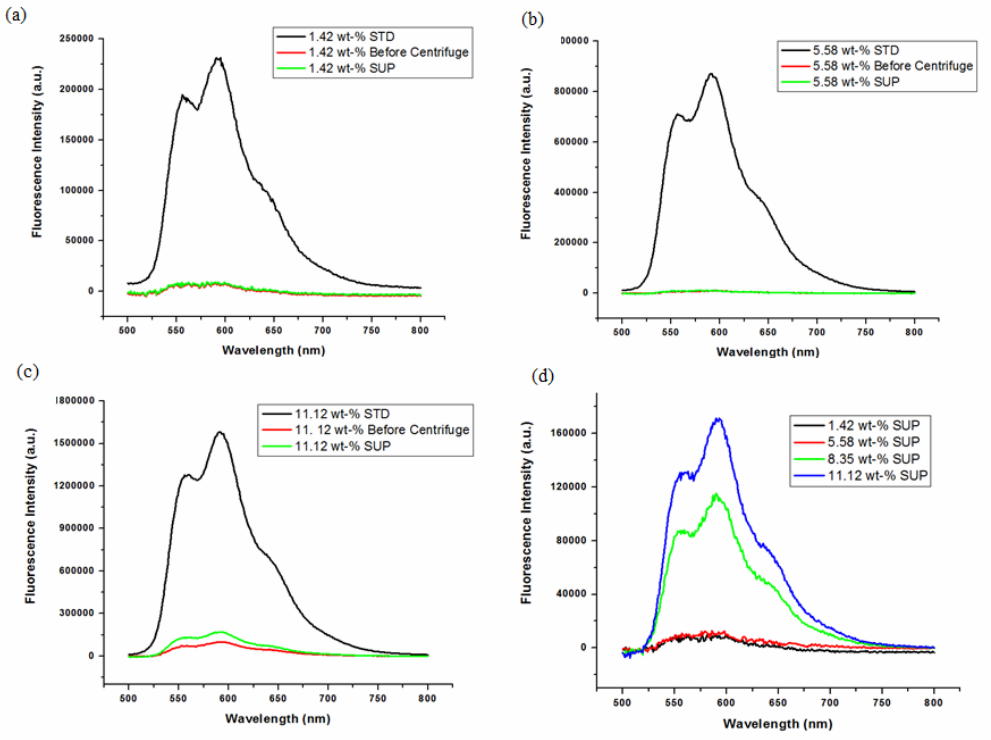

Figure 4.2. Maximum Drug Loading Efficiency using Fluorescence

To find the optimum PEG density for colloidal gold stability, dynamic light scattering measurement was used for size change. After subtracting the gold surface area occupied by modified doxorubicin, available surface area was coated with various concentrations of PEG. As we increased the PEG concentration, saturation point was reached for gold-drug-PEG size measurement (Table 4.1).

Table 4.1. PEG Coating and Gold Nanoparticle-Anticancer Agent-PEG (Au-DOX-PEG) System Size Change

% PEG[†]	Au-DOX-PEG Size (nm)
0 (Au-DOX Only)	7.0 ± 1.6
25	17.7 ± 1.5
50	18.0 ± 1.6
100	17.7 ± 1.4
150	17.9 ± 1.2
200	17.7 ± 1.5

[†]Indicates the amount of excess PEG added to free, available surface area on gold surface after adsorbing DOX-PDPH (~5.5 wt-%)

Saturation of gold nanoparticle surface at low % PEG values indicate that most of the gold surface is coated with modified doxorubicin, and PEG is bound onto the gold surface in a "mushroom conformation". Mushroom conformation is characterized by low surface grafting density and polymer tends to "lie" close to the surface that multiple points of a single polymer is covering the surface [115]. Despite the low PEG surface density, the resulting Au-DOX-PEG was colloidally stable in various mediums such as salt and serum solutions (APPX A Figure A.1). We suspect that in conjunction with DOX-PDPH coating, small-sized gold nanoparticle core (5nm) and long chain length (MW=5000) PEG resulted in a sufficient coverage of the gold surface for colloidal stability. It has been reported that nanoparticle stability increases with increasing PEG length and decreasing nanometer particle diameter [43]. In particular, PEG with a

molecular weight of ≥ 2000 Daltons can significantly reduce protein adsorption and result in colloidal stability in highly ionic strength media due to increased steric repulsive forces [43, 170-175]. Supporting our results, Liu, Y. et al found that 1) for any given PEG length, decrease in nanoparticle diameter resulted in a decreased amount of PEG per nanoparticle input to the reaction mixture and 2) for a given nanoparticle diameter, increase in PEG length resulted in a decrease in the amount of PEG amount input to the reaction mixture for colloidal stability. Furthermore, in accordance with DLVO theory, small-sized gold nanoparticles are more stable in general than the larger-sized gold nanoparticles due to minimized van der Waals attraction energy.

Finally, we also wanted to ensure that bound doxorubicin is not affected by the addition of PEG. Similar to the method used for drug loading efficiency, the supernatant collected from centrifugation of various concentrations of PEG coated gold-drug-PEG systems indicated that addition of PEG, especially excess amount of PEG, did not affect bound doxorubicin and there was no detectable replacement of the bound drug.

Drug Release Profile

Figure 4.3 shows pH-dependent release profile of doxorubicin linked to hydrazone bond of PDPH at 37°C. Initially, doxorubicin is slowly released for both acidic and basic conditions that no detectable release was observed up to 48 hours. More doxorubicin was released over time, especially for acidic condition, which led to approximately 4 times more doxorubicin release at the end of 96 hours for pH 5 condition compared to that of neutral condition. Previous studies also reported increased hydrolysis

of hydrazone bond and rapid release of doxorubicin in acidic conditions compared to neutral conditions [130, 156].

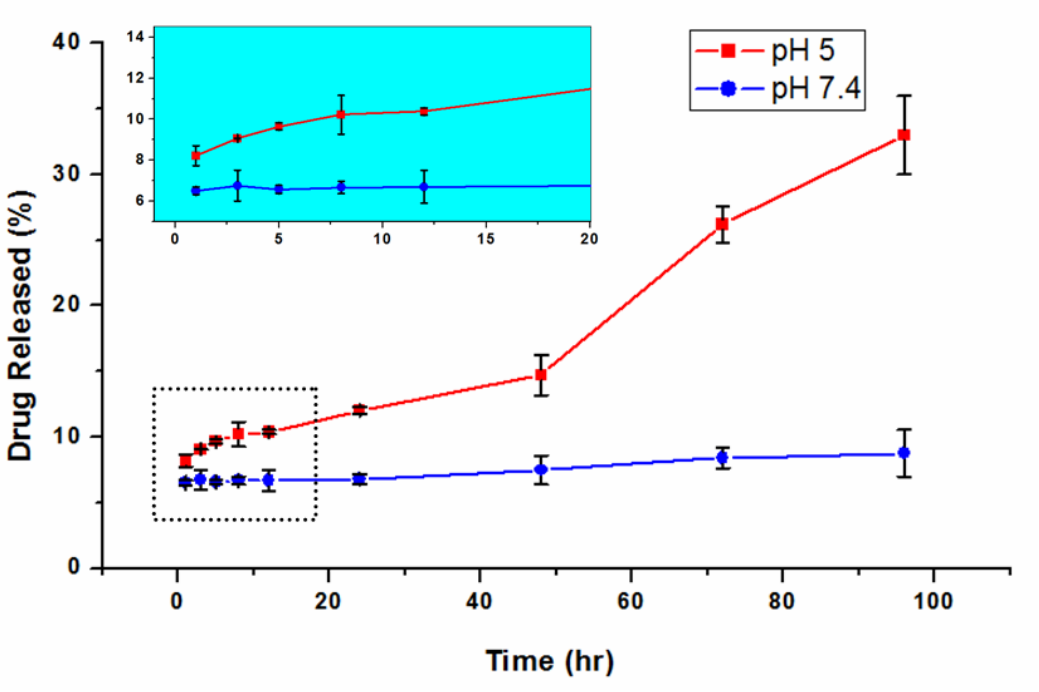

Figure 4.3. pH-Sensitive Drug Release

The slow, delayed release of doxorubicin from Au-DOX-PEG system is due to (1) the diffusion barrier created by PEG coating and (2) interactions between the polymer and the drug. PEG chains interact with one another that complex is formed amongst PEG chains by hydrogen bonding [157]. As polymer chain length increases and more inter-polymer complexes are formed, the release rate of the drug is decreased. Also, complexation affects PEG conformation that polymer coils provide additional diffusion barrier for more tortuous path for drug release [157, 158]. Because PEG is a hydrophilic polymer, as the hydrophobicity of the drug increases, the diffusion rate of the drug decreases. However, we believe that combination of the EPR effect and various *in vivo*

conditions will affect the release profile of Au-DOX-PEG system to be more effective system.

In Vitro Therapeutic Efficacy of Au-DOX- PEG System

MTT assay with 4T1 cell line was used to study the anticancer efficacy of Au-DOX-PEG system. Cell viability was inversely related to doxorubicin activity that absence or minimal efficacy of doxorubicin resulted in increased cell survival. Cell viability for each group (pure doxorubicin, Au-PEG, and Au-DOX-PEG) was compared to the control group which was free of doxorubicin (Figure 4.4 (b)).

Compared to the pure doxorubicin 96 hour toxicity, the slightly lower toxicity of Au-DOX-PEG could have resulted from slow release of doxorubicin within PEG shell (also seen in Figure 4.3) and different cellular localization of Au-DOX-PEG system compared to the pure drug.

The slow release of doxorubicin from Au-DOX-PEG system was also evident in the fluorescence images of the 4T1 murine breast cancer cells incubated with the gold conjugate system (Figure 4.4 (a)). When equal concentration of doxorubicin was used, cells that contained Au-DOX-PEG displayed less fluorescence intensity compared to the pure doxorubicin incubated cells. Also, when equal concentration of gold nanoparticle was used, only Au-DOX-PEG displayed fluorescence for doxorubicin and Au-PEG fluorescence images resembled that of CONTROL where no fluorescence was detected for doxorubicin. The actual uptake of gold nanoparticle by 4T1 cells is evident in TEM images in next section.

(a)

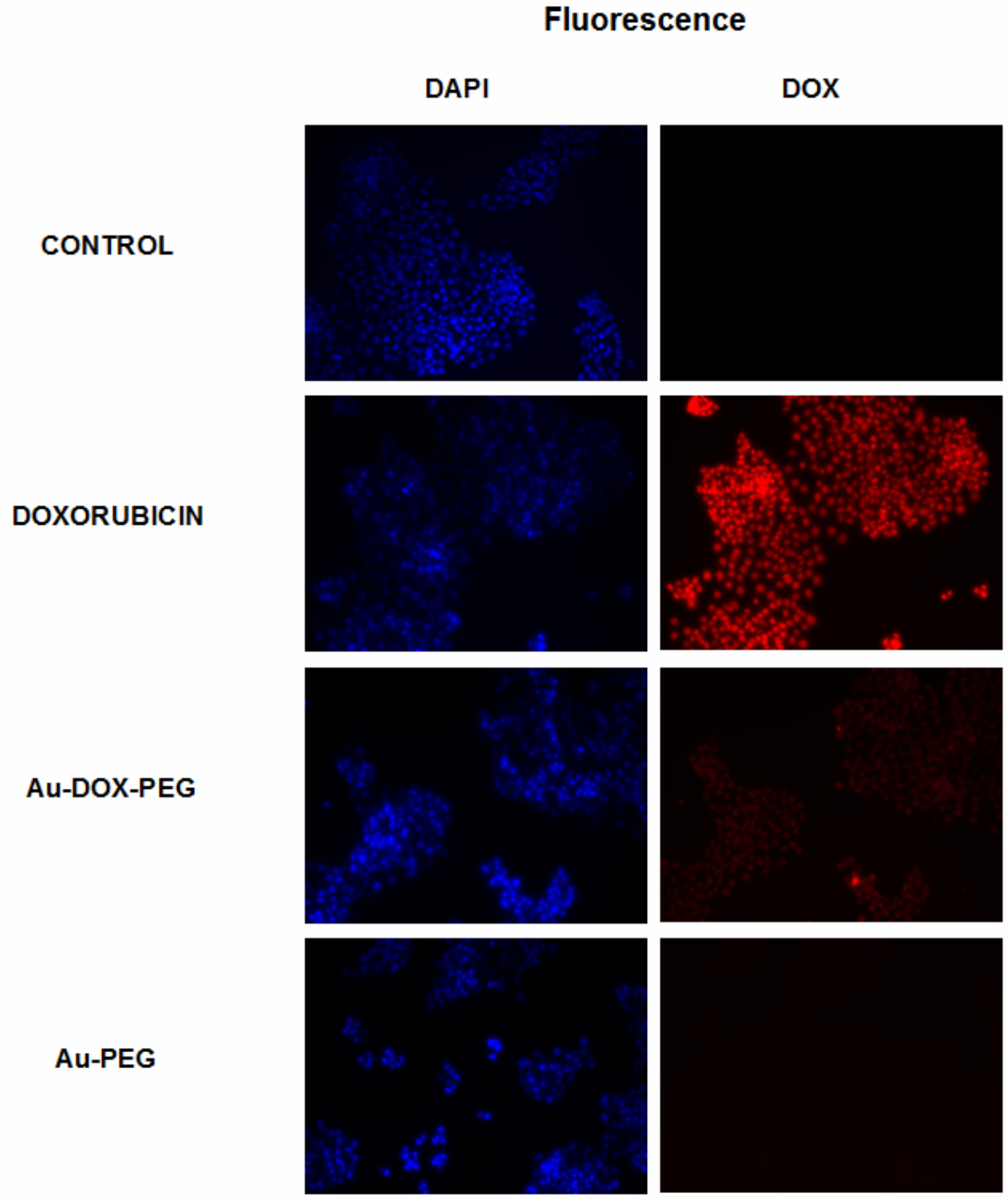

(b)

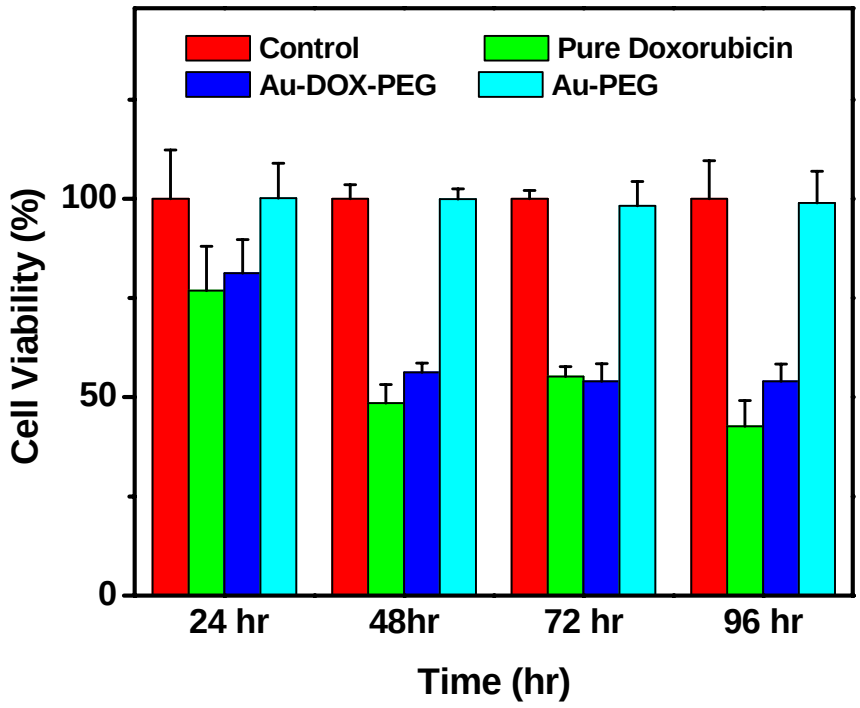

Figure 4.4. *In vitro* Therapeutic Efficacy of Au-DOX-PEG and Cellular Uptake of Gold Nanoparticle (a) 4T1 cells were incubated with doxorubicin, Au-DOX-PEG, and Au-PEG at 37°C for 2.5 hours and fluorescence images were taken for DAPI (nucleus staining) and DOX (Doxorubicin) (equal amount of gold was used for Au-DOX-PEG and AU-PEG groups; 5μg/mL of doxorubicin and equivalent was used for doxorubicin and Au-DOX-PEG, respectively) (b) MTT assay results with 4T1 murine breast cancer cells (equal amount of gold was used for Au-DOX-PEG and AU-PEG groups; 7 μg/mL of doxorubicin and equivalent was used for doxorubicin and Au-DOX-PEG, respectively)

In vivo Therapeutic Efficacy of Au-DOX-PEG Drug Delivery System for solid tumor

Body Weight, Tumor Volume, and Tumor Raw Weight Changes

To investigate the therapeutic efficacy of Au-DOX-PEG drug delivery system *in vivo*, we conducted a comparison study between pure doxorubicin versus Au-DOX-PEG system on 4T1 murine breast cancer mice model. 4T1 tumor cells were injected subcutaneously at the mammary fat pad of female BALB/c mice. Treatments were

carried out by injecting saline (control), pure doxorubicin, Au-DOX-PEG (at an equal doxorubicin dose of 2.4 mg/ kg), and Au-PEG into tail-vein for every 3 days over ~2 weeks (n=5 for each group). As shown in Figure 4.5, tumor volume was measured every other day by a caliper and it was observed that Control group (untreated) and gold nanoparticle only group (Au-PEG) displayed average *fractional tumor volumes* (i.e. final tumor volume divided by initial tumor volume) of 6.3 ± 1.8 and 6.6 ± 2.4, respectively, on day 16. Statistical analysis results indicated that there was no significant difference between the Control and Au-PEG groups ($P>0.05$ for Control versus Au-PEG). Pure doxorubicin treated group resulted in fractional tumor volume of 3.1 ± 1.2 on day 16, which represents *tumor group inhibition* or *TGI* of ~50 % (i.e. TGI= 100 * {[Control fractional tumor volume – Group of Interest fractional tumor volume]/ Control fractional tumor volumes}). The statistical analysis result indicated that there were no significant differences between the Control versus pure Doxorubicin groups and Au-PEG versus pure Doxorubicin groups ($P>0.05$ for doxorubicin versus control; $P> 0.05$ for doxorubicin versus Au-PEG). In contrast, Au-DOX-PEG treatment resulted in a fractional tumor volume of 1.8 ± 0.3 on day 16 ($P<0.01$ Au-DOX-PEG versus Control; $P<0.05$ Au-DOX-PEG versus Au-PEG; $P>0.05$ Au-DOX-PEG versus pure doxorubicin) with tumor group inhibition of ~71%, which was more effective than the pure Doxorubicin group.

Alternatively, therapeutic efficacy of Au-DOX-PEG system was studied by extracting tumor from mice and raw tumor weight was measured from each group on day 16. Similar to the tumor volume change results, there was no significant difference between the Control and Au-PEG average tumor raw weights ($P>0.05$ for Control versus

(a)

(b)

(c)

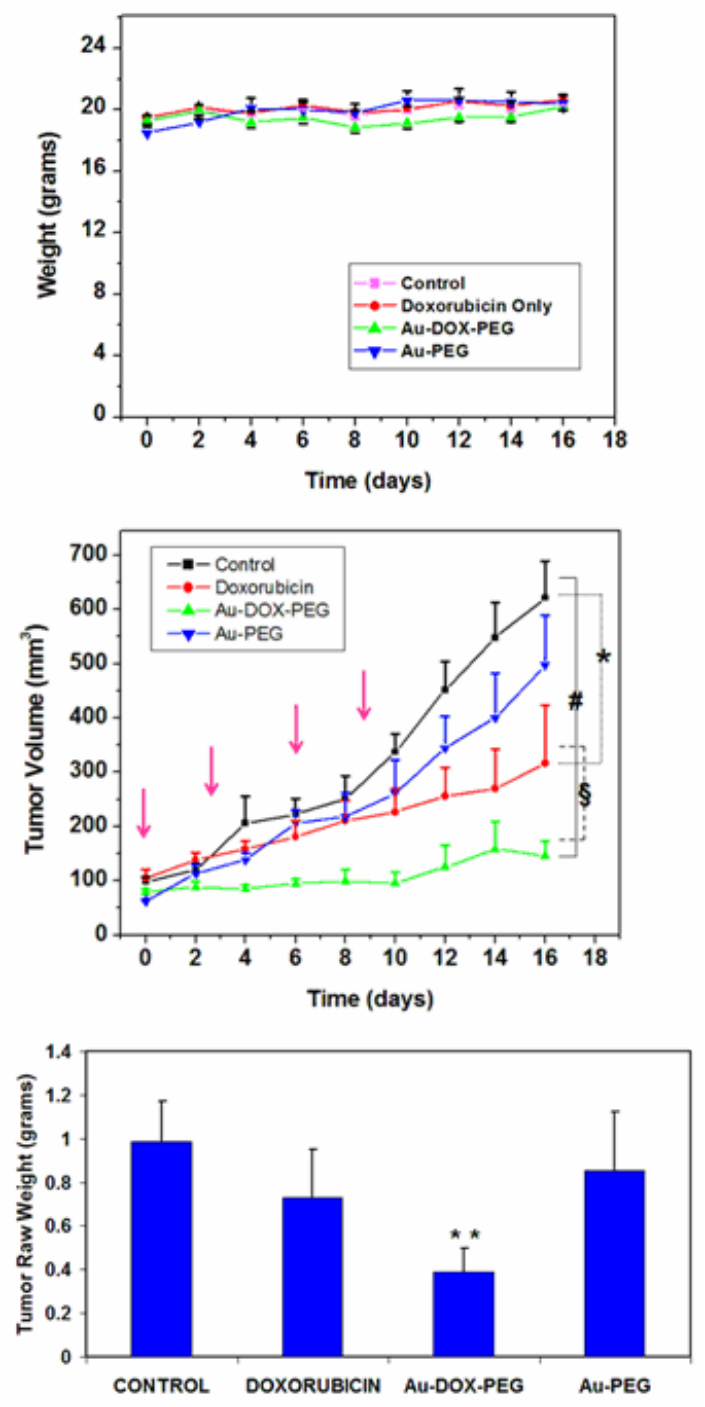

Figure 4.5. *In Vivo* Results (a) Weight Change: there was no visible weight changes amongst the group over the course of treatment (b) Tumor Volume Change: Tumor Volume Change for Control, Doxorubicin, Au-DOX-PEG, and Au-PEG (*: $p > 0.05$; # : $p < 0.01$; §: $p > 0.05$; pink arrow indicates treatment); Tumor Weight (**: $p < 0.05$ from control only) (c) Extracted Tumor Raw Weight [n=5 and standard error of mean were used for all figures]

Au-PEG). Compared to the average Control tumor raw weight, Doxorubicin group resulted in an average tumor weight of 0.73 ± 0.22 g, which was ~25% lighter than the Control group ($P>0.05$ for Doxorubicin versus Control). Au-DOX-PEG group had an average tumor weight of 0.38 ± 0.11 g, which was significantly lighter than the Control group (~61% lighter than the Control group with $P<0.05$ for Au-DOX-PEG versus Control). Compared to the pure Doxorubicin group, Au-DOX-PEG group was ~47% lighter but it was not statistically significant enough ($P< 0.05$ for Au-DOX-PEG versus pure Doxorubicin). Thus, consistent with the tumor volume change results, Au-DOX-PEG group resulted in a tumor raw weight that was significantly differently (all $P<0.05$) from the Control and Au-PEG groups at the end of the therapy. In contrast, Doxorubicin group did not display statistically significant difference between Control group or between the Au-PEG group tumor raw weights.

Finally, body weights amongst the Control, pure Doxorubicin, Au-DOX-PEG, and Au-PEG groups were measured throughout the therapy. The statistical analysis results indicates that there was no significant differences amongst the body weights for all four groups ($P>0.05$).

In summary, there was no significant difference between Control and Doxorubicin, whereas Au-DOX-PEG group showed statistically significant difference from the Control group. Moreover, Au-DOX-PEG group showed statistically significant difference from the Au-PEG group, whereas pure Doxorubicin group did not. Although Au-DOX-PEG group exhibited somewhat higher tumor group inhibition (TGI) index than the Doxorubicin group, there was no statistically significant difference ($P>0.05$) seen between Doxorubicin and Au-DOX-PEG groups. However, it should be noted that Au-

DOX-PEG displayed no apparent toxicity to the vital organs in contrast to pure Doxorubicin group as shown in the upcoming section.

Spatial Distribution of Au-DOX-PEG in Tumor

For the drug delivery nanoparticle system to exert its full therapeutic efficacy, it must reach the cancer cells in the solid tumor by (1) crossing (i.e. extravasate) the tumor blood vessel wall into the tumor interstitium (i.e vascular permeability), (2) migrating through the tumor interstitial space or penetration away from the blood vessel through the extracellular matrix, and then (3) penetrating or entering the cancer cell (i.e. cellular uptake) [176, 177]. Our system resulted in a successful extravasation by diffusion through the tumor blood vessel wall due to small size scale of Au-DOX-PEG (Figure 4.6). Tumor accumulation is a function of both the rate of extravasation from the blood to the tumor space and also the rate of clearance from the tumor. Hobbs et al. showed that the rate of extravasation ofs"small-sized" bovine serum albumin (BSA) of 7nm was independent of pore size over a variety of tumor models [28]. This demonstrates that for a ~7 nm molecule, which is much smaller than the transvascular pore, extravasation is not dependent on pore size but is instead a diffusive process that will depend on the concentration gradient between blood and tumor. Chilkoti et al. demonstrated that dextran drug carrier of molecular weights of 40 and 70 kDa (diameters of 11.2-14.6nm) resulted in a successful extravasation and penetration into the tumor [23]. Similarly, Tang et al. demonstrated that doxorubicin containing PEG-PE micelles with size of 10-20nm resulted in a successful extravasation, accumulation, and penetration of the nanoparticle at the tumor site [178].

The increased accumulation and retention of nanoparticle at the tumor interstitium increases the success rate of the drug delivery system. For normal vasculature, macromolecules and cell debris are cleared from the interstitium through lymphatic drainage. However, lymphatics in tumors are either poorly developed or nonfunctional that leads to decreased rate of clearance of particles [179, 180]. As seen in Figure 4.7, statistical analysis ($P>0.05$, Kruskal-Wallis Test) shows that there was no significant difference amongst the total gold amount accumulated in tumor over time after a single tail-vein injection of gold nanoparticle system. This indicates that the retention of our Au-DOX-PEG system within the tumor mass for prolonged period time for successful tumor therapy. Accumulation of Au-DOX-PEG in tumor was also evident by the color change of tumor mass itself as seen in Figure 4.6. Au-DOX-PEG displayed high accumulation in the tumors that they penetrated relatively long distance (radially) into the tumor (dark thick halo seen in the sliced open tumor mass picture of Figure 4.6 (a)), rather than being concentrated only near the vascular surface of short distance. Also, TEM Images from Figure 4.6 shows that gold nanoparticle are present in the extravascular compartment or the tumor interstitium, where concentration in this compartment represents the cumulative exposures of cancer cells to drug. It has been reported that when the particles are too small (molecular weight <40kDa), nanoparticles are rapidly cleared from the tumor extravascular compartment [23]. Thus, our Au-DOX-PEG system has the ideal size (5nm core with ~13nm shell) that resulted in successful vascular permeability and retention in the tumor interstitium.

(a)

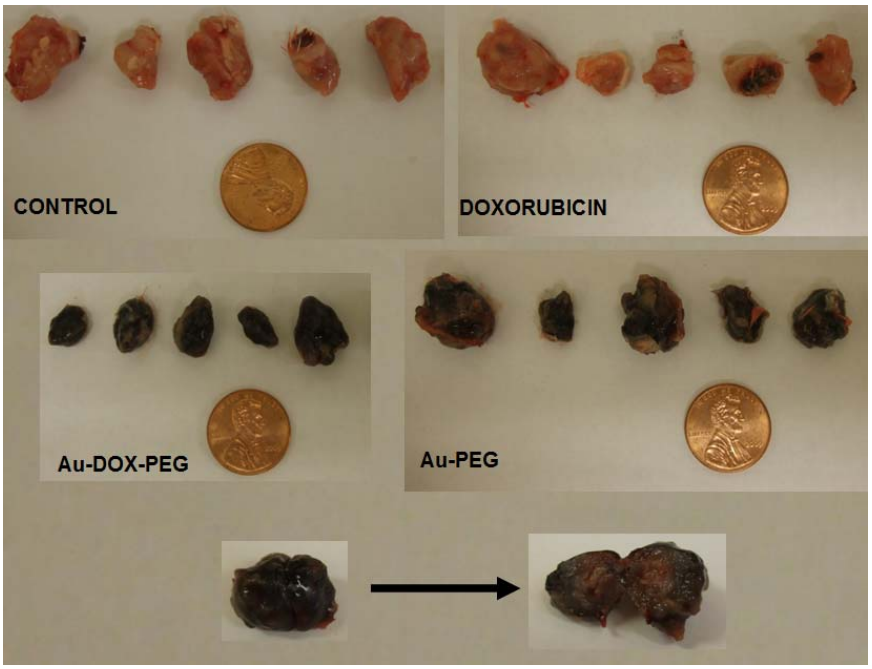

(b)

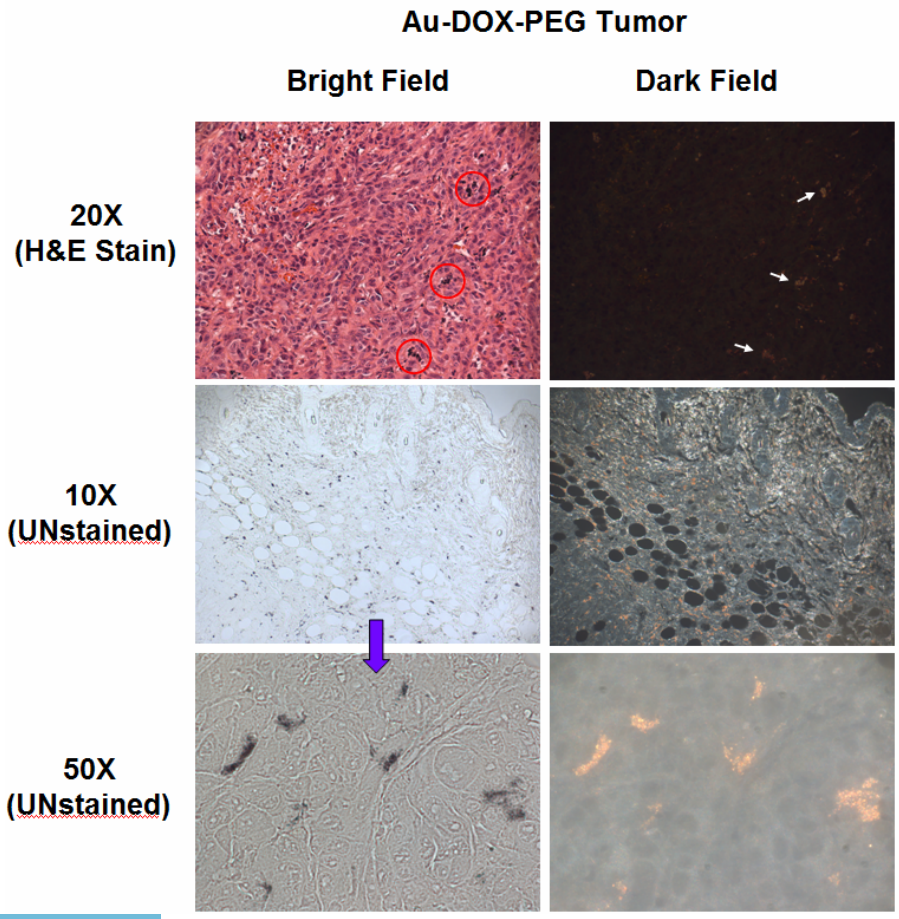

(c)

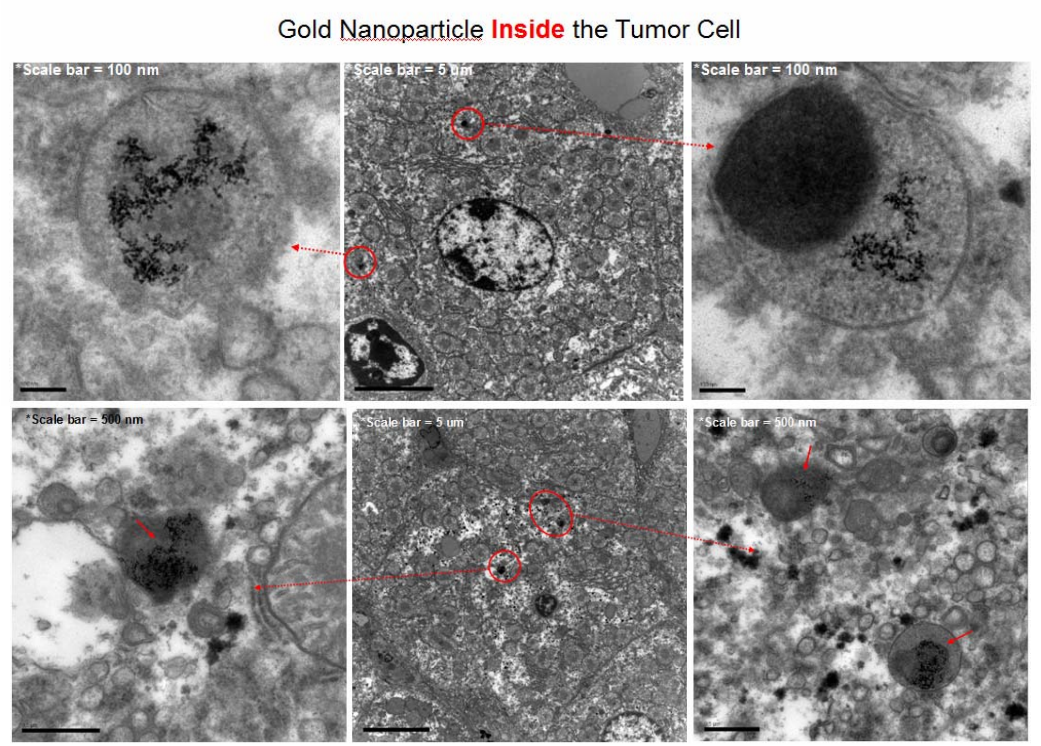

(d)

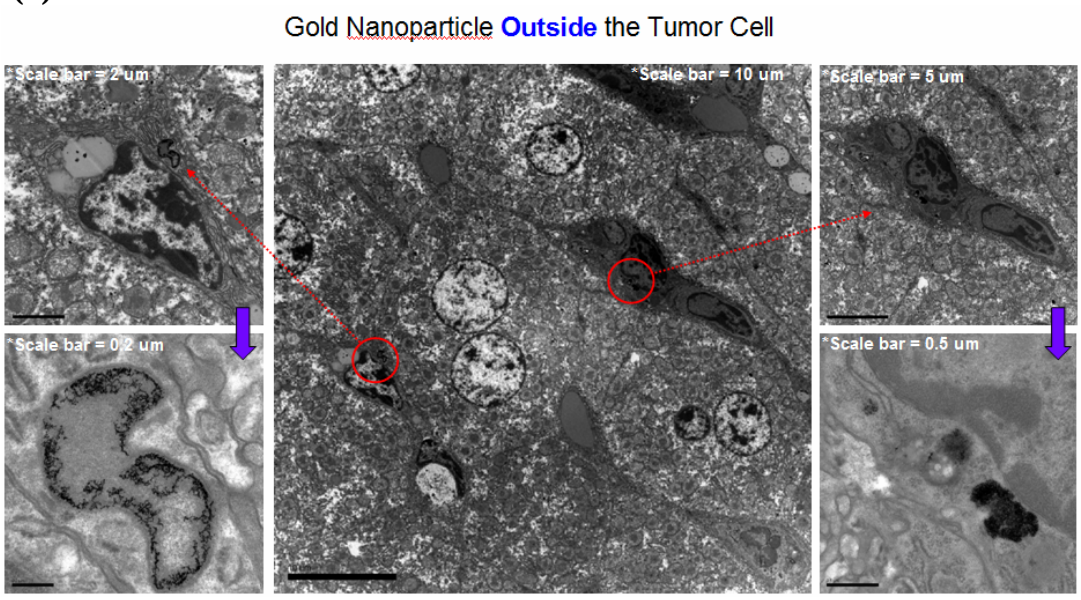

Figure 4.6. Spatial Distribution of Au-DOX-PEG within Tumor (a) Collection of extracted tumor from Control, Doxorubicin, Au-DOX-PEG, and Au-PEG groups. Bottom picture indicates the halved Au-DOX-PEG tumor. (b) Brightfield and darkfield microscopy images of Au-DOX-PEG present within tumor (arrows and orange chunks indicates Au-DOX-PEG) (c) TEM images of Au-DOX-PEG inside the tumor cell (d) TEM images of Au-DOX-PEG outside the tumor cell

Finally, the successful therapeutic efficacy of our Au-DOX-PEG resulted from the cellular uptake of Au-DOX-PEG by cancer cells (with the assumption that doxorubicin is released *inside* the cancer cells after cellular uptake of Au-DOX-PEG). It has been reported that particles transport to the tissues by convection in healthy tissues [176]. However, due to lack of lymphatic drainage, the interstitial hydrostatic pressure increases to severely restrict convective transport [181, 182]. As a result, diffusion becomes the dominant means of transport of nanoparticles in tumor tissues. The rate of transport through the extracellular matrix is determined by the effective interstitial diffusion coefficient, which decreases as molecular weight is increased [183]. Thus, as high concentrations of Au-DOX-PEG was injected to the system, concentration gradient acts as a driving force to result in the uptake of gold nanoparticle system by cancer cells.

Spatially, the TEM images in Figure 4.6 confirm that Au-DOX-PEG system is present *both* inside and outside of tumor cells. The uptake of Au-DOX-PEG by the tumor cells seems to be non-specific endocytosis, as they are usually found inside a vacuole or endosome-looking vesicles inside the cells. Within the cells, Au-DOX-PEG system is mostly present within the outer membrane of the endosome due to diffusion-limited, heavy gold core of Au-DOX-PEG system.

Three mechanisms can be suggested for the successful therapeutic efficacy of our Au-DOX-PEG system: (1) most of the Au-DOX-PEG was accumulated in the tumor stroma and doxorubicin was released from the acidic tumor stroma to be uptaken by tumor cells or extracellular components (it has been reported that drug carriers larger than 10kDa can localize near the vascular surface and release the drug from its carrier when it is near the vascular surface so that drug could penetrate much deeper into the tumor

tissue [23], (2) most of the Au-DOX-PEG was uptaken by the tumor cells by concentration gradient-driven diffusion process, where doxorubicin was released *inside* the tumor cells to exert its therapeutic efficacy, or (3) Au-DOX-PEG exerted its therapeutic efficacy by releasing doxorubicin *both* inside and outside the tumor cell (i.e. combination of both (1) and (2)). It is hard to conclude whether most of Au-DOX-PEG was inside or outside the tumor cell to exert therapeutic efficacy from Figure 4.6 TEM images. Kirpotin et al. reported that non-targeted (passive) colloidal gold encapsulating liposome drug delivery system were predominantly present within the tumor stroma, either in extracellular space or within tumor-resident macrophage but not within the tumor cells themselves, after 7 days of injection [184]. However, Kirpotin et al. used a larger nanoparticle of 86 nm in mean diameter for the experiment, whereas our Au-DOX-PEG is 18 nm in mean diameter. Thus, small-size scale of Au-DOX-PEG resulted in uptake of our system by the cancer cells via passive targeting.

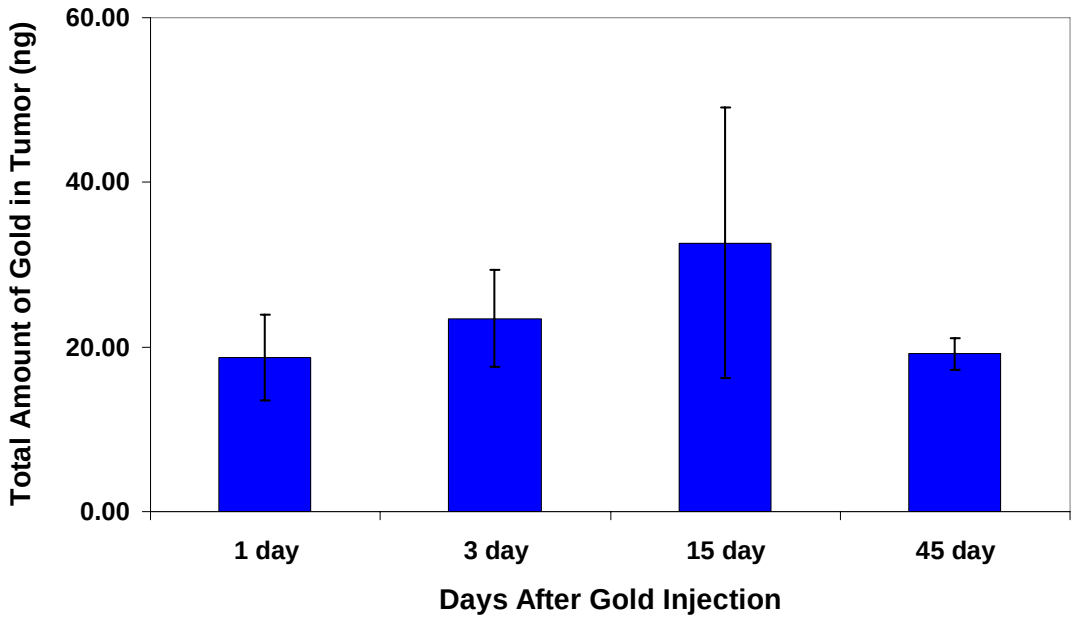

Figure 4.7. ICP-MS Analysis of Gold in Tumor After Single Injection

Additionally, PEGylation of our gold nanoparticle drug delivery system has affected the overall uptake of the Au-DOX-PEG. It has been reported that as the nanoparticles are transported within the tumor interstitium, nanoparticles can nonspecifically interact with various proteins and tissue compartments in the tumor interstitium or get metabolized [176]. PEGylation is known to render non-fouling surfaces that minimize nonspecific binding of proteins [169]. Also, PEGylation of our gold nanoparticle, along with attachment of modified doxorubicin, resulted in a near-neutrally charged nanoparticle that decrease the binding of proteins and increased the uptake of Au-DOX-PEG by the tumor cells.

In summary, the therapeutic efficacy of Au-DOX-PEG resulted from its "small-size" and "near neutral charge" that led to effective transport of the nanoparticle across the tumor microenvironment and reaching the cancer cells at optimal concentrations. Moreover, it is the combination of the EPR effect (leaky tumor vasculature and decreased clearance rate due to defective lymphatic drainage) along with the concentration-driven, diffusion-limited transport of Au-DOX-PEG system that resulted in successful high accumulation of Au-DOX-PEG at the tumor site. We believe that acidic tumor environment and endosome trigger the release of the bound doxorubicin through cleavage of pH-sensitive hydrazone bond to result in therapeutic efficacy [176].

Biodistribution of Au-DOX-PEG in Various Organs and Toxicity

To further understand the therapeutic efficacy of Au-DOX-PEG, biodistribution of Au-DOX-PEG in tumor and various organs were investigated through Inductive-Coupled Plasma Mass Spectroscopy (ICP-MS) analysis of gold. We observed significant accumulation of Au-DOX-PEG in tumor compared to other normal organs (Figure 4.8

(a)). High accumulation of Au-DOX-PEG is due to the size scale and prolonged circulation of Au-DOX-PEG, taking advantage of the EPR effect. Nanoparticle plasma retention time is one of the primary driving forces for nanoparticle tumor accumulation by the EPR effect [22] that drug concentration in plasma must remain high for more than 6 hours to satisfy the EPR effect in solid tumors [25, 36, 185]. For our Au-DOX-PEG system, PEGylation contributed to the prolonged blood circulation time of ~1.6 days compared to that of pure doxorubucin with few minutes. This prolonged circulation time promotes EPR effect and results in successful accumulation of Au-DOX-PEG at tumor site, where the small-sized Au-DOX-PEG easily extravasate out of the leaky tumor vessel to ultimately result in therapeutic efficacy.

The key to a successful anti-tumor efficacy of a drug system relies on the accumulation and spatial distribution within the tumor. Especially for passive targeting, molecular weight (or size) and charge become the dominant factors that govern the accumulation of drug delivery system at the tumor site [23]. The accumulation of Au-DOX-PEG at the tumor site was enhanced by the small molecular weight of the system (but greater than 40kDa to satisfy EPR condition [185]) that resulted in longer blood circulation half time of ~1.6 days. Moreover, the PEGylation of the small-sized gold nanoparticle core has enhanced the circulation time and minimized any non-specific binding by the serum proteins for RES clearance [169]. PEGylation also resulted in a slightly negative, near-neutrally charged Au-DOX-PEG system. It has been reported that anionic and neutral particles have prolonged blood circulation half-life [186]. In contrast to positively-charged particles, negatively-charged particles results in prolonged blood circulation half-life due to reduced interactions between tissue and cells [187]. Slightly

negative charge resulting from PEGylation was effective to give longer plasma half-life for Au-DOX-PEG, which ultimately led to higher accumulation at the tumor site.

Additionally, it is the ultra-structural differences between the normal and tumor vasculature that resulted in a higher concentrations of Au-DOX-PEG system in tumor site compared to other organs. The permeability of normal vasculature decreases with the increasing hydrodynamic diameter of 3.6 nm, which is below the size limit of our system [188]. On the other hand, the permeability/ transport across the tumor vasculature is poorly regulated that tumor vasculature allows molecules up to 2 μm, which allows our Au-DOX-PEG system to easily extravasate and penetrate into the tumor interstitium [25, 27, 189-191]. Thus, the leaky vasculature and the increased permeability of Au-DOX-PEG within the tumor interstitium ultimately led to high accumulation of Au-DOX-PEG at the tumor site. Similar to the STEALTH liposomal drugs [192, 193], we believe that our Au-DOX-PEG initially accumulated at the tumor site via EPR effect over the course of few days (as indicated by the blood circulation half-life of ~1.6 days). Then, the drug is slowly released over the few weeks in a controlled manner (as seen in Figure 4.3), where the drug penetrates deeper into the tumor tissue due to creation of diffusion gradient.

Here, we want to emphasize the fact that therapeutic efficacy of Au-DOX-PEG system resulted from "passive" transport of Au-DOX-PEG. Both active targeting and passive targeting require passage through the leaky tumor blood vessel and extravasate into the tumor interstitium or the perivascular region [176]. There has been a controversy where several works have shown that the use of tumor-targeting ligands does not increase the total accumulation of the nanoparticles in solid tumors [17, 184, 194, 195]. The

targeting-ligands rather increase the receptor-mediated internalization of the nanoparticles for improved therapeutic efficacy. According to Huang, X. et al, the targeted and non-targeted gold nanorods displayed "marginal" difference in terms of total gold accumulation in xenograft tumor models. However, targeted nanorods altered the intra- and extra-cellular distribution compared to non-targeted nanorods [17]. Moreover, targeting ligands shorten the blood circulation life through opsonization (adsorption of blood proteins) [196].

It is interesting to see our passive targeting Au-DOX-PEG system resulted in a high accumulation at the tumor site to exert its therapeutic efficacy. As seen in Figure 4.8 (a), the amount of gold accumulated per gram of organ at tumor was similar to that of spleen and greater than liver. In contrast, targeted nanorods (hydrodynamic diameters of 51nm for nanorod and ~80nm for coated nanorod) resulted in fewer amounts of gold accumulated per gram of organ at tumor compared to spleen and liver [17]. Indeed, majority of gold was taken up by the liver and spleen (60-90% of the total injected gold) and less than 2% of the total injected gold was taken up by tumor for targeted nanorods. Similar trend was seen for TNF-α coated gold nanoparticle (hydrodynamic diameter of 27nm with coating), where amount of gold accumulated per gram of organ at tumor site was significantly less than that of spleen and liver [197]. For our Au-DOX-PEG system, passive targeting resulted in 7.0% of the total single injected gold to be uptaken by the tumor itself. The high accumulation and uptake of Au-DOX-PEG is rendered from the size of our system (5nm core and 18nm for coated). However, we cannot exclude the fact that the higher doses used in this study may have altered the accumulation rate of Au-

DOX-PEG at tumor site, which could have led to increased nonspecific uptake of our system by the cancer cells.

(a)

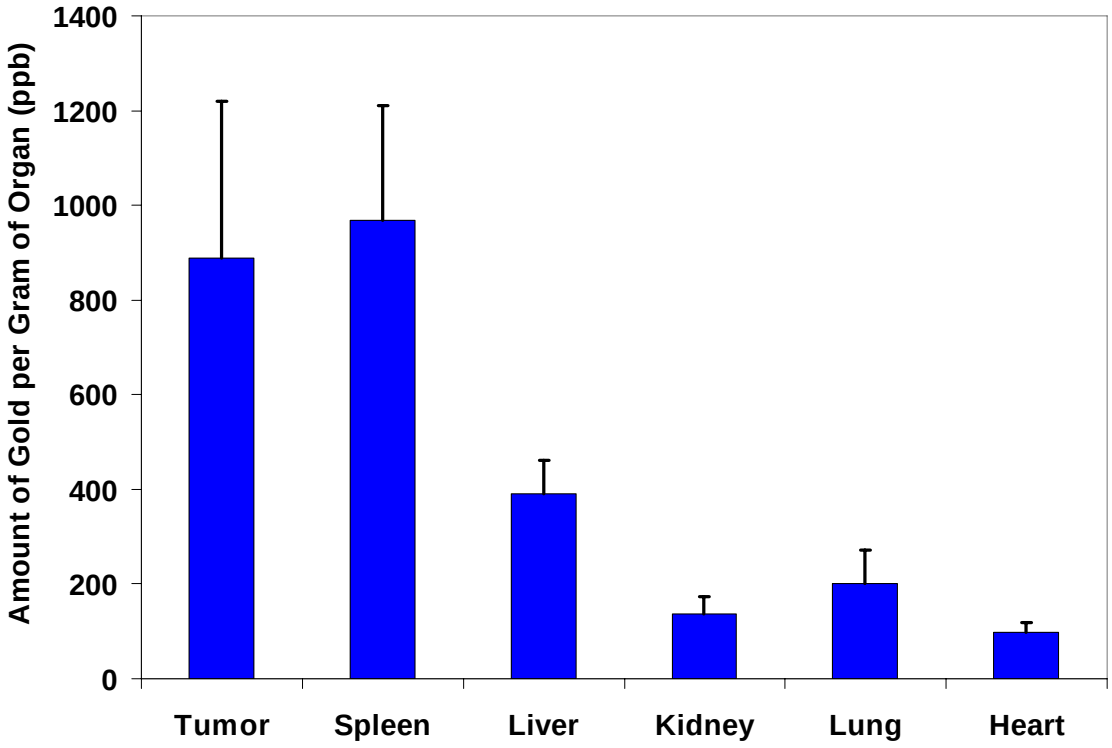

(b)

(c)

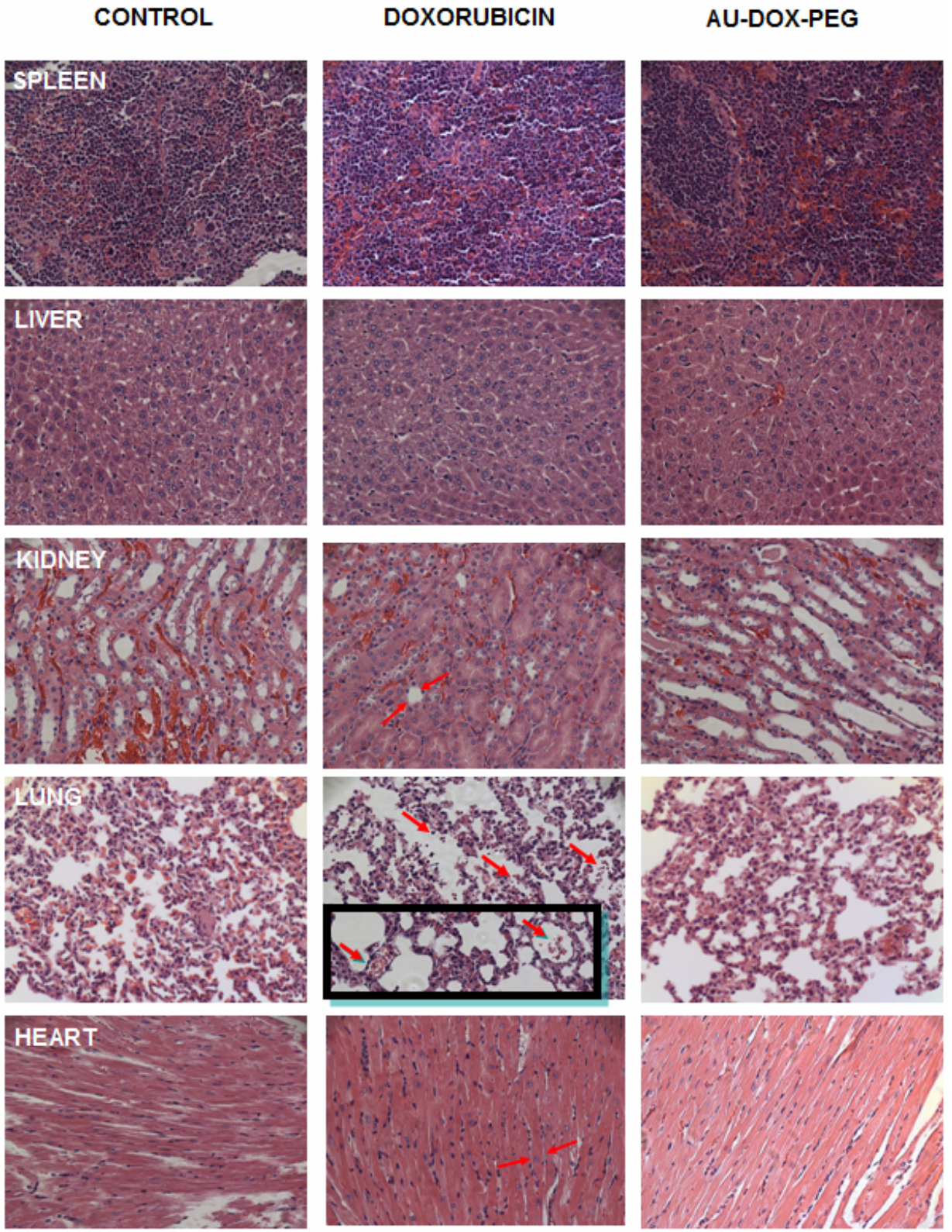

(d)

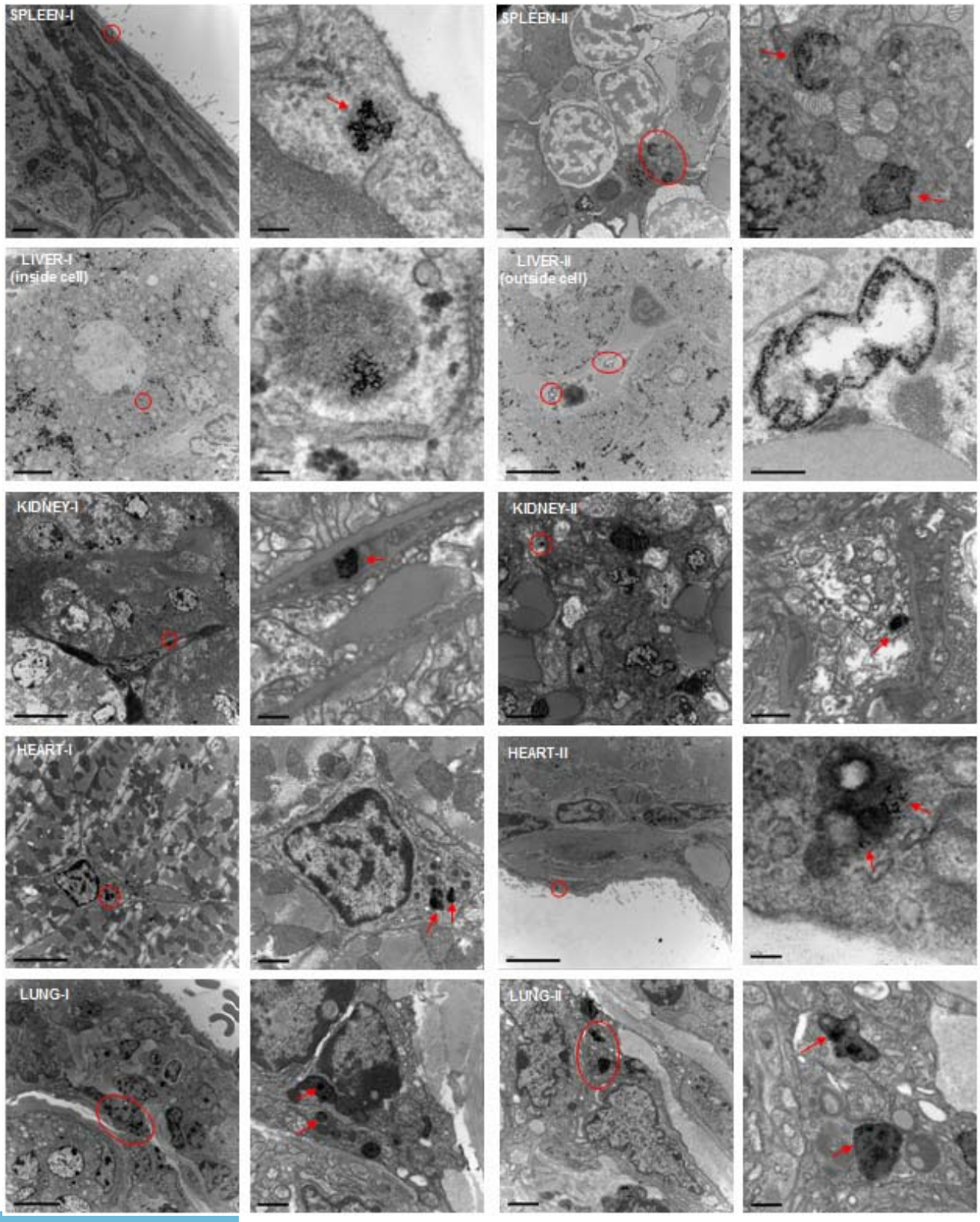

(e)

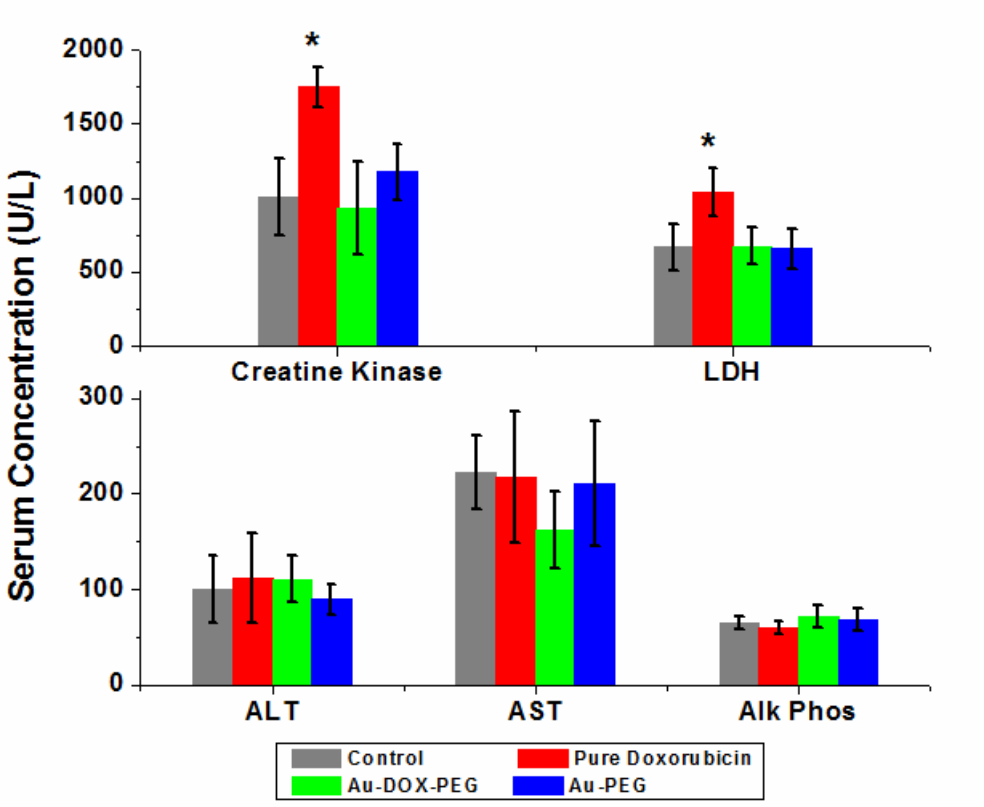

Figure 4.8. Biodistribution of Au-DOX-PEG in Various Organs and Low Toxicity After 2 weeks of Treatment (a) ICP-MS analysis of gold: the size resulted in high accumulation of Au-DOX-PEG at tumor site compared to other non-tumor sites (b) Au-DOX-PEG uptake in spleen and liver (c) Hematoxylin & Eosin staining of extracted organs after treatment (d) TEM images of various organ after Au-DOX-PEG administration [*Spleen*: Red blood cells are seen (polychromatophillic). ; *Liver*: Dark spots are glycogen granules. Gold nanoparticles are mostly inside the blood vessel cells (outside the cell) and some are seen inside the liver cell near the nucleus. ; *Kidney*: Some are inside the blood vessel cell and others are inside some cell. ; *Heart*: Gold nanoparticles are inside an irregular-shaped cell in between the heart muscle fiber. Some gold nanoparticles are in the cavity/muscle lignin of the heart.; *Lung*: Gold nanoparticles are overall inside the blood vessel (outside the lung cell).] (e) Blood serum analysis [*=P<0.05; LDH=lactate dehydrogenase; ALT= alanin transaminase; AST= aspartate aminotransferase; Alk Phos= alkaline phohphatase]

A successful drug delivery system not only exerts therapeutic efficacy but also reduces systemic toxicity when administered. Compared to pure doxorubicin, it is

important to note that Au-DOX-PEG system lacked any apparent toxicity in vital organs. Due to its small size, Au-DOX-PEG accumulated throughout the various organs, including tumor, in the system (Figure 4.8(a), (b)), consistent with the literature results. The smaller size and longer circulation time results in accumulation of Au-DOX-PEG at non-tumor sitesand concerns for toxicity at normal, healthy cells arises. However, as shown in Figure 4.8 (c), Au-DOX-PEG in spleen, liver, heart, kidney, and lung did not display any apparent toxicity compared to the Control (untreated) mice. Pure doxorubicin also did not display any apparent toxicity in the spleen and liver. However, pure doxorubicin treated mice displayed toxicity particularly in the heart, kidney, and lung. Edema, swelling of cells, was present in kidney for Doxorubicin group where nephric tubules exhibited swelling, along with congestion of renal glomeruli and narrowed Bowman's space. For heart, interstitial edema was seen for Doxorubicin group that swelling was present for heart muscle fibers. For lungs, red blood cells were present within the alveoli sac space for Doxorubicin group, in contrast to clear alveoli sac space of the Control and Au-DOX-PEG groups.

The inflammatory and oxidative response can be obtained by analyzing the blood serum. For example, when there is damage to the liver, there is an increased expression of certain immunological proteins in the blood that can be detected by serum analysis. Serum protein analysis results seen in Figure 4.8 (e) complements our toxicity results found in histological results. Serum proteins such as ALT, AST, and Alkaline phosphatase can be used to measure liver toxicity. Here, there were no significant differences amongst control (untreated), doxorubicin, Au-DOX-PEG, and Au-PEG groups for each ALT, AST, and Alkaline phosphatase level. This indicates minimal

toxicity to the liver, which is consistent with the histology results shown in Figure 4.8 (c). Similarly, kidney and heart toxicities seen in Doxorubicin group are further complemented with the serum protein profile results. Kidney toxicity can be measured through total bilirubicin, creatinine, and LDH levels, whereas heart toxicty can be measured via creatine kinase and LDH. Creatinine (~0.2 mg/dl) and total bilirubicin (~0.15 mg/dl) levels for all experimental groups were similar, but increased LDH level in Doxorubicin group suggests kidney toxicity in doxorubicin treated mice. Moreover, increased creatine kinase and LDH levels in Doxorubicin group also suggests cardiotoxicity in doxorubicin-treated mice, as evidenced in histology sections.

We believe that the pharmacokinetics of the encapsulated doxorubicin influences the toxicity profile of such formulation of Au-DOX-PEG. It is the competition between the tumor accumulation rate and the drug release rate that it is preferable for the drug to be released after significant amount of drug carrier has accumulated at the tumor site to exert its therapeutic effect and minimize any side effects to normal, healthy cells.

No apparent toxicity from Au-DOX-PEG system comes from change in pharmacokinetics and biodistribution of doxorubicin that was linked via pH-sensitive linker to gold nanoparticle. One hypothesis is that for our Au-DOX-PEG system, the slow, controlled release of the drug (Figure 4.3) resulted in no apparent toxicity in vital organs. If you manipulate the drug release rate, you can reduce the toxicity at healthy organs and not interfere with therapeutic activity of Au-DOX-PEG. Other hypothesis is that due to increased vascular permeability at the tumor site [193], Au-DOX-PEG accumulates more rapidly with higher concentration at the tumor site compared to non-tumor sites. Indeed, as seen in the ICP-MS results from Figure 4.8 (a), majority of gold

was concentrated at the tumor. Less than 16% of total single injected gold went to spleen and liver, whereas less than 1.5% of the total single injected gold went to kidney, lung, and heart. Addition to the small amount of total gold accumulating in the vital organs, the ultra-structural differences between tumor and vital organs have resulted in no apparent toxicities at non-tumor sites. As mentioned earlier, increased permeability and retention effect at the tumor site resulted in a toxicity or therapeutic efficacy toward cancer cells for Au-DOX-PEG. Due to their leaky vasculatures, Au-DOX-PEG is easily extravasated to access cancer cells. In contrast, normal, healthy cells have tightly regulated blood vessels (smaller pore size cutoff of 2-6nm) that transport of nanoparticles are restricted and Au-DOX-PEG have less chance of accessing the healthy, normal cells [26]. Furthermore, combined with clearance of Au-DOX-PEG within the normal tissues due to functional lymphatic drainage (unlike tumor lymphatics) might have reduced the exposure of Au-DOX-PEG to the vital organs. Also seen in the TEM images (Figure 4.8 (d)), most of the Au-DOX-PEG in vital organs are contained within the blood vessels or macrophages outside the cells, unlike the tumor.

Finally, there also has been a controversy for *in vivo* toxicity exerted by differently sized gold nanoparticles themselves. Indeed, it is hard to conclude what is the exact size of the gold nanoparticle to result in toxicity. Toxicity not only depends on the size of the nanoparticle but also depends on the surface-ligand chemistry, charge, shape, chemical composition of the particle itself, and the route of administration. The *in vivo* study done by Chen, Y et al. indicates no inherent toxicity exerted by the naked 5nm gold nanoparticles [198]. On the other hand, 13nm PEGlyated gold nanoparticle induced acute inflammation and toxicity to liver [199]. Similarly, Terentyuk G. et al. also reports

toxicity exerted by 15nm PEGylated gold nanoparticle in rabbit organs after intravenous injection [61]. They found that 15nm PEGylated gold nanoparticle resulted in hemodynamic disorders (congestion of the blood) in liver and spleen, along with thickening of kidney basal membrane. Niidome et al. have shown that the toxic potential is triggered by the surface modification of the gold nanoparticles. In fact, bromide-stabilized gold nanorods induced severe cytotoxicity in HeLa cells, whereas PEG-modified gold particles, which displayed a neutral surface, could only induce moderate toxicity [51]. Nevertheless, Connor et al. demonstrated that neither the surface characteristics nor the size of gold nanoparticles seemed to play a role in inducing cytotoxicity in the human leukemic cell line K562 [47]. Connor et al. stated that 4, 12, 18nm gold nanoparticles with various surface modifiers were not inherently toxic to human cells, despite being taken up by the cells. Similarly, Shukla et al. found that 3.5nm gold nanoparticles lacked toxicity towards macrophages but reactive oxygen and nitride species were observed [48]**.** For extremely small-sized gold nanoparticles or gold clusters (less than 2nm in diameter), Pan et al. and Tsoli et al. stated that they are toxic to cells [45, 46]. As far as we are concerned, our 5nm core Au-DOX-PEG gold nanoparticle did not display any apparent toxicity to the vital organs when administered in high dosage via tail-vein. This is evident in the MTT assay, serum anlaysis, and histology results in Figure 4.4 and Figure 4.8.

4.5 CONCLUSION

We took a "tumor activated prodrug therapy" approach, where drug bound to the gold surface remains inactive until it reaches the acidic tumor site or intracellular environment, where change in pH triggers the release of doxorubicin via cleavage of

hydrazone bond. We took doxorubicin as a model drug to test the feasibility of using small-sized 5nm gold nanoparticle for drug delivery applications. The water-soluble Au-DOX-PEG resulted in similar toxicity to cancer cells as pure doxorubicin *in vitro*. However, when tested *in vivo*, high concentration of Au-DOX-PEG accumulated at the tumor site via EPR effect to result in therapeutic efficacy. Unlike the pure doxorubicin, Au-DOX-PEG did not result in any apparent toxicity to vital organs.

The success of Au-DOX-PEG system resulted from (1) "high" accumulation at the tumor site compared to other non-tumor sites, (2) ideal spatial distribution and successful penetration at tumor site (i.e. Au-DOX-PEG were present both inside and outside the cancer cells), and (3) slow, controlled release of drug via pH-sensitive linker (i.e. state of the drug), all owing to the small size scale of the system. The small size of the system, along with PEGylation, gave prolonged blood circulation time to result in high accumulation of at the tumor site. Also, the small size scale allowed Au-DOX-PEG to easily extravasate into the tumor environment to result in therapeutic efficacy. The slow, controlled release of drug and high accumulation at the tumor site resulted in no apparent toxicity at vital organs, whereas pure doxorubicin displayed heart, kidney, and lung toxicity. Thus, our results demonstrated that functionalized 5nm gold nanoparticle-based drug delivery system represents a highly attractive candidate as a potential drug delivery carrier for cancer nanotherapy.

CHAPTER 5

SIZE-DEPENDENT BIODISTRIBUTION AND CLEARANCE OF GOLD NANOPARTICLE

5.1 ABSTRACT

Here, we closely looked at the size-dependent biodistribution and clearance of both 5nm and 60nm gold nanoparticle systems. In addition to therapeutic efficacy of colloidal gold system, it is important to study the long-term clearance and the fate of the delivered colloidal gold system for *in vivo* applications. Compare to the short blood circulation half time (9 hours) for 60nm gold system, 5nm gold system resulted in a longer circulation half time (1.6 days). Larger 60nm gold nanoparticles were mostly uptaken in the liver and the spleen, whereas smaller sized 5nm gold nanoparticle was visible in the various organs in the system, especially resulting in pigmentation in the skin and the lymph nodes. Size dependent clearance was observed that 5nm gold system was excreted via renal and hepatobiliary pathways, whereas 60nm gold was mostly retained in the spleen and liver after 6 months. Thus, 5nm gold system is a potential candidate for biomedical applications, where 5nm gold core displays inherently different biodistribution and clearance characteristics than larger nanoparticles.

5.2 INTRODUCTION

The unique physico-chemical properties of nanoscale particles results in an increased reactivity with the biological systems that it renders different effects in the system compared to the larger, bulk materials. It is important to know the distribution and the effects of absorbed nanoparticle in various organs after an exposure. Moreover, it is

important for the particle to be delivered to the desired, targeted site, such as tumor for drug delivery applications, and "size" plays a critical role.

Generally, when the system is injected with the nanoparticle, it is uptaken by the reticulo-endothelial System (RES) such as spleen or liver [200]. The surface modification of the nanoparticle can change the dynamics of nanoparticle circulation time that various coating techniques can be adopted to prolong the circulation time of the nanoparticle in the blood. In particular, coating the surface of the nanoparticle with hydrophilic polymer such as poly(ethylene glycol) or PEGylation can render "stealth" characteristics to the nanoparticles, thus resulting prolonged circulation time [169, 201]. Moreover, the circulation time of this the nanoparticle not only depends on the coating but also depends on the core size of the nanoparticle. Consequently, the circulation time of the nanoparticle will affect the distribution and efficacy of the nanoparticle within the system, especially for intravenously injected nanoparticles.

Currently, several studies have been reported on the size-dependent biodistribution and clearance of gold nanoparticles. There is a correlation between size and biodistribution of nanoparticles. Generally, nanoparticles with size less than 10nm gets distributed throughout the system, whereas larger particles like ~60nm is mostly confined to the liver and spleen after intravenous injection [49]. Furthermore, in detailed studies on various nanoparticle size and its distribution confirm that majority of nanoparticles accumulated in the "liver" and "spleen" regardless of size (1.9nm~250nm), shape (sphere or rod), type (carbon nanotube, quantum dots, iron oxide, gold nanoparticle), and dose of exposure (0.01~2700 mg/kg) after intravenous injection [18, 49-51, 53, 56, 57, 59-62, 199, 202-204]. Thus, if all the particles accumulate and

distribute in a similar manner despite of size, shape, and dose, then "clearance" plays a critical role that determines the success of the nanoparticle for *in vivo* applications.

After delivering the therapeutic or imaging agent with a nanocarrier to the target site, it is desirable to see the delivery vehicle to clear out from the body, minimizing any harm to the healthy, normal cells. It has been reported that larger particles such as 20nm gold nanoparticle is minimally excreted through feces and urine that there is significant and persistent accumulation of gold nanoparticle in the liver and spleen through intravenous exposure [202]. Similarly, metal-based 13nm quantum dot showed accumulation in kidney but there was no urinary excretion up to 28 days after the injection in mice [63]. Also, 40nm gold nanoparticle was removed from the circulation primarily by Kupffer cells in the liver and remained as clusters even after six months [204]. In contrast, particles with less than ~6nm in diameter displayed clearance from the system. For example, 77% of the injected 1.9nm gold nanoparticle was rapidly cleared through the kidney and excreted 5 hours after the intravenous injection in the mouse [56]. Similarly, Choi et al showed rapid clearance of zwitterionic coated quantum dots (4.36-5.52nm) through kidney and urinary excretion within 4 hours after the intravenous injection. Based on these findings, we believe that nanoparticle "size" plays a critical role for not only delivering the drug delivery system to the target site but also determining the *in vivo* behavior such as clearance and distribution of the nanoparticle throughout the body [64]. However, there is no golden standard for the optimal size to be used in cancer nanotechnology and it is still debatable.

In this study, we look closely at the special properties inherent to 5nm gold nanoparticle, compared to the larger 60nm gold nanoparticle. It was found that 5nm gold

nanoparticle distributed throughout the system, slowly clearing out of the system with time via urine and feces. Furthermore, it was found that lymphatic system was involved in the clearance of 5nm gold nanoparticle. In contrast, the larger 60nm gold nanoparticle system steadily accumulated in the spleen and liver at a greater amount than the 5nm system over time and showed decreased clearance from the system in long term. Thus, we *hypothesize* that it is the "nano-size scale", under the renal and urinary excretion threshold, of the polymer-gold system that is responsible for clearance of polymer-gold system over time. This study will provide insight on specific size of nanoparticle that could be applicable for other nanoparticle delivery systems.

5.3 MATERIALS AND METHODS

Materials

Chemical Reagents

Citrate-stabilized gold colloids, 5 nm and 60nm in size, were obtained from Ted Pella, Inc. (Redding, CA). Poly(ethylene glycol) (CH_3O-PEG-SH) of molecular weight 5000 was purchased from Rapp Polymere (Germany). Mili-Q deionized water (Millipore, 18.2 MΩ cm^{-1}) was used throughout the experiments. All of the products were used without modification or purification unless as noted.

Instrumentation

Nanoparticle surface charge (zeta potential) and size were measured by ZetaSizer Nano-ZS90 (Malvern Instrument). Adsorption spectra were obtained through ultraviolet-visible spectrophotometer (Beckman Coulter DU530). Gold content was analyzed by ICP-MS (HP 4500, Agilent Technologies). TEM were taken by using Hitachi H7500 high-magnification electron microscope.

Mouse Model

5-6 weeks old CrTac: NCr-Foxn1^{nu} male nude mice were obtained from a commercial vendor (Taconic). The protocols were approved by the Institutional Animal Care and Use Committee (IACUC) of Emory University.

Statistical Analysis

Statistical analysis was performed using one-way ANOVA followed by multiple comparison Bonferroni's test. Data were collected from at least three different animals and $P<0.05$ was considered statistically significant.

PEGylation of colloidal gold

Methoxy thiol-PEG (MW 5000) solution was added drop-wise to the colloidal gold solution. PEG solution was added accordingly to correspond to a complete coverage for PEG monolayer on gold particle surface. Simple geometric calculations showed that each thiol-PEG occupied a footprint area of 0.35 nm^2 on the gold surface, consistent with the literature data reported for brush conformation of thiol-PEG. Excess of 10-20 fold PEG solution was added to the colloidal gold to ensure stability of gold colloids against aggregation under various *in vivo* conditions. The resulting 5nm and 60nm gold-PEG solutions were centrifuged to remove any unbound thiol-PEG. Then UV-vis spectrometer, DLS, and zeta potential were used to characterize the system.

Blood, urine, and feces collection

Blood was drawn from the cheeks of the mice at different time points (1, 5, 10, 30 minutes; 1, 2, 4, 8, 20, 30 hours; 2, 3,4,5,6,7…25 days). Blood was weighed then further digested in nitric acid for ICP-MS analysis. Similarly, urine and feces were collected at different time points (30 minutes; 2.5, 4, 7.5 hours; 1,2,3,4….25 days). Note that urine

and feces were collected at specific time points and was not cumulative. Collected urine and feces were weighed then further digested in nitric acid for ICP-MS analysis.

***In vivo* study of biodistribution and clearance**

Due to the nature of long term clearance and biodistribution study, non-tumor bearing nude mouse will be used with PEGylated 5nm and 60nm gold nanoparticles. Mice were divided (n=4) randomly into three groups of control, 5nm, and 60nm groups. Equal concentration of gold (0.04g/kg of body weight) was injected once for both 5nm and 60nm groups via tail vein. Mice were housed in sterile cages and any abnormal changes in body weight and behavior were observed every day. After the single injection, critical time points such as 1, 3, 10, 20, 35, 60, 90, and 180 day were chosen for harvesting organs (heart, kidney, liver, lung, brain, spleen, and skin) to quantify any gold concentration changes over time. Concurrently, pictures will be taken to document any skin and lymph node color changes over time. Presence of gold in various organs was verified by ICP-MS and TEM.

5.4 RESULTS AND DISCUSSION

PEGylation of Gold Nanoparticle and Blood Circulation Time

For biocompatibility and colloidal stability, 5nm and 60nm gold nanoparticles were coated with thiolated methoxy-PEG (MW 5000). The resulting gold nanoparticle had an average hydrodynamic size (diameter) of 18.2 ± 0.9 nm with a surface charge (zeta potential) of -5.04 ± 0.6 mV for 5nm gold nanoparticle system, whereas 60nm gold nanoparticle system had 78.5 ± 1.2 nm for average hydrodynamic diameter and -14.5 ± 1.4 mV for zeta potential. The resulting gold nanoparticle was injected once through the mouse tail vein to study the pharmacokinetics and its behavior.

After a single tail vein injection, blood samples were collected for 5nm gold nanoparticle system at various time points (between 0 and 25 days) from the mouse cheek, and ICP-MS was used to measure the gold concentration in blood. Using a simple mono-exponential decay model, the experimental data were fitted to result in a half decay time ($t_{1/2}$) of ~1.6 days for the PEGylated gold nanoparticle. This is consistent with the previous literature reports where small-sized gold nanoparticles (1.4 nm and 15nm in diameter) resulted in high blood concentrations even after 24 hours after the intravenous injection [60, 205].

It has been reported that surface modification with long-chain PEG (with molecular weight of ≥2000 Da) significantly reduces protein adsorption on a surface [169], which in turn increases the circulation time of the nanoparticle in blood. The so-called "non-fouling" or protein resistant surface is controlled by two principles of 1) terminal hydrophilicity of the head group combined with 2) formation of a dense but disordered PEG brush with significant penetration of water into the PEG layer [171]. As seen in the TEM image from Figure 5.1, it is this thick and high surface density of PEG layer on the gold surface that resulted in a long blood circulation time. It has been reported that smaller gold nanoparticle (10nm) resulted in a higher surface density of the adsorbed single-stranded DNA compared to the larger gold nanoparticle (50nm) by 13 times [206]. Thus, it is the nature of the small 5nm gold nanoparticle core that resulted in dense "brush" configuration layer of PEG to minimize opsonization (adsorption of blood protein). Additionally, it is the non-targeted nature of the particle that resulted in a longer circulation time. It has been reported that targeted ligand exposed on the surface can accelerate the opsonization process [196, 207]. Finally, high concentration of small gold nanoparticle in the blood stream have possibly saturated the reticuloendothelial system (RES) and retarded the uptake by the RES. In comparison, larger gold nanoparticle of 60nm core that has been PEGylated (MW 5000) resulted in a half decay time of 9 hours (not shown). Thus, our 5nm core gold nanoparticle system resulted in ~4 times increase

in half decay time compared to 60nm, having more advantage for the EPR effect for tumor accumulation.

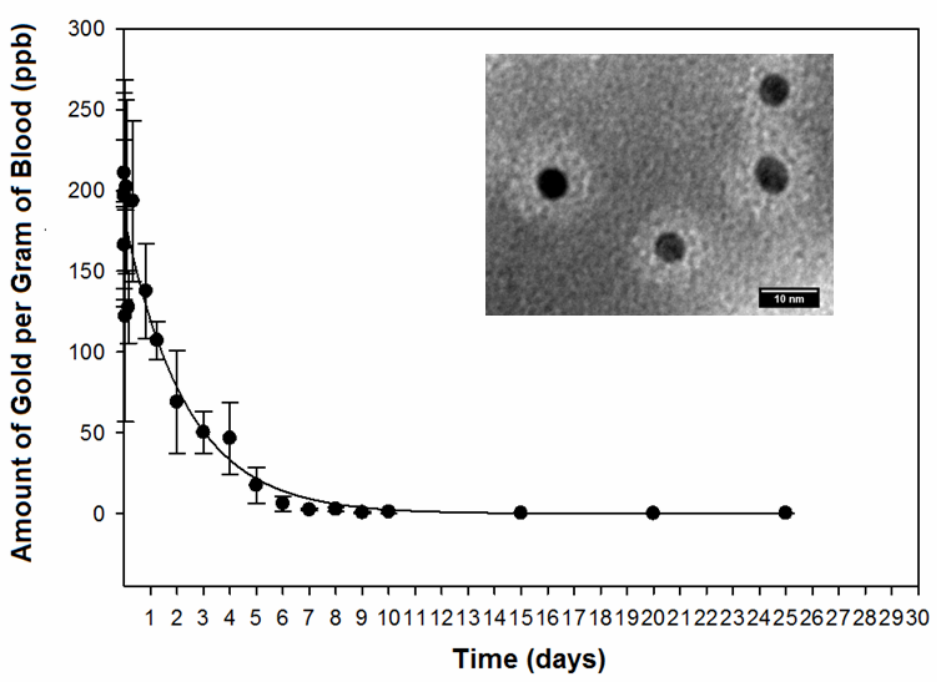

Figure 5.1. Blood Circulation Half Life of 5nm Gold Nanoparticle (~1.6 days)

Biodistribution of Gold Nanoparticle in Skin and Pigmentation

Skin is the largest organ in the body. Here, skin is used as a semi-quantitative assessment measure that is related to the gold concentration inside the body. It was found that internal gold concentration was related to the degree of visible skin pigmentation. The skin pigmentation qualitatively measures and reflects the gold distribution and clearance within the system that has been injected with 5nm gold nanoparticle.

The deposition of cutaneous gold occurred in the reticular and papillary dermis in the absence of inflammatory change. Most of the gold nanoparticles were confined in the dermal macrophage, inside a lysosome, in an aggregated form as seen Figure 5.2.

The following skin pigmentation was due to presence of 5nm gold nanoparticle and was not a melanin-induced pigmentation. The mice used for this experiment were derived from an albino mouse (i.e. lacking melanin pigmentation) and further examination of epidermis under TEM confirmed the absence of melanin granules in the mouse skin. Thus, this reversible skin pigmentation was solely due to injection of 5nm gold nanoparticle. We believe that reversible characteristic (i.e skin darkening then lightening) is due to the clearance of small-sized 5nm gold nanoparticle over time (as seen in next section). Interestingly, the skin pigmentation was also size dependent. When equal amount of gold concentration of 60nm gold nanoparticle was injected, no skin pigmentation was present in the 60nm gold injected mouse (Figure 5.2).

For humans, it has been reported that high concentration of crystalline and amorphous gold "salt" (not nanoparticle) ingestion leads to an "irreversible" skin pigmentation called "chrysiasis". Similar to the mouse skin pigmentation seen in our experiment, chrysiasis is characterized by the grayish-blue pigmentation of the skin but is "irreversible". Also, unlike our mouse skin pigmentation, chrysiasis skin pigmentation preferentially occurs in the areas of sun exposure, where metal deposits stimulate melanin production [208].

To our knowledge, we are the first team to report the mouse skin pigmentation which qualitatively correlates to internal biodistribution and clearance of gold nanoparticle over time. Sonavane et al. reported that *in vitro* experiments revealed size-dependent gold nanoparticle accumulation in rat skin [209]. Similar to our results, Sonavane et al. reported that compared to the larger size gold nanoparticles, small-sized gold nanoparticle (15nm) displayed higher permeation and accumulation in the dermis

and epidermis of the rat skin. Furthermore, Semmler-Behnke et al. briefly mentions high accumulation of 1.4 nm gold nanoparticle in the subcutaneous fatty tissue, which could not be explained. However, both papers mentioned gold nanoparticle accumulation in the skin, but not skin pigmentation [205].

(a)

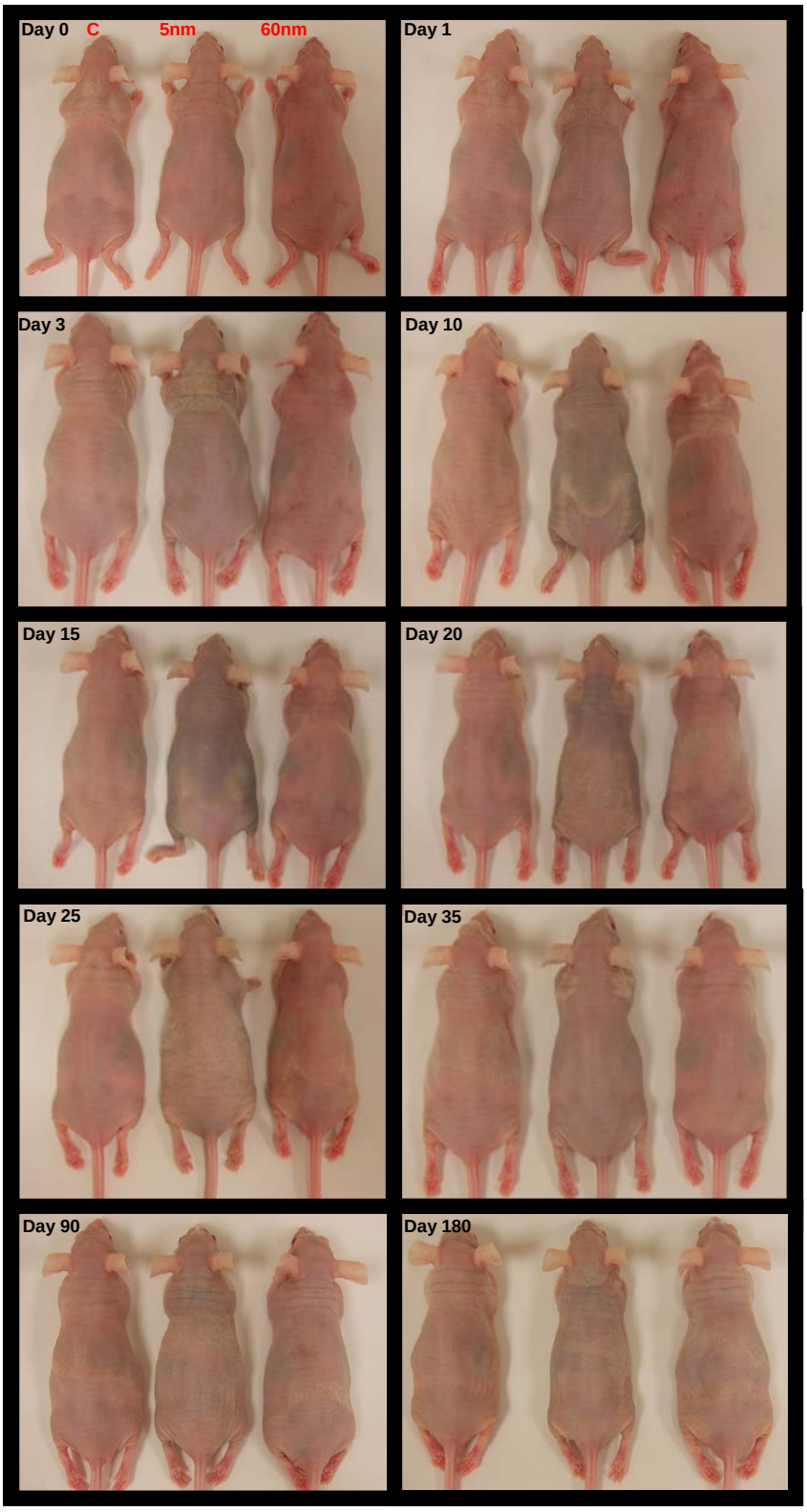

(b)

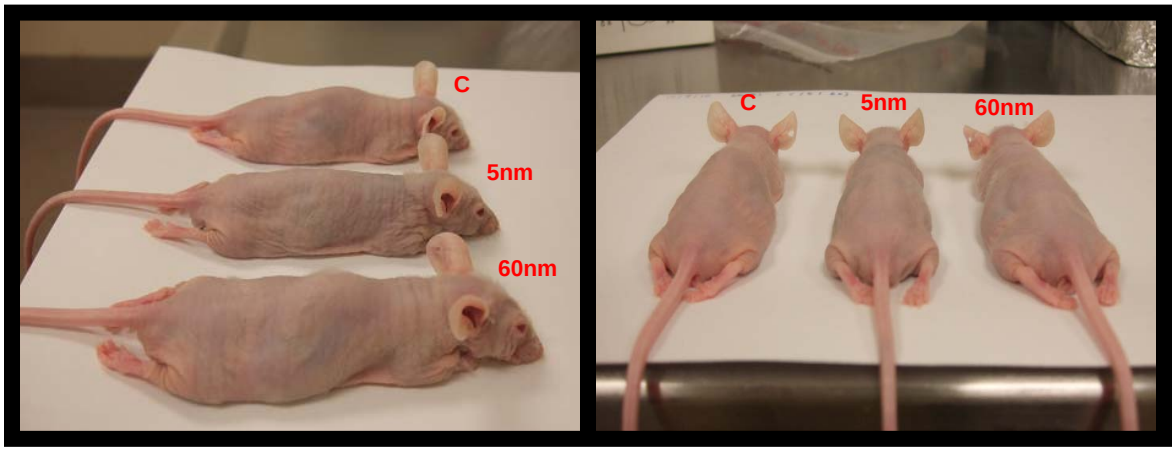

(c)

5nm 3D

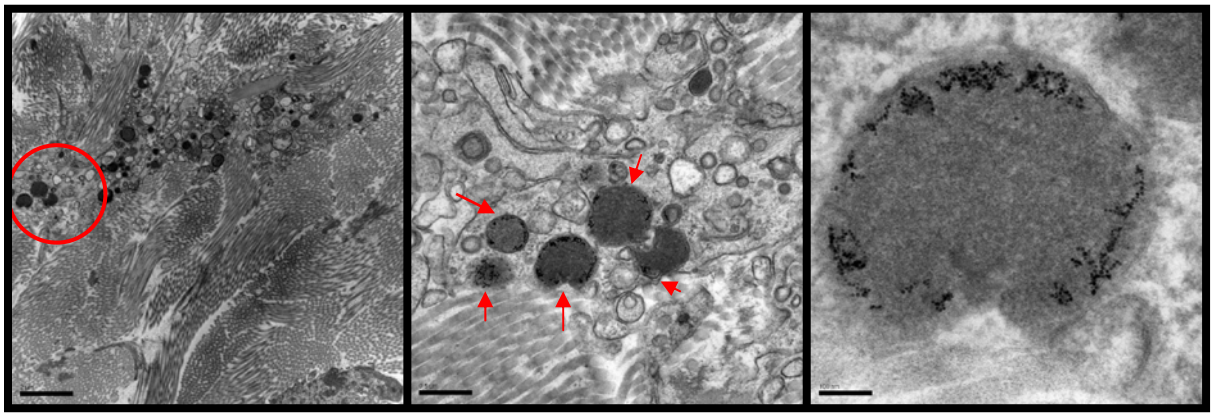

5nm 6M

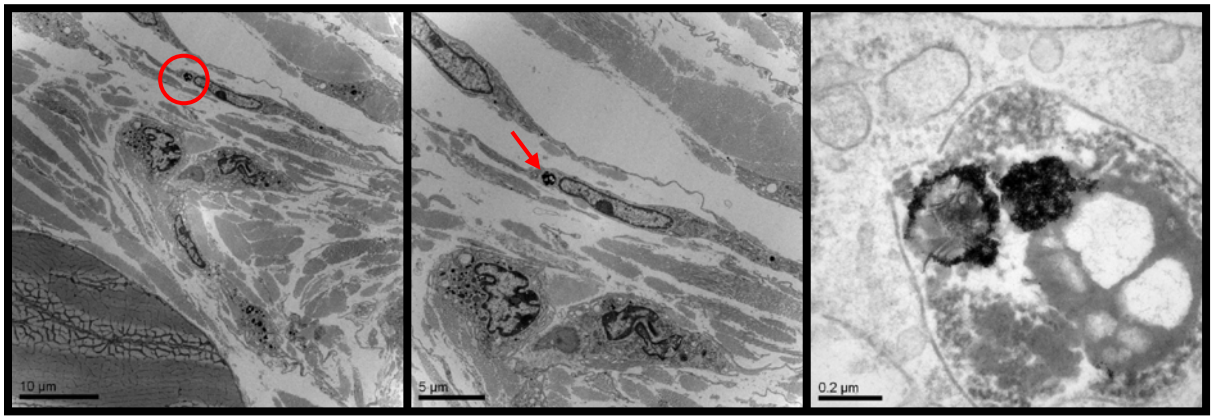

(d)

60nm 10D

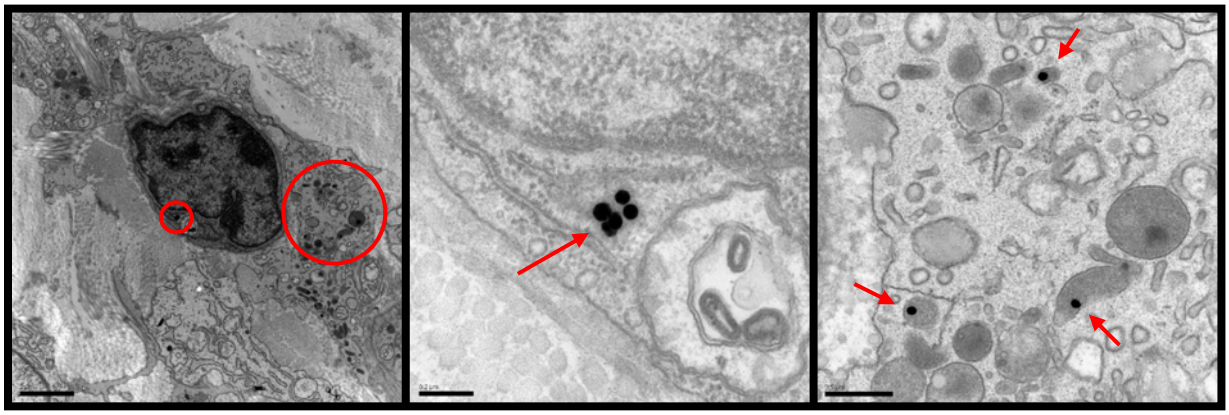

60nm 6M

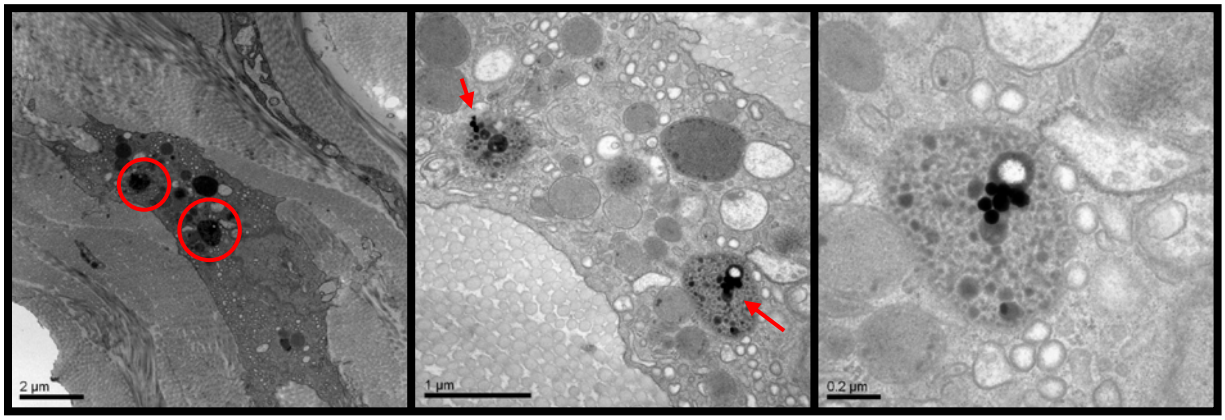

Figure 5.2. Gold Nanoparticle Induced Skin Pigmentation and Qualitative Monitoring of Distribution of 5nm versus 60nm Gold Nanoparticle (a) Skin Color Change versus Time Picture (in order of Control vs. 5nm vs. 60nm) (b) 6 month multi-view of Control vs. 5nm vs. 60nm (c) TEM images of 5nm gold nanoparticle inside the skin around the head area for 3 day and 6 months (d) TEM images of 60nm gold nanoparticle inside the skin around the head area for 10 day and 6 months

Despite same concentration of gold was injected for both 5nm and 60nm, the mouse injected with 60nm gold lack skin pigmentation due to its large size. As seen in Figure 5.2, the TEM images reveal that only few number of particles actually reach the dermis of the skin. Due to its large size, 60nm is not readily diffused to the dermis like the small-

sized 5nm gold. Moreover, for both 5nm and 60nm, gold nanoparticles were only visible within the dermis layer, which is in proximity to the blood vessel. Based on the observation via TEM, deeper layers of dermis (closer to blood vessel and muscle layer), you see more gold. Gold nanoparticles were confined in an irregular-shaped cells, suspected to be a type of a macrophage, inside a lysosome.

Also, gold distributes in different patterns within skin over time for 5nm gold nanoparticle system. At the beginning, the gold spreads out evenly throughout the body, giving an even pigmentation in the skin. Then as the gold gets cleared out from the body, gold tend to concentrate more around the head and the buttocks area, and the dark pigmentation line appeared on the sides of the mice. The ICP-MS data in Figure 5.3 was measured by taking three points in the body (head, torso, and buttocks), then averaged the ICP-MS values for each time point.

Biodistribution of 5nm Gold Nanoparticle versus 60nm Gold Nanoparticle in Various Organs

There was a size-dependent biodistribution of gold nanoparticles within the system (Figure 5.3). In general, smaller 5nm gold system resulted in a wide spread of gold in various organs with total gold mass being liver > spleen> kidney> lung> heart, skin, lymph> brain at day 180. Although, the spleen exhibited higher capacities per gram of tissue (ng/g or ppb) for gold nanoparticle uptake, the liver took up the majority of the nanoparticle due to its larger mass. The amount of 5nm gold system in the liver did not decrease significantly until day 35. After day 35, significant amount of 5nm gold system was cleared out from the liver. The gold in the liver decreased from 263.66 ± 66.14 ng/g at day 35 to 142.43 ± 19.71 ng/g ($P<0.05$) at day 90 and further decreased to 53.39 ng/g at day 180 (n=1 for day 180). For spleen, significant decrease in gold was also observed

after day 35. The gold in the spleen decreased from 832.99 ± 138.57 ng/g at day 35 to 509.43 ± 27.57 ng/g ($P<0.05$) at day 90 and further reduced to 291.8127 ng/g at day 180 (n=1 for day 180). Interestingly, the amount of total gold in the lymph also decreased significantly after day 35 that gold decreased from 494 ± 33.91 ng/g at day 35 to 228.36 ± 25.2 ng/g at day 90 ($P<0.05$) and further reduced to 48.13 ng/g at day 180 (n=1 for day 180). For heart, kidney, lung, and skin, there was more gradual decrease in gold over time. Small amount of 5nm gold system was detected in the brain but it was less than 0.1% of the total injected dose. Approximately 44% of the total injected dose was uptaken by the liver and spleen at 3 day (36% in the liver and 8% in the spleen). After 180 days, approximately 15% of the total injected gold was detected in the liver and the spleen (10% in liver and 5% in spleen). Thus, the long-tern study in a naïve, non-tumor bearing mice study indicated that the majority of 5nm gold system accumulated in the liver and spleen, and it gradually cleared out over time at day 180. Unlike the 60nm gold system, the unexpected bell-shaped biodistribution (Figure 5.3 (a) histogram for lymph, spleen, liver, and skin) of 5nm gold system would most likely resulted from the high concentration (0.04g Au/kg of body weight) of gold injected to the mouse. As reported by literature, high concentrations (0.85mg/kg of body weight) of small-sized 4nm gold were detected in the blood up to7 days and continuted to detect gold in the blood up to one month [210]. Similarly, our 5nm gold system resulted in a prolonged blood half-time (1.6 days) that most likely the high concentrations of 5nm gold system did not get fully uptaken by the various organs up to ~35 days from circulation. The animals remained healthy for the entire duration of the study (up to 180 days) and no observable signs of weight loss, behavioral changes, and toxicity were detected.

(a)

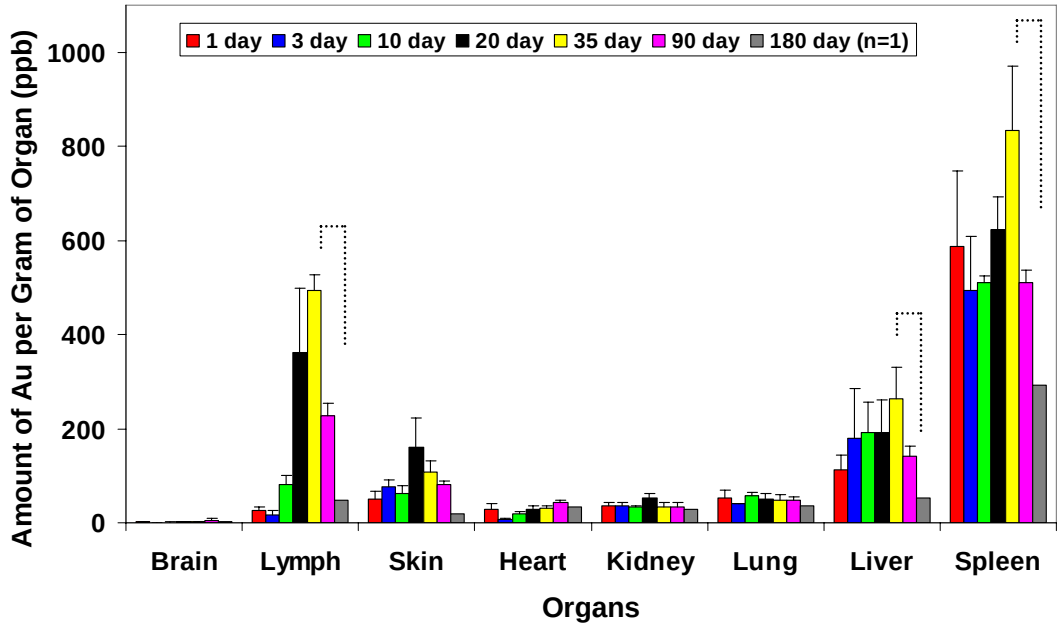

(b)

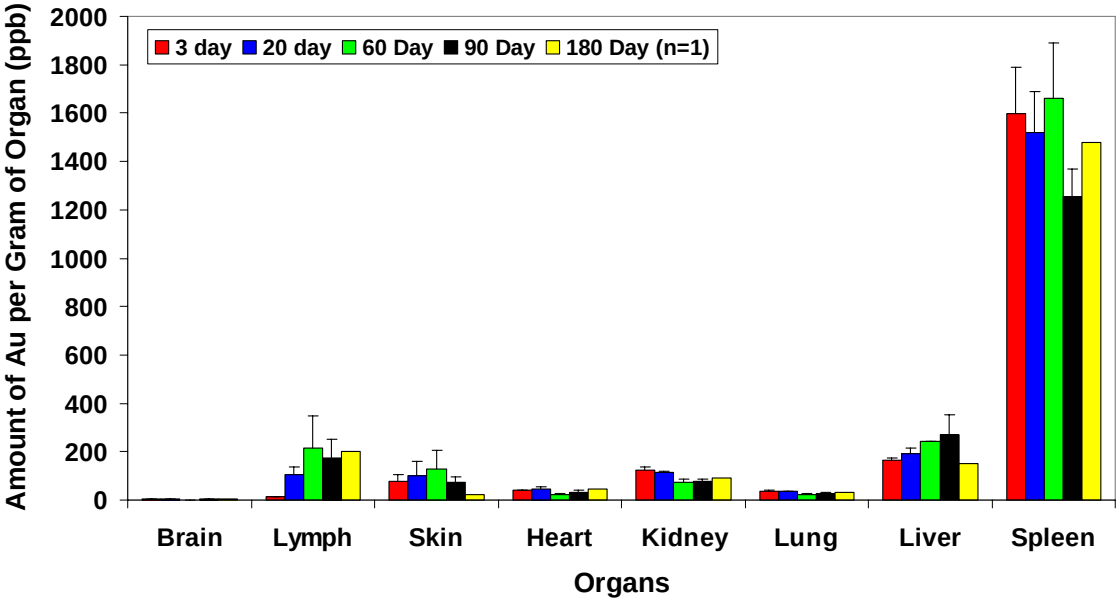

Figure 5.3. Biodistribution of (a) 5nm versus (b) 60nm Gold Nanoparticles in Various Organs up to 180 days (dashline: $P<0.05$)

60nm gold system also displayed similar biodistribution as 5nm gold system with highest uptake being the liver and the spleen. Overall, unlike the 5nm gold system, majority of gold was present in the liver and the spleen and much less so in other evaluated organs. Initially, approximately 60% of the total injected gold was uptaken by the liver and spleen (40% liver and 19 % spleen) at day 3. After 180 days of initial injection, there was no observable change in the amount of gold in the spleen (~23% of total injected gold). However, there was a slight decrease in the amount of 60nm gold system in the liver that the total injected gold decreased to ~37% after 180 days. The slight decrease in the gold concentration in the liver suggests hepatobiliary clearance of gold in the liver over time. Similar trend was seen for other organs (i.e. lymph, kidney, skin, heart, and lung) that there were no significant changes in the gold concentration over the span of 6 months. Consistent with the literature results, no gold was found in the brain for 60nm (but for 5nm gold system), which reflects the tight restriction of blood brain barrier for the passage of nanoparticles. It has been reported that particles smaller than 20nm in diameter results in translocation of nanoparticle into the brain, whereas the passage of larger particles (>50nm) into the brain is restricted [49, 52].

Even though *equal* gold concentration was injected for both 5nm and 60nm gold systems, small-sized 5nm gold system exhibited less uptake by the liver and the spleen. Furthermore, less gold was retained for 5nm gold system after 180 days that there was a significant decreased in the gold concentrations in the liver and the spleen, whereas 60nm gold system displayed minimal decrease and increased retention of gold in the liver and the spleen. We believe that the size plays a critical role in the biodistribution and clearance of the nanoparticle over time.

Indeed, previous literature supports our size dependent biodistribution and clearance results. It has been reported that when four different sizes of gold nanoparticles (10, 50, 100, and 250nm) were intravenously injected in rats, 10nm gold nanoparticles were found in all organs evaluated (total gold amount highest in liver> blood> spleen> kidney> lungs> brain> testis> heart) whereas 50, 100, 250 nm gold nanoparticles were almost solely distributed to liver, spleen, and blood after 24 hour of injection [49]. Similarly, when 15, 50, 100, and 200 nm gold nanoparticles were injected intravenously in mice, smallest 15nm gold nanoparticle resulted in a wide spread of gold in liver, lung, kidney, spleen, brain, heart and blood; particles larger than 50nm were mostly confined to the liver, lung, kidney, and spleen after 24 hours [60]. Finally, the accumulation of 1.4-nm gold nanoparticles in the liver and spleen was significantly lower compared to that of 18-nm gold nanoparticles where twice as more total injected gold accumulated in the liver and spleen for 18nm gold nanoparticle [205]. Similar to our 5nm gold nanoparticles, smaller 1.4nm resulted in wide spread in the system where 1.4nm gold nanoparticles accumulated in liver, lung, spleen, kidney, brain, heart, and skin in rat.

As seen with our 5nm versus 60nm gold system study, majority of gold was accumulated in the liver and the spleen. Previous studies reports accumulation of gold in the liver and the spleen for long durations of time regardless of size, shape, dose, and types of materials. 10-20nm carbon nanotubes in mice resulted in 80% and 5% of total gold in the liver and the spleen, respectively, at a nearly constant level throughout 28 days [211]. Single injection of 13nm quantum dot, coated with MW5000 methoxy PEG, resulted in accumulation in the liver (29-40% of the injected dose) and spleen (4.8-5.2% of injected dose) over 28 days [212]. Similarly, iron oxide (11 nm) injected in rats

resulted in 50 % and 25 % of injected dose in liver and spleen after 21 days [213]. When gold nanorods (65nm in length and 11 nm in width) were injected intravenously, 35 % of total gold accumulated in the liver and 2 % in spleen after 3 days [51]. Within 24hr, 18nm gold nanoparticle AuNP was completely removed from the blood and predominantly present in the liver (93.9% of injected gold) then in spleen (2.2% injected gold) [205]. Injected gold nanoparticles of four sizes (10, 50, 100, and 250nm) in rats resulted in accumulation mainly in the liver (20-46% injected dose) an spleen (1.2-2.2% injected dose) after 24 hours [49]. When 12.5nm gold nanoparticle was injected everyday for 8 days intraperitoneally, gold nanoparticles accumulated in various organs (amount of gold/ gram of tissue being spleen> liver=kidney> lungs> brain) with liver having the highest total % of injected gold [214]. For long term studies like ours, Sadauskas, E. et al. reported that intravenously injected 40nm gold nanoparticle was removed from the circulation primarily by the Kupffer cells in the liver and remained as clusters even after 6 months [58]. Study from a company called CytImmune also reported intravenous injection of 27nm gold nanoparticle coated with TNF-α and PEG in a tumor mouse model resulted in gold uptake by the liver and spleen (~35% of the total gold) at 120 days [197].

The significant and persistent accumulation of gold nanoparticle in liver and spleen through intravenous exposure could be due to their fenestrated, discontinuous endothelia which allow nanoparticles up to 100 nm in diameter to exit from the bloodstream into the parenchyma. In addition, organs of the reticuloendothelial system (RES) including the liver and spleen can efficiently accumulate nanoparticles via opsonization that nanoparticles could bind to antibody in the plasma and are subsequently

recognized by the phagocyte-rich RES [215]. Also, higher uptake in the liver could be due to (1) larger organ size and (2) the momentary saturation of the uptake capacity of the spleen, which allows uptake in the liver when high concentrations of gold nanoparticles are introduced in a bolus intravenous injection. From various studies reported in the literature, several factors such as particle size, their surface charge, surface hydrophobicity, and the presence and/or absence of surface ligand are responsible for particle uptake by the RES [200].

(a)

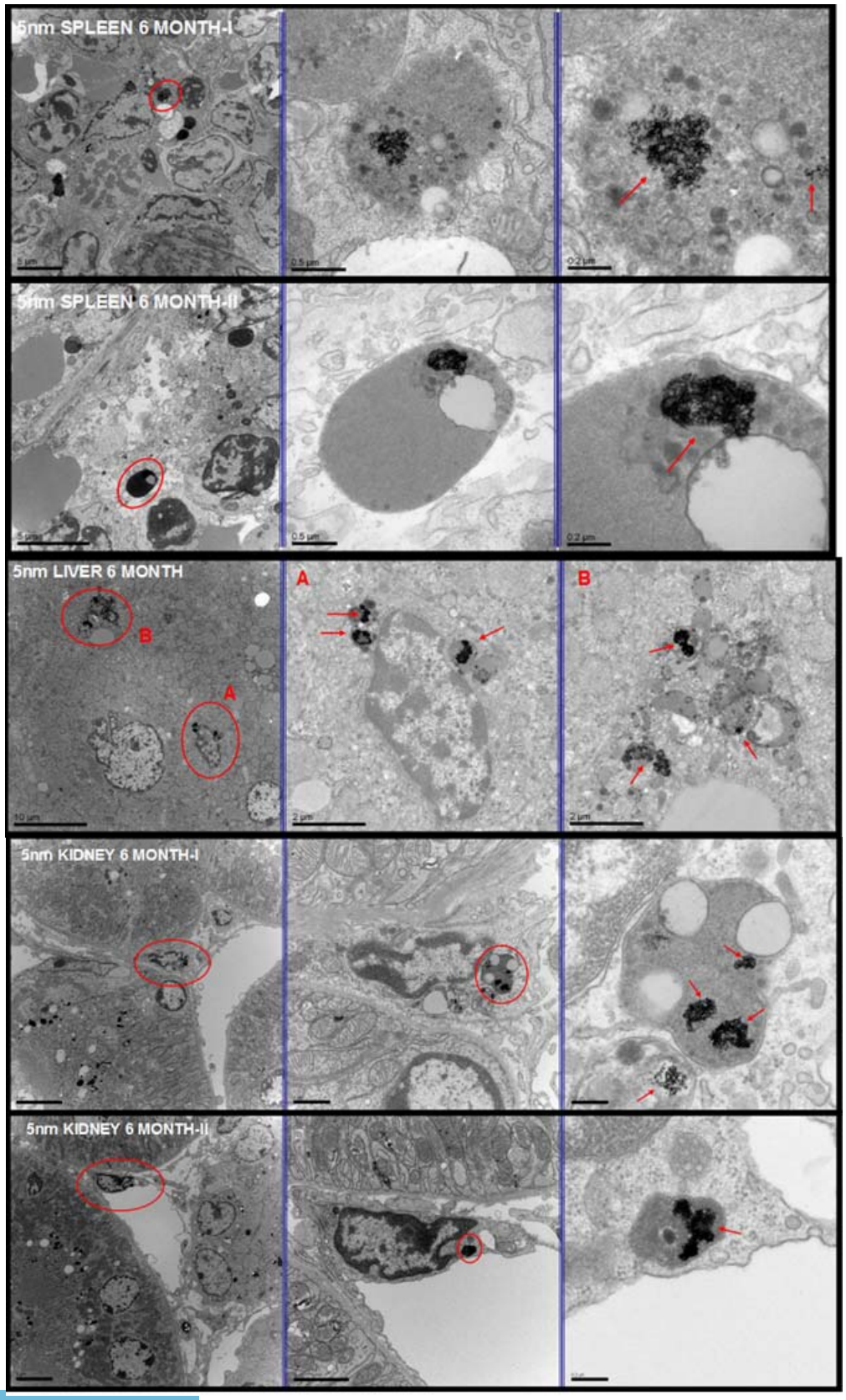

(b)

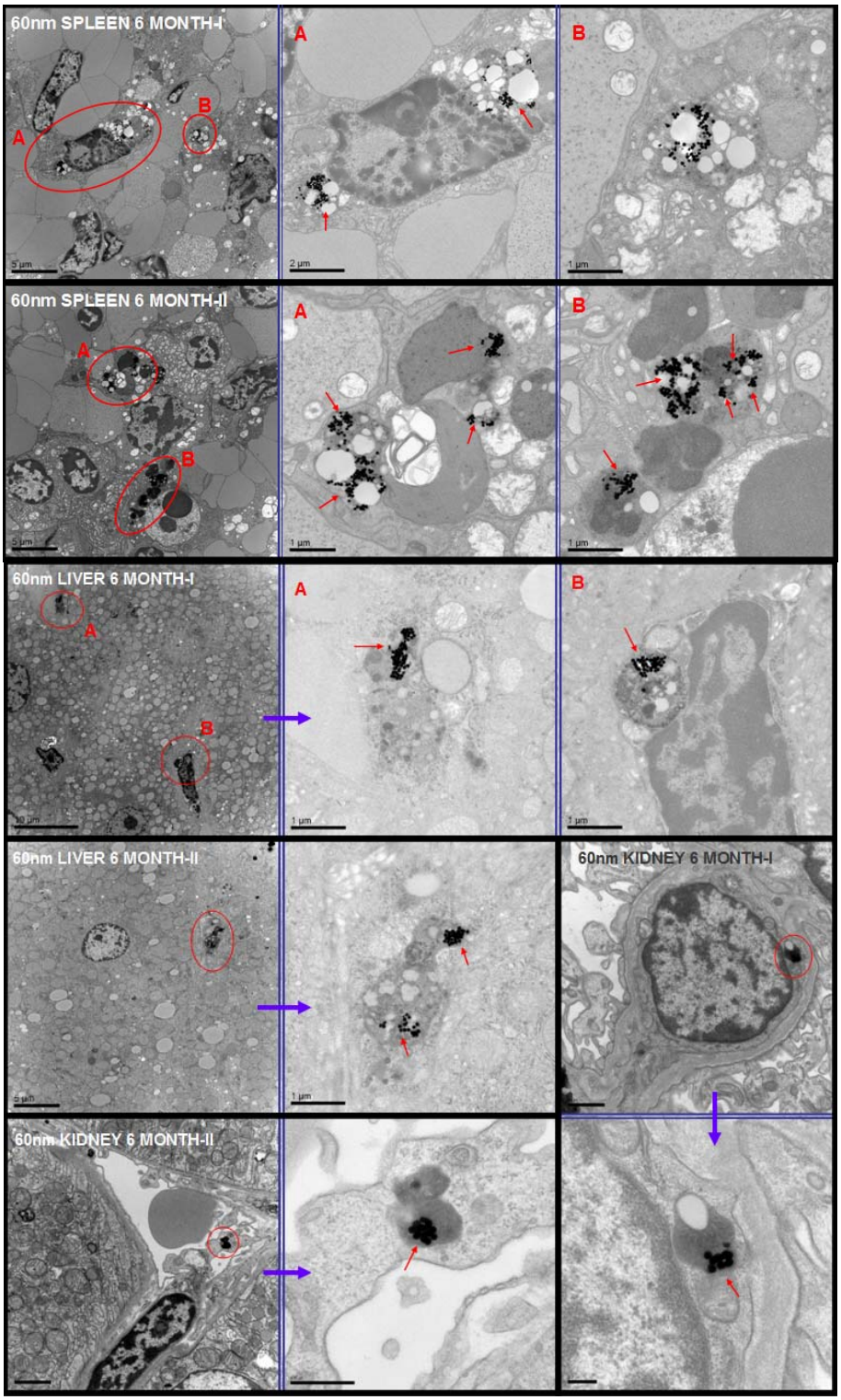

Figure 5.4. TEM Images of (a) 5nm and (b) 60nm Gold Nanoparticles in Various Organs at 6 Months

TEM images in Figure 5.4 show 5nm and 60nm gold nanoparticles present in small clusters in the various organs of liver, spleen, and kidney at 6 months. Most of the gold nanoparticles are contained in a membrane-bound vesicles inside irregularly-shaped (suspected to be macrophages) cells. The arrangement of nanoparticles in the sample indicated that the clusters were most likely agglomerates with weak binding forces. After intravenous administration, the gold nanoparticles may have been covered with various proteins present in the blood such as serum albumin and apolipoproteins that may facilitate the cellular uptake of the nanoparticle, as demonstrated for polymeric nanoparticles [216]. It has been observed that nanoparticles are rapidly uptaken, sequestered, and retained by the RES, mainly in the liver and spleen [200]. In the liver, the particles are mainly retained by the scavenging periportal and midzonal Kupffer cells, while hepatocytes and liver endothelial cells may play a secondary role under special pathophysiolgical conditions. It has been reported that Kupffer cells in the liver are mainly responsible for uptaking polymeric nanoparticles with hydrophobic surface. In the spleen, the marginal zone and red pulp macrophages are the major scavengers, while peritoneal macrophages and dendritic cells have a minor contribution.

Clearance of Gold Nanoparticle

Generally, renal and hepatobiliary systems are involved in the clearance of nanoparticles via urine and feces. Renal clearance or urinal pathway is more desirable that kidney is capable of rapidly removing the nanoparticles from the vascular compartment in an unaltered, original form [217]. There is minimal involvement of intracellular catabolism associated with the renal route that minimizes toxicity and agent

retention. In contrast, hepatobiliary system requires intracellular enzymatic modification. In hepatobiliary clearance, hepatocytes are directly related to bile excretion, and Kupffer cells are responsible for intracellular degradation of uptaken nanoparticles [217]. The uptake of hepatic system is quick, with the preferential uptake of particles in 10-20nm size range, but the hepatic clearance is a very slow process and most of the time nanoparticles result in prolonged retention in parenchyma itself [64, 217].

Various studies have been reported for clearance of nanoparticles. For 1.9nm gold nanoparticle, ~77% of the injected gold was excreted through kidney within 5hours in mice [56]. Choi et al. also reports rapid clearance of zwitterionic quantum dots (4.36nm-5.52nm) within 4 hours of intravenous injection through kidney [64]. 1.4nm gold nanoparticle were both excreted by kidney and hepatobiliary systems (8.6% injected gold in urine and 5% injected gold in feces), whereas 18nm gold nanoparticle resulted in relatively small hepatobiliary excretion (0.5% injected gold) and hardly any renal excretion in rats [205]. 13nm quantum dots displayed accumulation in kidney without any renal excretion [63] when 13 nm PEGylated gold nanoparticle accumulated in the liver and spleen without any hepatobiliary excretion up to 7 days [55]. Interestingly, larger 27nm PEGylated gold nanoparticles were significantly cleared out from the liver via hepatobiliary clearance after 4 months of intravenous injection in mouse [197]. Also, Balasubramanian et al. found that 20nm gold nanoparticle filtered from the bloodstream and excreted via urine (1.7ng/g at day 1 and 0.8 ng/g at 1 week) [52]. It is puzzling to see various sizes of nanoparticles get cleared out, especially via renal filtration, when the literature reports effective pore size of the filtration barrier (i.e. glomerular basement

membrane (GBM)) and podocytes to be ~8nm in the kidney [218]. Thus, it is not only the size but also other factors like charge affects the clearance of nanoparticles.

As seen in Figure 5.5, our 5nm gold nanoparticle coated with MW 5000 thiolated methoxy- PEG (average hydrodynamic diameter of 18.2 ± 0.9 nm) resulted in both renal and hepatobiliary clearance. Since urine and feces were collected at the indicated, particular time point (i.e. not cumulative), we can not conclude how much of the total injected gold was excreted via urine or feces. However, it is clear that our 5nm gold system was significantly excreted via urine and feces up to 25 days. We believe that 5nm gold system was excreted rapidly via urine and feces at the initial time point (~ up to 9-10 days) and rest of the 5nm gold system was excreted slowly as gold nanoparticle accumulates in the kidney, liver, and spleen. It has been reported that PEGylation dramatically reduces particle renal filtration due to increased hydrodynamic diameter (HD). Cho et al. reported that PEGylation of 4nm gold nanoparticle (HD of 14.8 ± 3.3 nm) resulted in hardly any renal and hepatic excretion [210]. In contrast to our results, they concluded that PEGylated 4 nm gold nanoparticle had a similar excretion profile as larger 13nm and 100nm PEGylated gold nanoparticles. Even though we are unclear of the exact mechanism at which allowed the passage of 5nm PEGylated gold nanoparticle through renal filtration, we believe that the successful excretion of 5nm PEGylated gold nanoparticle, particularly in renal system, was due to the surface charge (Cho et al. does not report the zeta potential or the MW of PEG used for their system) and perhaps coating replacement. It has been reported that filtration is greatest for cationic then neutral then anionic molecules being the least [217]. Molecular charge is of particular significance for molecules within 6-8nm range, as these particles are not small enough to

undergo charge-independent filtration, yet may still be filtered if molecular charge is favorable. The fact that our 5nm gold system is excreted, however, suggests that factors other than pore size may be important in the filtration of nanoparticle. The effective filtration pore diameter of 8nm applies to proteins with negative charges which are effectively repelled from the GBM barrier. The neutral or slightly negatively- charged 5nm gold nanoparticle may not be so effectively repelled, and manage to pass through the barrier. It has been reported that hydrodynamic diameter greater than 15nm cannot be excreted renally [64]. Furthermore, unlike the hard 5nm core, the shell created by PEG is soft and flexible that might have changed its conformation, thus allowing the passage of gold system. PEG coating on the surface of the gold might have been replaced with other ligands in the serum (i.e. proteins) that could have led to alteration of shape, charge, and hydrodynamic diameter of our gold system. Finally, high concentrations of gold injected into the mice have resulted in excretion of gold via urine and feces, where high concentration gold resulted in the uptake capacity of the RES. The slight decrease in the rate of urine excretion in the later phase might suggest gradual accumulation of nanoparticles in the kidney over months might diminish the permeability of GBM and podocytes, further reducing the excretion of gold nanoparticles.

Hepatobiliary excretion of gold nanoparticles have been reported by Renaud et al. that colloidal gold taken up as a complex with low-density lipoprotein was excreted into the feces via the common bile duct at a maximal rate of about 5% daily, 4 to 12 days after injection [219]. Hardonk et al. also reports excretion of gold nanoparticles via hepatocytes at the earlier phase then via Kupffer cells at later phase [220]. For chrysiasis in humans, gold salt, concentrated particularly in the RES, are excreted in feces and urine

continuing for years after cessation of the therapy [208]. Excretion profile of 60nm gold nanoparticle was excluded, as previous literature reports hardly any excretion of larger particles via urine and minimal excretion via hepatic system [58, 210].

(a)

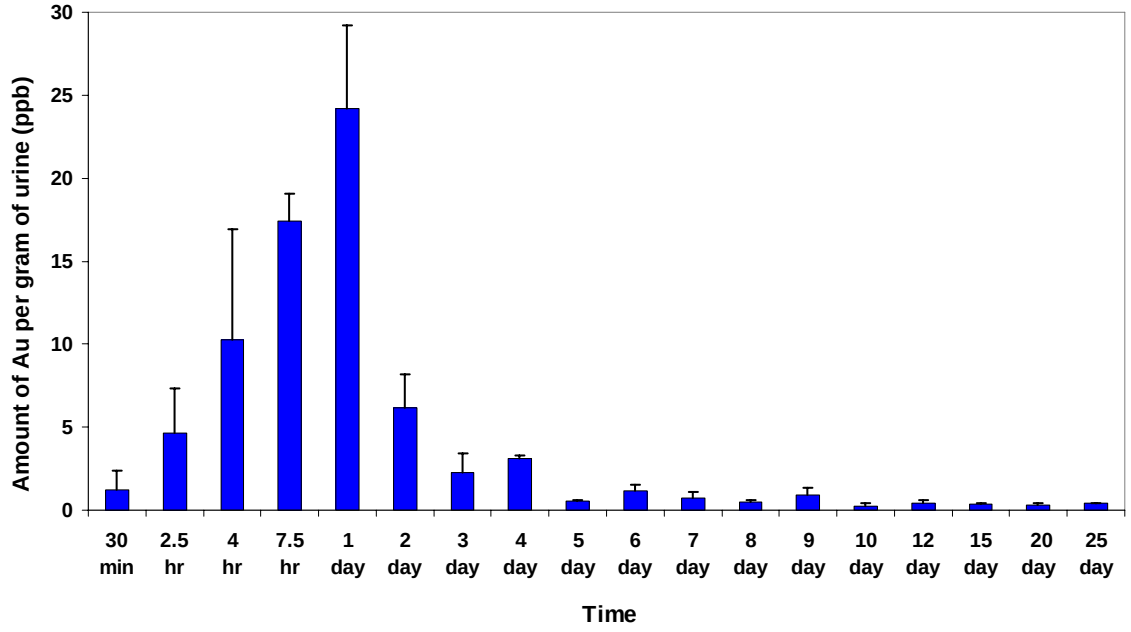

(b)

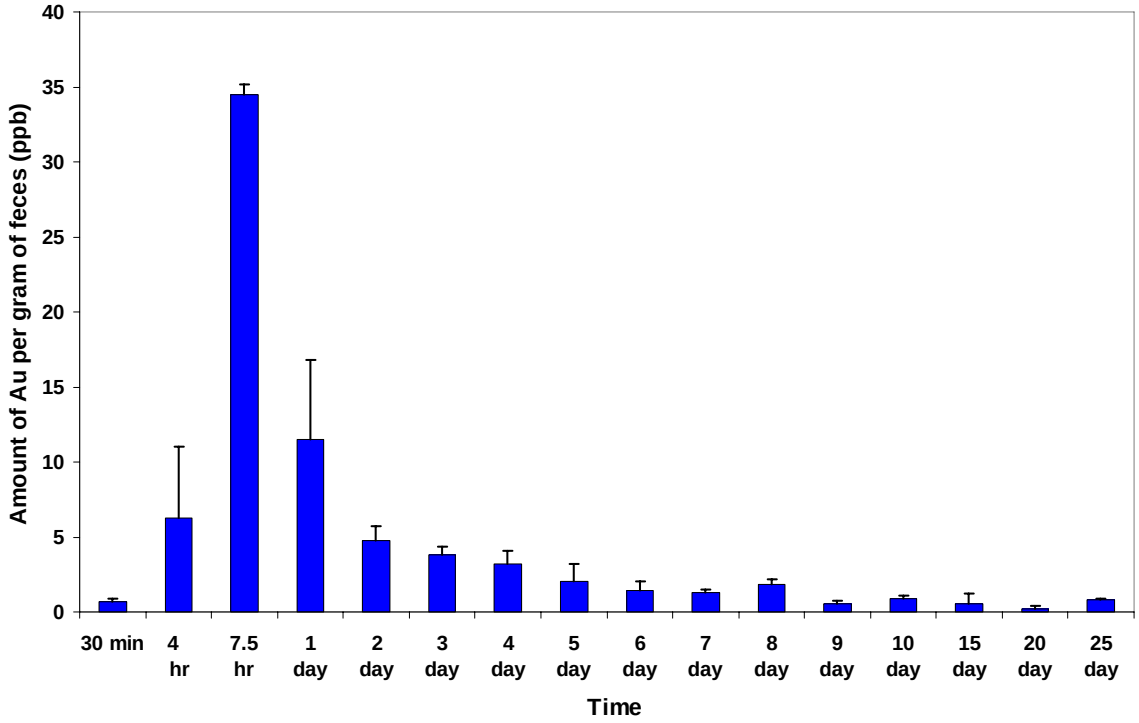

Figure 5.5. Renal (a) and Hepatobiliary (b) Clearance of 5nm PEGylated Gold Nanoparticle [each time point represent urine or feces collected at that particular time point (i.e. not cumulative)]

Previous research study states that given the same surface chemistry and similar chemical properties/composition of the gold core, the size governs the uptake by the lymph nodes [221]. This was consistent with our study where small-sized 5nm gold system was visible as dark brown circle in the extracted lymph nodes (Figure 5.6). Initially, dark brown circles were visible within the lymph nodes and as the time progressed, the pigmentation of the dark brown circle in the lymph node lightened up. This visible cue also corresponds to the ICP-MS analysis of lymph nodes (Figure 5.3 (a)) where concentration of gold decreased over time in the lymph nodes. Interestingly, larger 60nm gold system did not display any pigmentation within the lymph node that it looked similar in hue compared to the Control lymph nodes. This is also evidenced in the TEM images of the lymph nodes (Figure 5.7) where only fewer number of particles were seen in the 60nm gold system images compared to 5nm gold system. We believe that large size of 60nm limited the lymphatic clearance of the gold system and resulted in decreased appearance in the lymph nodes. Also, TEM images demonstrate number of particles within the lymph nodes decreases over time for the 5nm gold system, whereas there seems to be an increase in the number of particles in the lymph nodes for 60nm gold system over time. Again, this is also consistent with the ICP-MS results in Figure 5.3 (b) where the concentration of 60nm gold system in the lymph nodes did not decrease over time in contrast to 5nm gold system. Accumulation of gold nanoparticle after intravenous injection has been reported in previous literature that high concentrations of 4, 13, and 100 nm gold nanoparticles were detected in the mesenteric lymph nodes [210].

(a)

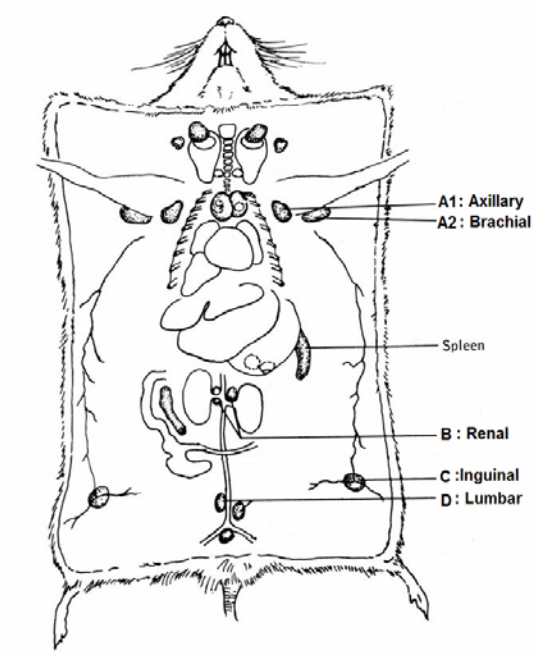

(b)

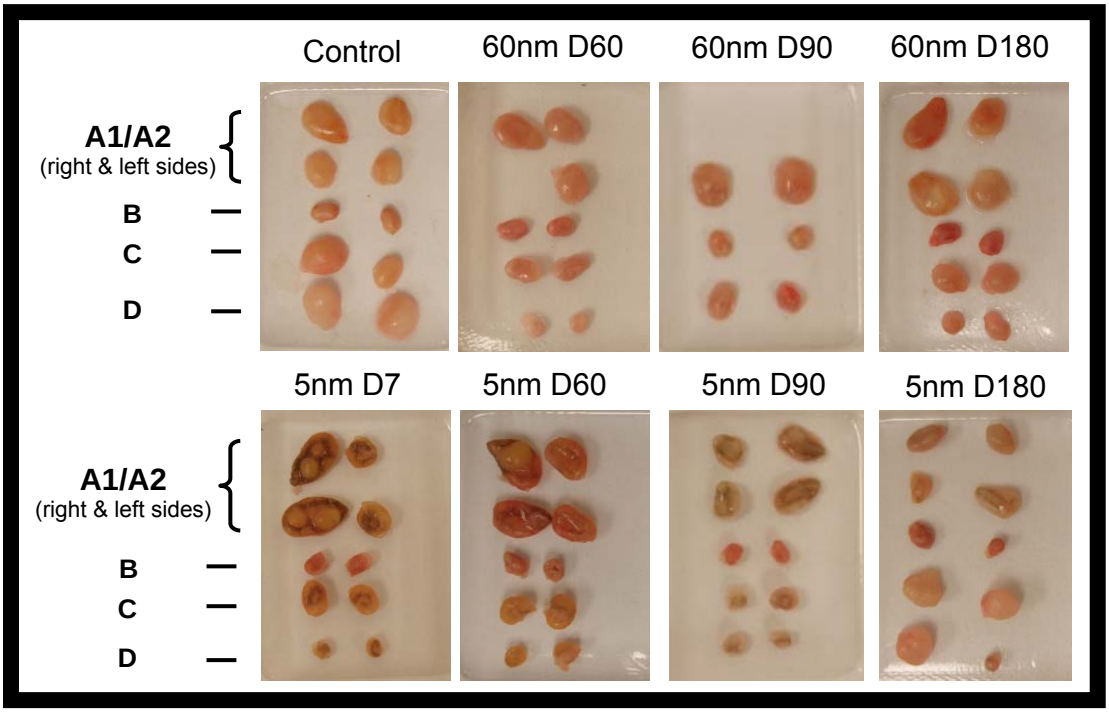

Figure 5.6. Lymphatic Clearance of Gold Nanoparticle (a) Schematic drawing of general lymph node locations (b) Pictures of extracted raw lymph nodes for Control versus 5nm versus 60nm gold nanoparticle [Mouse drawing modified from <http://www.informatics.jax.org/greenbook/figures/figure13-4.shtml>; D#=day#]

Detection of gold nanoparticles in the lymph nodes could be due to translocation of gold nanoparticles from the lungs. It has been reported that lymphatic drainage plays an important role in the uptake of particulates in the respiratory system [222, 223]. The findings indicate that lung could serve as a reservoir for nanoparticles after acute exposure, and there is significant translocation of nanoparticles out of the lungs through lymphatic vessels and/or the bloodstream to other organs with time. Balasubramanian et al. reported that gold nanoparticle concentration in the lungs increased dramatically after an injection then there was a continual decrease of nanoparticle in the lungs with time after an initial peak [52]. Thus, this could account for the higher accumulation of gold nanoparticles in the lymph nodes at earlier times. As the amount of gold in the lung decreases over time, the according gold nanoparticle being translocated from lung to lymph nodes also decrease over time.

In a typical lymphatic clearance, molecules leak out of the blood vessels into the interstitial space and are cleared via the lymphatic system [224, 225]. Thus, small-sized 5nm gold nanoparticles could have easily extravasated from the blood vessels and into the interstitial space to result in lymphatic clearance. Indeed, dark circles seen in the lymph node pictures (Figure 5.4) indicate high accumulation of extravasated 5nm gold nanoparticles. Compared to the 5nm, 60nm lymph nodes did not display any discoloration in the lymph nodes (Figure 5.4), even though same concentration of gold was injected for both 5nm and 60nm. This suggests that larger 60nm gold nanoparticle was unable to extravasate from the blood vessel as easily as the 5nm gold nanoparticles that less of them end up in the lymph node. Another reason for gold detection in the

lymph nodes could be accounted from general lymphatic clearance from the interstitial spaces of various organs, including the RES.

(a) 5nm Lymph

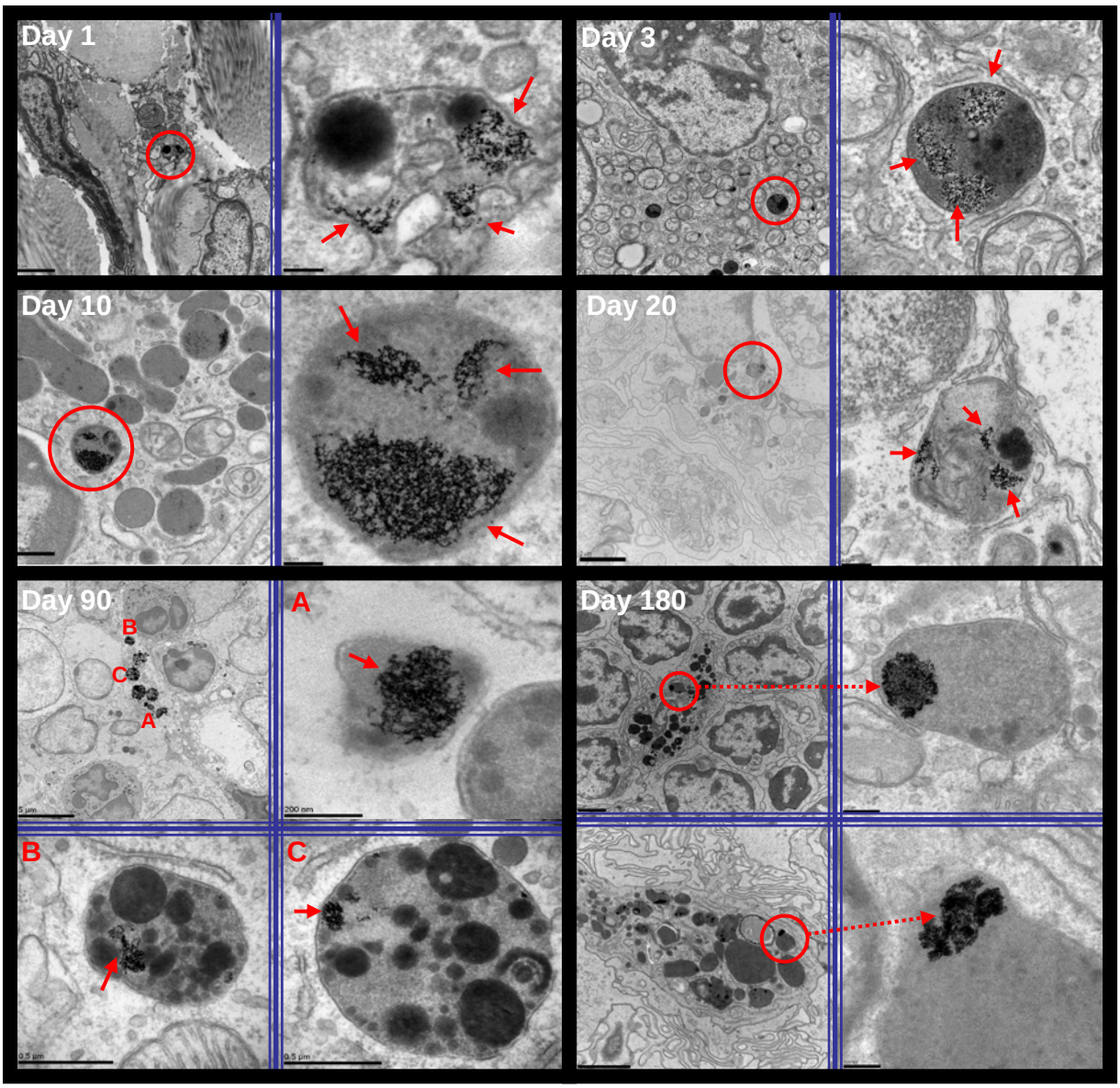

(b)
60nm
Lymph

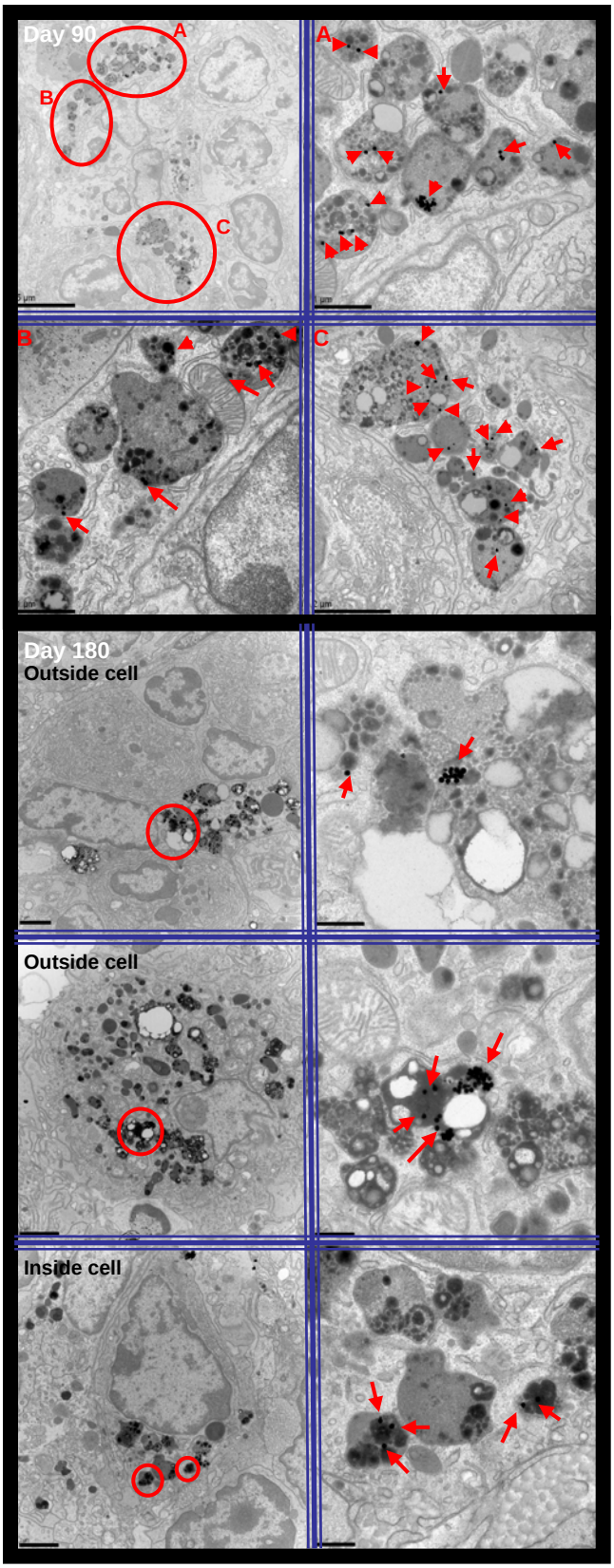

Figure 5.7. TEM Images of (a) 5nm Versus (b) 60nm Gold Nanoparticles in lymph nodes

5.5 CONCLUSION

Here, we showed the size-dependent biodistribution and clearance of colloidal gold nanoparticles that (1) increased circulation time for 5nm gold system (due to size and PEG) resulted in biodistribution of gold in various organs compared to 60nm gold system, (2) larger 60nm gold nanoparticles were mostly uptaken in the liver and the spleen, whereas smaller sized 5nm gold nanoparticle was visible in the various organs in the system, especially resulting in pigmentation in the skin and the lymph nodes, and (3) size dependent clearance was observed where 5nm gold system gets cleared out via renal (urine) and hepatobiliary (feces) pathways, whereas 60nm gold was mostly retained in the spleen and liver after 6 months. Thus, 5nm gold system is a potential candidate for biomedical applications, where 5nm gold core displays inherently different biodistribution and clearance characteristics than 60nm or larger nanoparticles.

CHAPTER 6

SUMMARY AND FUTURE DIRECTIONS

6.1 ABSTRACT

In this chapter, we summarize the important findings from previous chapters and significance of our work in cancer nanotechnology. We then examine the future applications of gold nanoparticles in drug delivery applications, specifically focusing on the size and its impact on biological applications.

6.2 SUMMARY

This dissertation focused on the design and development of various sizes of colloidal gold nanoparticle drug delivery systems for cancer nanotherapy. In particular, two representative sizes of gold nanoparticles, 5nm and 60nm, were investigated for the size effect on therapeutic efficacy, toxicity, and biodistribution in cancer nanotherapy. In the first chapter, we described the general background on cancer and emphasized the role of nanotechnology, particularly focusing on the size effect for successful detection, diagnosis, and treatment of cancer. The complexity and heterogeneity nature of cancer makes it difficult to successfully diagnose and treat cancer, and nanotechnology plays a critical role in overcoming the obstacles in cancer biology. It is the size-scale of nanotechnology that provides a powerful tool to easily manipulate the complex cancer environment by distinctively size-tuning the nanomaterial to interact with biological molecules in tumor.

In the second chapter, we closely looked at one class of nanoparticles, namely colloidal gold nanoparticle, and its unique physical and chemical properties that are attractive for applications in cancer nanotechnology. Gold nanoparticles confer several advantages such as biocompatibility, size-tunability, and easy surface modification

methods. Furthermore, due to its unique optical properties, multiple analytical chemistry methods such as UV-vis spectrophotometry, SERS, TEM, ICP-MS, darkfield microscopy, fluorescence can be used. Previously, gold nanoparticles have been mainly used for chemical sensing, photothermal therapy, and diagnostic purposes. The idea of using gold nanopartcle as a carrier for drug delivery is recent that further attention and study is required.

In the third chapter, we start off our drug delivery study with larger 60nm colloidal gold nanoparticle system. Here, we report development and characterization of multifunctional drug delivery system for *simultaneously* treatment and SERS spectroscopic detection of tumor. Doxorubicin, serving a *dual* function of chemotherapeutic agent and SERS reporter molecule, was chemically conjugated to gold nanoparticle via pH-sensitive hydrazone linker then PEG was added to develop multifunctional delivery system. Doxorubicin occupied maximum of 20% of total surface area of gold nanoparticle to result in colloidal stability. The multifunctional delivery system demonstrated pH-dependent drug release profile, therapeutic effect on tumor cells, along with *in vitro* spectroscopic detection based on SERS. SERS spectra were detected for *non-aggregated* gold system at near-infrared wavelength. Thus, the development of multifunctional drug delivery system raises exciting opportunities for simultaneous spectroscopic detection and therapy for tumors.

In the fourth chapter, we switched our focus to smaller-sized 5nm gold nanoparticle for drug delivery applications. Despite successful treatment and SERS spectroscopic detection in tumor, 60nm gold nanoparticle system resulted in a limitation of low drug-loading efficiency (0.1 wt-%). In order to test *in vivo*, our calculation results

showed that high concentration of gold nanoparticles were needed for 60nm gold nanoparticle system (calculation not shown). Thus, in order to increase the drug loading efficiency and minimize the amount of gold injected *in vivo*, 5nm gold nanoparticle was selected for the study. Similar to 60nm gold system, 5nm gold nanoparticles were coated with doxorubicin which was modified with pH-sensitive hydrazone linker. Then the resulting gold system was coated with PEG to give colloidal stability and biocompatibility. 5nm gold nanoparticle drug delivery system resulted in a higher drug loading efficiency of 5.5 wt-%. However, as a trade off for having a higher drug loading efficiency, 5nm gold system no longer displayed SERS like the 60nm gold system due to its size. When tested in a tumor mouse model, 5nm gold drug delivery system resulted in therapeutic efficacy against tumor with no apparent systemic toxicity. In contrast, pure doxorubicin resulted in kidney, heart, and lung toxicity, along with insignificant therapeutic efficacy compared to other groups tested. The success of 5nm gold system resulted from (1) "high" accumulation at the tumor site compared to other non-tumor sites via EPR effect, (2) ideal spatial distribution and successful penetration at tumor site, and (3) slow, controlled release of drug via pH-sensitive linker to result in no apparent systemic toxicity. All of these factors owe to the small size scale of our 5nm gold system.

Finally, in the fifth chapter, we closely looked at the biodistribution and clearance of both 5nm and 60nm gold nanoparticle systems. In addition to therapeutic efficacy of colloidal gold system, it is important to study the long-term clearance and the fate of the delivered colloidal gold system for *in vivo* applications. Compare to the short blood circulation half time (~9 hours) for 60nm gold system, 5nm gold system resulted in a longer circulation half time (1.6 days) that led to size-dependent biodistribution of gold

nanoparticles. We showed that larger 60nm gold nanoparticles were mostly uptaken in the liver and the spleen, whereas smaller sized 5nm gold nanoparticle was visible in the various organs in the system, especially resulting in pigmentation in the skin and the lymph nodes. We also demonstrated size dependent clearance where 5nm gold system was excreted via urine and feces, whereas 60nm gold was mostly retained in the spleen and liver after 6 months. Thus, 5nm gold system is a potential candidate for drug delivery applications where 5nm gold core displays inherently different biodistribution and clearance characteristics than 60nm or larger nanoparticles.

In summary, we believe that nanoparticle "size" plays a critical role for not only delivering the drug delivery system to the target site but also determining the *in vivo* behavior such as clearance and biodistribution in the system.

6.3 FUTURE DIRECTIONS

The work presented in this thesis mainly focuses on the two different systems to represent application of colloidal gold nanoparticle in cancer nanotherapy. While the drug delivery application and the *in vivo* fate of gold nanoparticles have been demonstrated conclusively, there is still a large amount of further developments needs to be made for optimization. In the following section, we suggest specific studies and future directions to be undertaken for futher improvement of our study.

Improvement of Drug Loading Efficiency

Maximum drug loading is desired for high therapeutic efficacy for drug delivery system. Currently, drug loading is limited to the "surface" of the gold nanoparticle, thus somewhat limiting the drug loading efficiency. Drug loading can be further enhanced by increasing the surface area for drug-hydrazone linker conjugation site by adopting a

different type of polymer coatings such dendrimers. Dendrimeric polymer provides multiple conjugation sites per polymer by branching characteristics. However, further study on toxicity of dendrimeric system, along with drug release profile has to be investigated.

In this study, 60nm gold nanoparticle system had a low drug loading efficiency, thus limiting its use for *in vivo* applications. Also, as seen from the biodistribution and clearance studies, larger 60nm gold system was retained in the RES and was not cleared over time. Thus, the 60nm gold system could be more optimal for *ex vivo* diagnostic purposes in a long run. The SERS feature of 60nm gold system makes it an attractive candidate for cancer diagnostics where antibody-targeted 60nm gold nanoparticle with SERS tag could be used to capture cancer cells from the blood drawn from patients.

Improvement of Therapeutic Efficacy

Hydrazone bond is highly sensitive to pH changes that it is cleaved under mild acidic conditions of less than pH 5.5. The slow, delayed release of doxorubicin from gold nanoparticle-anticancer agent-PEG system is due to (1) the diffusion barrier created by PEG coating and (2) interactions between the polymer and the drug. To ensure rapid release of the bound drug, drug needs to be placed closer to the outer most layer of the system to decrease any diffusional barrier and accessibility of drug release triggering molecules. However, placing the drug near the outer most layer will limit the drug loading efficiency and change the property of the system compared to the current system. On the other hand, the PEG layer can be decreased to smaller size (or lower molecular weight) to minimize any diffusional barrior. However, decreasing the protective PEG

layer will compromise the colloidal stability of the gold nanoparticle. Alternatively, different linker system such as glutathione-activated prodrug system could be adopted.

Alternatively, assuming that the drug loading percentage is fixed, doxorubicin (our model drug for the study) can be replaced with more potent drug to increase the therapeutic efficacy of the system.

Finally, targeting ligand can be adopted to increase the therapeutic efficacy of the system. It has been reported that targeting ligands increase the internalization of drug carrier by the cancer cells at tumor site. This requires testing the optimal concentration of targeting ligands to be used, pharmacokinetics of the carrier, and toxicity exerted by the targeting ligand itself.

Improvement of Biodistribution, Toxicity, and Clearance Studies

As seen with our studies, smaller-sized nanoparticles accumulate at various organs in the system. Thus, wide and even spread of smaller-sized gold nanoparticle in the sytem requires further investigations in other parts (rather than focusing only on the vital organs) of the system. Also, to strenghthen the toxicity studies, changes in gene expressions in various organs can be studied, along with in depth serum protein analysis for organ toxicity.

Different sizes, rather than 5nm and 60nm, of gold nanoparticles needs to be tested for further generalization of the biodistribution and clearance of nanoparticles. Even smaller particles (like 2-3nm) and particles in between 5nm and 60nm can be used to study the different patterns in biodistribution and clearance. Additionally, different coating can be adopted to further strengthen the study. Different coatings on gold surface render different charge, shape, colloidal stability, and size. Thus, wide ranges of coatings

such as multidentate polymer can be tested. Furthermore, different dosages of gold system can be used to test the therapeutic efficacy, biodistribution, and clearance.

For clearance study, urine and feces needs to be collected cumulatively. Due to limited resources, our study was conducted by collecting urine and feces at each specific time point. By collecting urine and feces cumulatively, we can accurately calculate the amount excreted after the intravenous injection.

Finally, alternative methods other than ICP-MS can be used to further verify the gold quantification results. Analysis of collected organs, feces, urine, and blood through ICP-MS is an extremely costly and time-consuming process that it requires extensive drying and acid digestion of the samples. Other analytical chemistry methods such as atomic emission spectroscopy could be utilized.

Future of Gold Nanoparticles in Drug Delivery Applications

Nanotechnology plays a critical role in treatment of cancer. Currently, there are many ongoing clinical trials for various types of nanoparticles for cancer treatment. In particular, Doxil® and Abraxane® are one of few FDA approved nanoparticles for cancer therapy.

Doxil®, PEGylated liposomal doxorubicin, is widely used to treat ovarian cancer or multiple myeloma [226]. Doxil® has been approved in the United States since 1995, and there are over 1219 clinical trials related to Doxil® alone [227, 228]. Doxil® is formulated by encapsulating anthracycline (i.e. doxorubicin hydrochloride) drug in liposomes with surface-bound methoxy-polyethylene glycol to result in mean size of 80-90 nm and doxorubicin concentration of 2 mg/mL [229]. Due to its unique pharmacokinetic properties such as long circulation time (i.e. elimination half-life of 20-

30 hours), restricted volume of distribution (i.e. close to blood volume), and stable retention of anthracycline inside the liposome during circulation, Doxil® has shown 6-fold enhancement in antitumor activity compared to free doxorubicin with reduced cardiac toxicity [229]. However, Doxil® induces dose-limiting toxicities such as asthenia, fatigue, fever, anorexia, nausea, vomiting, stomatitis (i.e. painful sores in mouth), diarrhea, constipation, hand-foot syndrome, rash, neutropenia (i.e. low white blood cell count), thrombocytopenia, and anemia [230]. In particular, skin represents the major liposome accumulating site for long-circulating Doxil® that results in bothersome redness, flaking, swelling, and burning sensation on palms of hands or soles of feet.

Abraxane® was also approved by FDA in 2005, which overcomes the limitations of paclitaxel by formulating albumin-bound form of paclitaxel with a mean particle size of ~130nm [231]. In general, paclitaxel is highly hydrophobic and conventionally delivered via Cremphor EL® and ethanol, which leads to hypersensitivity reactions, severe neuropoenia, and peripheral neuropathy in patients during therapy [232]. When injected, this 130nm albumin-paclitaxel complex quickly dissolves into smaller endogenous albumin-sized (~10nm) complexes for effective accumulation at tumor sites. Several clinical trials show that Abraxane® improves the solubility of paclitaxel and also improves the toxicity profile of conventional paclitaxel therapy with Cremphor EL® with greater anti-tumor activity [231]. A Phase III clinical trial with metastatic breast cancer patients resulted in higher response rate, significantly lower rate of grade 4 neutropenia, but higher rates of grade 3 sensory neuropathy [231].

As seen above, despite advances made in toxic effects and therapeutic efficacy for cancer therapy, cancer patients still suffer from long-term adverse effects of the drug and

cancer mortality rate is still unacceptably high. Nanotechnology still faces challenges in the drug delivery area for further improvement and solutions to resolve these issues. To pinpoint, the biggest problems in current drug delivery are 1) presence of systemic toxicity imposed by nanoparticles due to changed pharmacokinetics and 2) drug stabilization and increased accumulation at target site for improved drug efficacy.

New formulations introduced for particular chemotherapeutic agent can reduce or eliminate the toxicity native to that drug, but it can also introduce unexpected, new toxicities to the system. For example, prolonged circulation time of Doxil® resulted in a high accumulation of liposomes in the skin. Due to small size, pure doxorubicin gets cleared out from the system within few minutes. However, change in pharmacokinetics of the doxorubicin by increasing the delivery vehicle size and PEGylation allowed retention of the drug in the blood for longer periods of time and exposed other organs, such as skin, to result in toxicity. Longer circulation time does lead to increased accumulation of the drug at the target site, but at the same time there is a risk of exposing other, unrelated organs for potential toxicity.

In addition to high accumulation of drug at the target site, efficacy of the drug is determined by the stability of drug during circulation and appropriate release/delivery of drug at the tumor site. In other words, drug needs to be stable during circulation and get properly released at the desired target site. For both Doxil® and Abraxane®, active drug is loosely bound, not covalently linked, to the delivery vehicle that there is a chance for leakage of parent drug during circulation. Leakage of drug not only reduces the efficacy of the drug delivery system but also increases the risk for potential toxicity in the system. Nanoparticle needs to be appropriately formulated so that drug is retained until it reaches

its target site, and gets released in a controlled manner. Thus, there should be a balance between systemic toxicity and efficacy of the drug to optimally treat the disease.

Similarly, our gold nanoparticle drug delivery system also faced the same issues dealt above. Due to its stealth PEG layer and the size, our gold nanoparticle drug delivery system circulated in the blood for long period of time (~1.6 days), which led to wide distribution of the drug delivery system in non-tumor organs. Similar to Doxil®, we observed increased accumulation at the skin but no skin toxicity. Surprisingly, we observed non-toxic skin pigmentation, which faded with time. Unlike Doxil® and Abraxane®, our parent drug doxorubicin was covalently bound to the gold nanoparticle surface for stability during blood circulation. Due to smart, pH-activated drug release mechanism, delivery system was observed to release drug in acidic environment such as tumor stroma. Despite the accumulation at non-tumor sites, no apparent toxicity was observed for the given experimental period. Extremely high concentration of gold drug delivery system accumulation and retention at tumor site, relative to non-tumor site, outweighs the potential toxicity exerted on non-tumor sites. Furthermore, gold drug delivery system seems to be present mostly outside the cells in non-tumor sites. No apparent toxicity present in non-tumor site is mostly due to minimal or slow release of hydrazone-bound drug from the gold surface in non-acidic environment.

Overall, our gold drug delivery system provided new insight on 5nm gold system that led to "increased" tumor accumulation due to changed pharmacokinetics (i.e. covalently bound doxorubicin was well-camouflaged or protected by PEG layer that stayed intact throughout the half-life circulation time of ~1.6 days) for "improved" therapeutic efficacy and overall "reduction" of side effects. Furthermore, small-sized gold

drug system was slowly "cleared" out from the body over time after cessation of treatment. We believe that 5nm gold drug delivery system is an ideal candidate for future drug delivery application *only when* intricate balance amongst nanoparticle formulation, dosage, dosing schedule, and nanoparticle pharmacokinetics are met, as seen in our study. Due to high surface-to-volume ratio, 5nm core allows increased drug loading efficiency. Furthermore, 5nm core is right below the renal clearance threshold and above 2nm, which has been reported to result in cellular toxicity. The only issue with 5nm drug delivery was skin pigmentation, which seems to be mostly cosmetic issue. This can be resolved by adopting different dosage, dosing schedule, or different types of potent drugs.

Nanotechnology allows different delivery strategies in cancer therapy that balance between toxicity and efficacy of the drug system is crucial. Furthermore, combining effective dosing schedule for improved efficacy of the drug and safety profile is essential. Nanotechnology offers new opportunities for currently available chemotherapeutic agents by 1) increasing solubility of drug, 2) increasing maximum allowed dosage, 3) decreasing toxicity of the native drug (but not complete elimination of toxicity related to the original drug and sometimes occurrence of unexpected, new toxicity), 4) allowing various delivery strategies by various formulation methods (i.e. biodegradable materials, liquid-to-gel transitioning material, thermal ablation, etc.), 5) allowing controlled release of the drug, 6) allowing different methods of metabolism to bypass certain metabolic pathway, and 7) allowing different methods of administration (i.e. intravenous, intraperitoneal, local tumor administration).

Thus, future opportunities with gold nanoparticles in drug delivery, particularly with 5nm, are positive and limitless. As an ideal drug delivery vehicle, gold nanoparticle

selectively delivers various kinds of drugs in a discrete quantity at specific time intervals, while minimizing systemic toxicity.

6.4 CONCLUSION

In conclusion, it is the "size" that affects the behavior and fate of the nanoparticle in biological system. By choosing the appropriate size for the system, we were able to successfully demonstrate the use of gold nanoparticles in drug delivery applications, along with desirable clearance from the biological system.

This work is *significant* by providing an insight on a potential ideal candidate for gold nanoparticle-based drug delivery system that uses small (5nm) gold nanoparticle to study therapeutic efficacy on solid tumor and *in vivo* clearance and biodistribution. To our knowledge, we are the first team to investigate in detail for 5nm gold nanoparticle drug delivery system *in vivo* and its complete behavior for better understanding of the gold nanoparticle-based drug delivery. The findings from this study will have implications in the chemical design of nanostructures for biomedical applications.

APPENDIX A

COLLOIDAL STABILITY OF PEGYLATED GOLD NANOPARTICLE

UV-vis spectroscopy can be used to characterize the coatings on the gold nanoparticle. For 5nm gold nanoparticle, it displays maximum absorption peak around 514nm for raw, non-aggregated 5nm particle. To ensure that bound doxorubicin or PEG on gold surface does not affect the colloidal stability, absorption spectra were measured for gold-drug (Au-DOX) and gold-drug-PEG (Au-DOX-PEG) in water (Figure A.1). Furthermore, to prevent formation of aggregates in various biological mediums such as salt, PEGylated drug-gold nanoparticle (Au-DOX-PEG) was incubated in 0.5M salt solution (reflecting the biological salt concentration). As seen in Figure A.1, Au-DOX-PEG was stable in salt solutions when tested up to 1 week, as indicated by smooth tail in the red wavelength region of the spectrum measured by UV-vis spectroscopy. In contrast, when raw 5nm gold nanoparticle was incubated in 0.5M salt solution, broadening of spectra was observed, along with the red shift in the maximum absorption peak. This indicates formation of aggregates of gold nanoparticles, as black precipitates were seen in the solution.

Additionally, when Au-DOX only was incubated in 10% serum solution (not shown here), dark precipitates (gold nanoparticle aggregates) were seen within few hours, whereas Au-DOX-PEG was stable (no precipitates seen) in 10% serum solution when observed up to 4 days at 37°C.

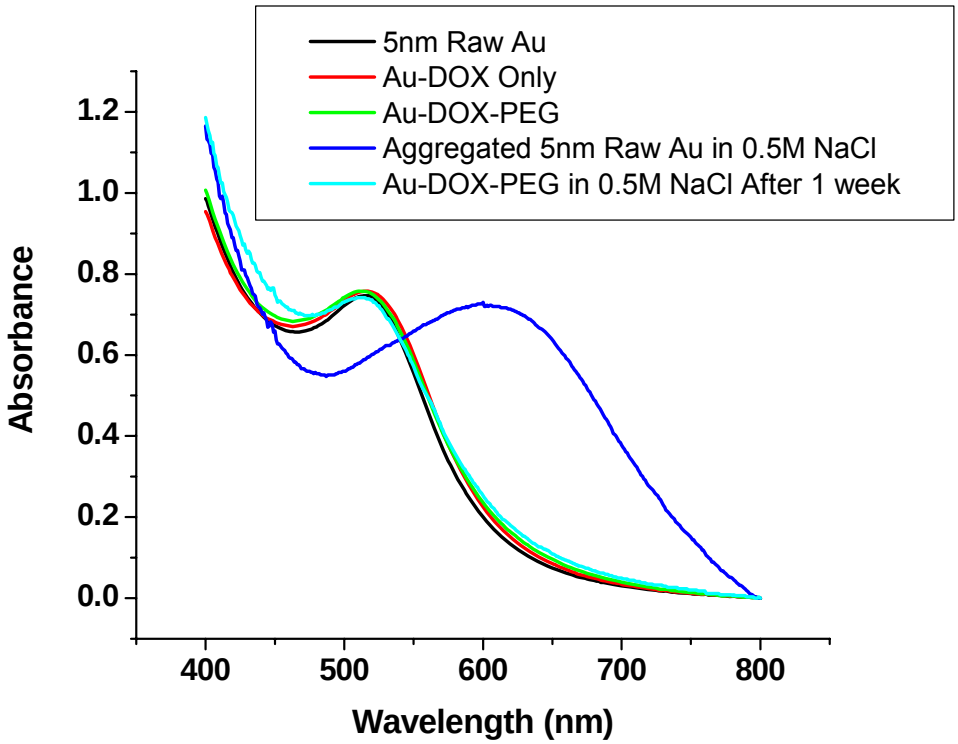

Figure A.1. Characterizaion of 5nm Gold Drug Delivery System (Au-DOX-PEG) with UV-vis Spectrometer (spectra were scaled for better visualization).

APPENDIX B

DARKFIELD IMAGING OF COLLOIDAL GOLD NANOPARTICLES IN VARIOUS ORGANS AFTER TREATMENT

Due to its unique optical property, colloidal gold nanoparticles can be imaged via darkfield microscopy. After mouse was treated with Au-DOX-PEG, various organs were harvested and embedded in paraffin for thin sections. The images obtained in Figure B.1 are unstained that orange dots spotted in various organs are solely from the deposited gold itself.

(a)

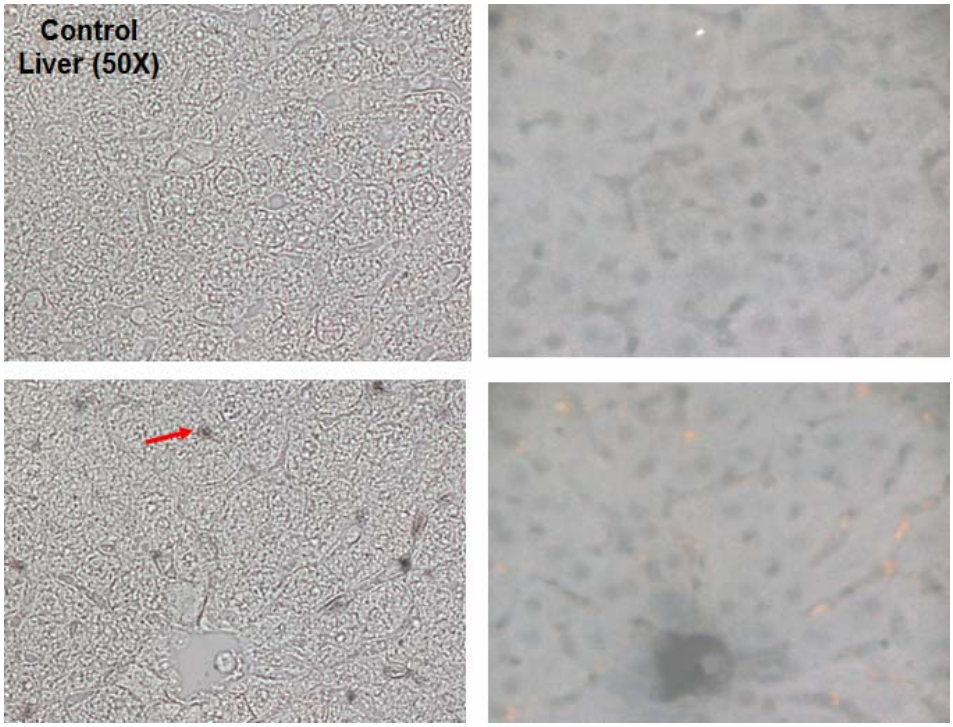

(b)

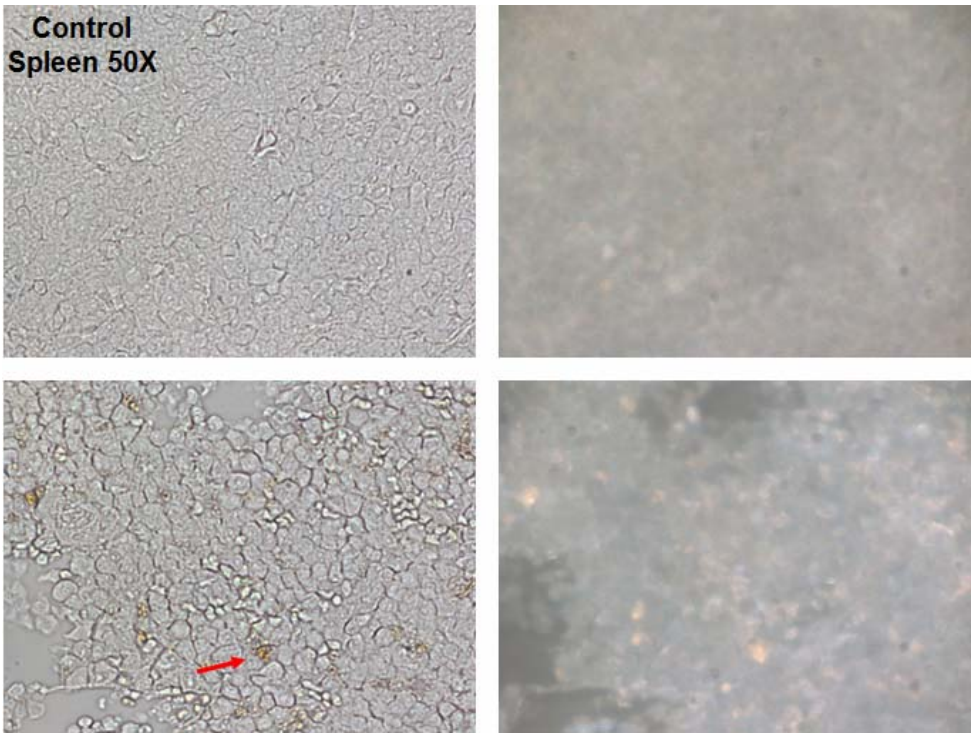

(c)

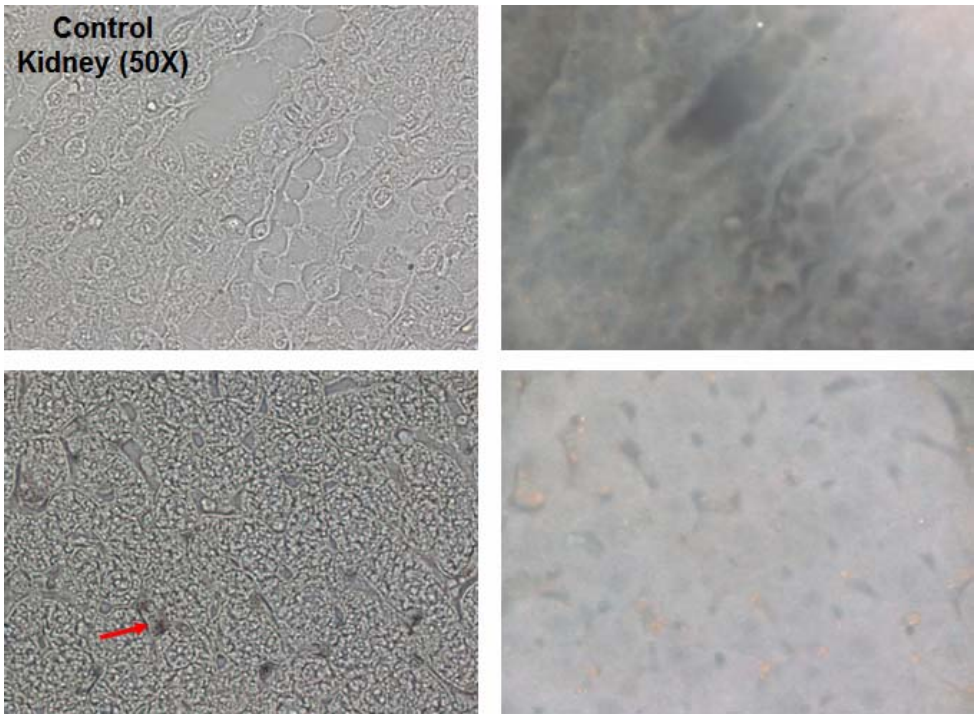

(d)

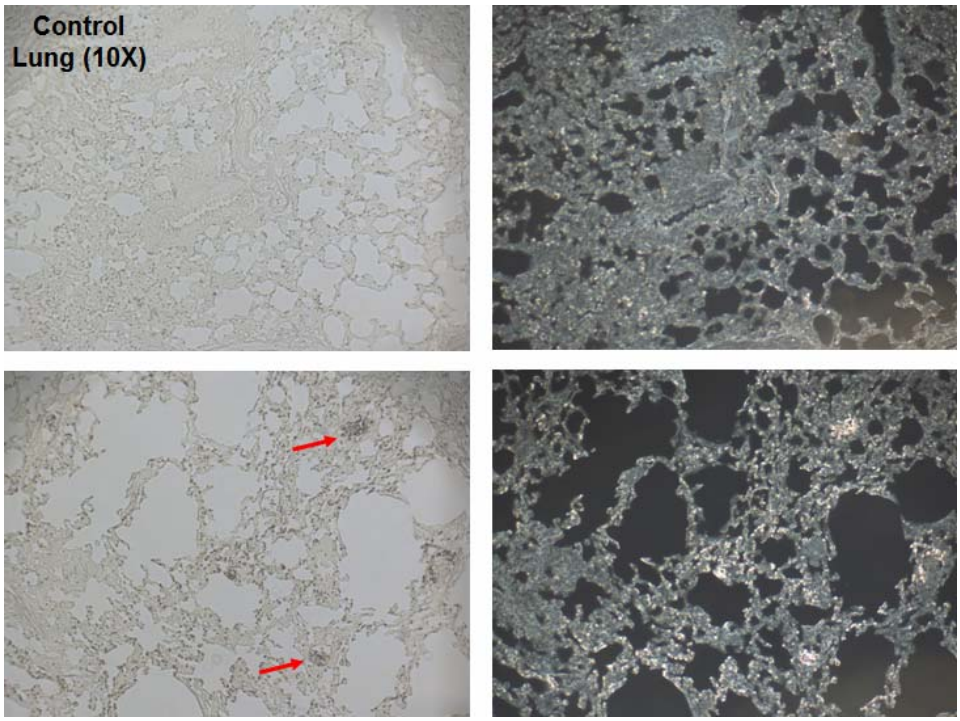

(e)

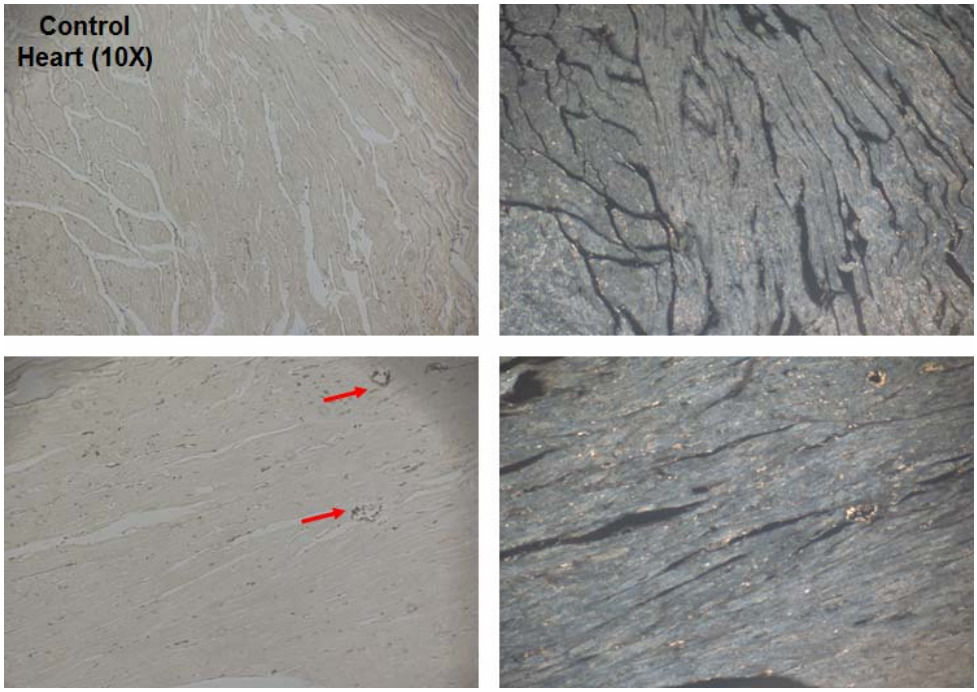

Figure B.1. Darkfield Imaging of Liver, Spleen, Kidney, Lung, and Heart after 16 Days of 5nm Gold Nanoparticle Drug Delivery System Au-DOX-PEG Treatment (red arrows indicate dark grey spots which represent gold deposited within the tissue)

REFERENCES

1. Lopez AD, Mathers CD, Ezzati M, Jamison DT, Murray CJ. Global and regional burden of disease and risk factors, 2001: systematic analysis of population health data. Lancet 2006 May 27;367(9524):1747-1757.

2. Cancer Statistics 2010. American Cancer Society, Inc.

3. Cai W, Chen X. Nanoplatforms for Targeted Molecular Imaging in Living Subjects. Small 2007;3(11):1840-1854.

4. Gao XH, Cui YY, Levenson RM, Chung LWK, Nie SM. In vivo cancer targeting and imaging with semiconductor quantum dots. Nature Biotechnology 2004 Aug;22(8):969-976.

5. Xing Y, Chaudry Q, Shen C, Kong KY, Zhau HE, Wchung L, et al. Bioconjugated quantum dots for multiplexed and quantitative immunohistochemistry. Nature Protocols 2007;2(5):1152-1165.

6. Wu XY, Liu HJ, Liu JQ, Haley KN, Treadway JA, Larson JP, et al. Immunofluorescent labeling of cancer marker Her2 and other cellular targets with semiconductor quantum dots. Nature Biotechnology 2003 Jan;21(1):41-46.

7. Rhyner MN, Smith AM, Gao XH, Mao H, Yang LL, Nie SM. Quantum dots and multifunctional nanoparticles: new contrast agents for tumor imaging. Nanomedicine 2006 Aug;1(2):209-217.

8. Thorek D, Chen A, Czupryna J, Tsourkas A. Superparamagnetic Iron Oxide Nanoparticle Probes for Molecular Imaging. Annals of Biomedical Engineering 2006;34(1):23-38.

9. Peng XH, Qian XM, Mao H, Wang AY, Chen Z, Nie SM, et al. Targeted magnetic iron oxide nanoparticles for tumor imaging and therapy. International Journal of Nanomedicine 2008;3(3):311-321.

10. Harisinghani MG, Barentsz J, Hahn PF, Deserno WM, Tabatabaei S, van de Kaa CH, et al. Noninvasive detection of clinically occult lymph-node metastases in prostate cancer. New England Journal of Medicine 2003 Jun;348(25):2491-U2495.

11. McCarthy JR, Kelly KA, Sun EY, Weissleder R. Targeted delivery of multifunctional magnetic nanoparticles. Nanomedicine 2007 Apr;2(2):153-167.

12. Torchilin VP. Micellar nanocarriers: Pharmaceutical perspectives. Pharmaceutical Research 2007 Jan;24(1):1-16.

13. Duncan R. Polymer conjugates as anticancer nanomedicines. Nature Reviews Cancer 2006 Sep;6(9):688-701.

14. Pridgen EM, Langer R, Farokhzad OC. Biodegradable, polymeric nanoparticle delivery systems for cancer therapy. Nanomedicine 2007 Oct;2(5):669-680.

15. Liu Z, Cai W, He L, Nakayama N, Chen K, Sun X, et al. In vivo biodistribution and highly efficient tumour targeting of carbon nanotubes in mice. Nature Nanotechnology 2007;2(1):47-52.

16. Huang X, El-Sayed IH, Qian W, El-Sayed MA. Cancer Cell Imaging and Photothermal Therapy in the Near-Infrared Region by Using Gold Nanorods. Journal of the American Chemical Society 2006;128(6):2115-2120.

17. Huang X, Peng X, Wang Y, Wang Y, Shin DM, El-Sayed MA, et al. A Reexamination of Active and Passive Tumor Targeting by Using Rod-Shaped Gold Nanocrystals and Covalently Conjugated Peptide Ligands. ACS Nano 2010;4(10):5887-5896.

18. Huang XL, Zhang B, Ren L, Ye SF, Sun LP, Zhang QQ, et al. In vivo toxic studies and biodistribution of near infrared sensitive Au-Au(2)S nanoparticles as potential drug delivery carriers. J Mater Sci Mater Med 2008 Jul;19(7):2581-2588.

19. Qian XM, Peng XH, Ansari DO, Yin-Goen Q, Chen GZ, Shin DM, et al. In vivo tumor targeting and spectroscopic detection with surface-enhanced Raman nanoparticle tags. Nature Biotechnology 2008 Jan;26(1):83-90.

20. Ferrari M. Cancer nanotechnology: Opportunities and challenges. Nature Reviews Cancer 2005 Mar;5(3):161-171.

21. Hanahan D, Weinberg RA. The Hallmarks of Cancer. Cell 2000;100(1):57-70.

22. Modi S, Jain JP, Domb AJ, Kumar N. Exploiting EPR in Polymer Drug Conjugate Delivery for Tumor Targeting. Current Pharmaceutical Design 2006;12(36):4785-4796.

23. Dreher MR, Liu W, Michelich CR, Dewhirst MW, Yuan F, Chilkoti A. Tumor vascular permeability, accumulation, and penetration of macromolecular drug carriers. J Natl Cancer Inst 2006 Mar 1;98(5):335-344.

24. Fang J, Nakamura H, Maeda H. The EPR effect: Unique features of tumor blood vessels for drug delivery, factors involved, and limitations and augmentation of the effect. Advanced Drug Delivery Reviews 2010;In Press, Corrected Proof.

25. Matsumura Y, Maeda H. A New Concept for Macromolecular Therapeutics in Cancer Chemotherapy: Mechanism of Tumoritropic Accumulation of Proteins and the Antitumor Agent Smancs. Cancer Research 1986 December 1, 1986;46(12 Part 1):6387-6392.

26. Takakura Y, Mahato RI, Hashida M. Extravasation of macromolecules. Advanced Drug Delivery Reviews 1998;34(1):93-108.

27. Hashizume H, Baluk P, Morikawa S, McLean JW, Thurston G, Roberge S, et al. Openings between Defective Endothelial Cells Explain Tumor Vessel Leakiness. Am J Pathol 2000 April 1, 2000;156(4):1363-1380.

28. Hobbs SK, Monsky WL, Yuan F, Roberts WG, Griffith L, Torchilin VP, et al. Regulation of transport pathways in tumor vessels: Role of tumor type and microenvironment. Proceedings of the National Academy of Sciences of the United States of America 1998 April 14, 1998;95(8):4607-4612.

29. Yuan F, Dellian M, Fukumura D, Leunig M, Berk DA, Torchilin VP, et al. Vascular Permeability in a Human Tumor Xenograft: Molecular Size Dependence and Cutoff Size. Cancer Research 1995 September 1, 1995;55(17):3752-3756.

30. Smith AM, Gao X, Nie S. Quantum Dot Nanocrystals for In Vivo Molecular and Cellular Imaging. Photochemistry and Photobiology 2004;80(3):377-385.

31. Weissleder R, Elizondo G, Wittenberg J, Rabito CA, Bengele HH, Josephson L. Ultrasmall superparamagnetic iron oxide: characterization of a new class of contrast agents for MR imaging. Radiology 1990 May 1, 1990;175(2):489-493.

32. Jain TK, Morales MA, Sahoo SK, Leslie-Pelecky DL, Labhasetwar V. Iron Oxide Nanoparticles for Sustained Delivery of Anticancer Agents. Molecular Pharmaceutics 2005;2(3):194-205.

33. Gref R, Minamitake Y, Peracchia MT, Trubetskoy V, Torchilin V, Langer R. Biodegradable long-circulating polymeric nanospheres. Science 1994 March 18, 1994;263(5153):1600-1603.

34. Murphy CJ, Gole AM, Stone JW, Sisco PN, Alkilany AM, Goldsmith EC, et al. Gold Nanoparticles in Biology: Beyond Toxicity to Cellular Imaging. Accounts of Chemical Research 2008 Dec;41(12):1721-1730.

35. Maeda H, Wu J, Sawa T, Matsumura Y, Hori K. Tumor vascular permeability and the EPR effect in macromolecular therapeutics: a review. Journal of Controlled Release 2000 Mar 1 2000;65(1-2):271-284.

36. Noguchi Y, Wu J, Duncan R, Strohalm J, Ulbrich K, Akaike T, et al. Early Phase Tumor Accumulation of Macromolecules: A Great Difference in Clearance Rate between Tumor and Normal Tissues. Cancer Science 1998;89(3):307-314.

37. Perrault SD, Walkey C, Jennings T, Fischer HC, Chan WCW. Mediating Tumor Targeting Efficiency of Nanoparticles Through Design. Nano Letters 2009;9(5):1909-1915.

38. Chithrani BD, Ghazani AA, Chan WCW. Determining the Size and Shape Dependence of Gold Nanoparticle Uptake into Mammalian Cells. Nano Letters 2006;6(4):662-668.

39. Osaki F, Kanamori T, Sando S, Sera T, Aoyama Y. A Quantum Dot Conjugated Sugar Ball and Its Cellular Uptake. On the Size Effects of Endocytosis in the Subviral Region. Journal of the American Chemical Society 2004;126(21):6520-6521.

40. Nakai T, Kanamori T, Sando S, Aoyama Y. Remarkably Size-Regulated Cell Invasion by Artificial Viruses. Saccharide-Dependent Self-Aggregation of Glycoviruses and Its Consequences in Glycoviral Gene Delivery. Journal of the American Chemical Society 2003;125(28):8465-8475.

41. Oh W-K, Kim S, Choi M, Kim C, Jeong YS, Cho B-R, et al. Cellular Uptake, Cytotoxicity, and Innate Immune Response of Silica Titania Hollow

Nanoparticles Based on Size and Surface Functionality. ACS Nano 2010;4(9):5301-5313.

42. Tan SJ, Jana NR, Gao S, Patra PK, Ying JY. Surface-Ligand-Dependent Cellular Interaction, Subcellular Localization, and Cytotoxicity of Polymer-Coated Quantum Dots. Chemistry of Materials 2010;22(7):2239-2247.

43. Liu Y, Shipton MK, Ryan J, Kaufman ED, Franzen S, Feldheim DL. Synthesis, Stability, and Cellular Internalization of Gold Nanoparticles Containing Mixed Peptide-Poly(ethylene glycol) Monolayers. Analytical Chemistry 2007;79(6):2221-2229.

44. Chung T-H, Wu S-H, Yao M, Lu C-W, Lin Y-S, Hung Y, et al. The effect of surface charge on the uptake and biological function of mesoporous silica nanoparticles in 3T3-L1 cells and human mesenchymal stem cells. Biomaterials 2007;28(19):2959-2966.

45. Tsoli M, Kuhn H, Brandau W, Esche H, Schmid G. Cellular uptake and toxicity of Au55 clusters. Small 2005 Aug;1(8-9):841-844.

46. Pan Y, Neuss S, Leifert A, Fischler M, Wen F, Simon U, et al. Size-dependent cytotoxicity of gold nanoparticles. Small 2007 Nov;3(11):1941-1949.

47. Connor EE, Mwamuka J, Gole A, Murphy CJ, Wyatt MD. Gold Nanoparticles Are Taken Up by Human Cells but Do Not Cause Acute Cytotoxicity. Small 2005;1(3):325-327.

48. Shukla R, Bansal V, Chaudhary M, Basu A, Bhonde RR, Sastry M. Biocompatibility of Gold Nanoparticles and Their Endocytotic Fate Inside the Cellular Compartment: A Microscopic Overview. Langmuir 2005;21(23):10644-10654.

49. De Jong WH, Hagens WI, Krystek P, Burger MC, Sips AJAM, Geertsma RE. Particle size-dependent organ distribution of gold nanoparticles after intravenous administration. Biomaterials 2008;29(12):1912-1919.

50. Paciotti GF, Myer L, Weinreich D, Goia D, Pavel N, McLaughlin RE, et al. Colloidal gold: A novel nanoparticle vector for tumor directed drug delivery. Drug Delivery 2004 May-Jun;11(3):169-183.

51. Niidome T, Yamagata M, Okamoto Y, Akiyama Y, Takahashi H, Kawano T, et al. PEG-modified gold nanorods with a stealth character for in vivo applications. Journal of Controlled Release 2006 Sep;114(3):343-347.

52. Balasubramanian SK, Jittiwat J, Manikandan J, Ong C-N, Yu LE, Ong W-Y. Biodistribution of gold nanoparticles and gene expression changes in the liver and spleen after intravenous administration in rats. Biomaterials 2010;31(8):2034-2042.

53. Balogh L, Nigavekar SS, Nair BM, Lesniak W, Zhang C, Sung LY, et al. Significant effect of size on the in vivo biodistribution of gold composite nanodevices in mouse tumor models. Nanomedicine 2007 Dec;3(4):281-296.

54. Bergen JM, von Recum HA, Goodman TT, Massey AP, Pun SH. Gold Nanoparticles as a Versatile Platform for Optimizing Physicochemical Parameters for Targeted Drug Delivery. Macromolecular Bioscience 2006;6(7):506-516.

55. Cho W-S, Cho M, Jeong J, Choi M, Cho H-Y, Han BS, et al. Acute toxicity and pharmacokinetics of 13 nm-sized PEG-coated gold nanoparticles. Toxicology and Applied Pharmacology 2009;236(1):16-24.

56. Hainfeld JF, Slatkin DN, Focella TM, Smilowitz HM. Gold nanoparticles: a new X-ray contrast agent. Br J Radiol 2006 Mar;79(939):248-253.

57. Hainfeld JF, Slatkin DN, Smilowitz HM. The use of gold nanoparticles to enhance radiotherapy in mice. Phys Med Biol 2004 Sep 21;49(18):N309-315.

58. Sadauskas E, Danscher G, Stoltenberg M, Vogel U, Larsen A, Wallin H. Protracted elimination of gold nanoparticles from mouse liver. Nanomedicine: Nanotechnology, Biology and Medicine 2009;5(2):162-169.

59. Sadauskas E, Wallin H, Stoltenberg M, Vogel U, Doering P, Larsen A, et al. Kupffer cells are central in the removal of nanoparticles from the organism. Part Fibre Toxicol 2007;4:10.

60. Sonavane G, Tomoda K, Makino K. Biodistribution of colloidal gold nanoparticles after intravenous administration: Effect of particle size. Colloids and Surfaces B: Biointerfaces 2008;66(2):274-280.

61. Terentyuk GS, Maslyakova GN, Suleymanova LV, Khlebtsov BN, Kogan BY, Akchurin GG, et al. Circulation and distribution of gold nanoparticles and induced alterations of tissue morphology at intravenous particle delivery. J Biophotonics 2009 May;2(5):292-302.

62. Zhang G, Yang Z, Lu W, Zhang R, Huang Q, Tian M, et al. Influence of anchoring ligands and particle size on the colloidal stability and in vivo biodistribution of polyethylene glycol-coated gold nanoparticles in tumor-xenografted mice. Biomaterials 2009 Apr;30(10):1928-1936.

63. Yang RS, Chang LW, Wu JP, Tsai MH, Wang HJ, Kuo YC, et al. Persistent tissue kinetics and redistribution of nanoparticles, quantum dot 705, in mice: ICP-MS quantitative assessment. Environ Health Perspect 2007 Sep;115(9):1339-1343.

64. Choi HS, Liu W, Misra P, Tanaka E, Zimmer JP, Ipe BI, et al. Renal clearance of quantum dots. Nature Biotechnology 2007 Oct;25(10):1165-1170.

65. Shukla S, Priscilla A, Banerjee M, Bhonde RR, Ghatak J, Satyam PV, et al. Porous Gold Nanospheres by Controlled Transmetalation Reaction: A Novel Material for Application in Cell Imaging. Chemistry of Materials 2005;17(20):5000-5005.

66. Chen J, Saeki F, Wiley BJ, Cang H, Cobb MJ, Li Z-Y, et al. Gold Nanocages:Bioconjugation and Their Potential Use as Optical Imaging Contrast Agents. Nano Letters 2005;5(3):473-477.

67. Yang P-H, Sun X, Chiu J-F, Sun H, He Q-Y. Transferrin-Mediated Gold Nanoparticle Cellular Uptake. Bioconjugate Chemistry 2005;16(3):494-496.

68. Hirsch LR, Stafford RJ, Bankson JA, Sershen SR, Rivera B, Price RE, et al. Nanoshell-mediated near-infrared thermal therapy of tumors under magnetic resonance guidance. Proceedings of the National Academy of Sciences of the United States of America 2003 November 11, 2003;100(23):13549-13554.

69. Chen JWBC, D.; Saeki, F.; Cang, L.; Au, L.; Lee,, J.; Li XX, Y. Gold Nanocages: Engineering the Structure for Biomedical Applications. Advanced Materials 2005;17:2255-2261.

70. Hainfeld JF, Slatkin, D. N., Smilowitz, H. M. . The use of gold nanoparticles to enhance radiotherapy in mice Physics in Medicine and Biology 2004;49(18):N309-N315.

71. Higby GJ. Gold in medicine: a review of its use in the West before 1900. Gold Bull 1982;15(4):130-140.

72. Richards DG, McMillin DL, Mein EA, Nelson CD. Gold and its relationship to neurological/glandular conditions. Int J Neurosci 2002 Jan;112(1):31-53.

73. Merchant B. Gold, the noble metal and the paradoxes of its toxicology. Biologicals 1998 Mar;26(1):49-59.

74. Walz DT, DiMartino MJ, Griswold DE, Intoccia AP, Flanagan TL. Biologic actions and pharmacokinetic studies of auranofin. Am J Med 1983 Dec 30;75(6A):90-108.

75. Wagner FE, Haslbeck S, Stievano L, Calogero S, Pankhurst QA, Martinek KP. Before striking gold in gold-ruby glass. Nature 2000 Oct 12;407(6805):691-692.

76. Edwards PP, Thomas JM. Gold in a metallic divided state--from Faraday to present-day nanoscience. Angew Chem Int Ed Engl 2007;46(29):5480-5486.

77. von Maltzahn G, Centrone A, Park JH, Ramanathan R, Sailor MJ, Hatton TA, et al. SERS-Coded Gold Nanorods as a Multifunctional Platform for Densely Multiplexed Near-Infrared Imaging and Photothermal Heating. Adv Mater 2009 Apr 20;21(31):3175-3180.

78. El-Sayed IH, Huang X, El-Sayed MA. Selective laser photo-thermal therapy of epithelial carcinoma using anti-EGFR antibody conjugated gold nanoparticles. Cancer Lett 2006 Jul 28;239(1):129-135.

79. Alivisatos AP. Semiconductor Clusters, Nanocrystals, and Quantum Dots. Science 1996;271(5251):933-937.

80. Link S, El-Sayed, M.A. Shape and Size Dependence of Radiative, Non-radiative and Photothermal Properties of Gold Nanoparticle. Int Reviews in Physical Chemistry 2000;19(3):409-453.

81. El-Sayed MA. Some interesting properties of metals confined in time and nanometer space of different shapes. Acc Chem Res 2001 Apr;34(4):257-264.

82. Bohren CF, Huffman, D.R. Absorption and Scattering of Light by Small Particles. New York: Wiley, 1983.

83. Link S, El-Sayed MA. Optical properties and ultrafast dynamics of metallic nanocrystals. Annu Rev Phys Chem 2003;54:331-366.

84. Mie G. Ann Phys 1908;25:329.

85. Burda C, Chen X, Narayanan R, El-Sayed MA. Chemistry and Properties of Nanocrystals of Different Shapes. Chemical Reviews 2005;105(4):1025-1102.

86. Yguerabide J, Yguerabide EE. Light-Scattering Submicroscopic Particles as Highly Fluorescent Analogs and Their Use as Tracer Labels in Clinical and Biological Applications: II. Experimental Characterization. Analytical Biochemistry 1998;262(2):157-176.

87. Sokolov K, Aaron J, Hsu B, Nida D, Gillenwater A, Follen M, et al. Optical systems for in vivo molecular imaging of cancer. Technol Cancer Res Treat 2003 Dec;2(6):491-504.

88. Jain PK, Lee KS, El-Sayed IH, El-Sayed MA. Calculated Absorption and Scattering Properties of Gold Nanoparticles of Different Size, Shape, and Composition: Applications in Biological Imaging and Biomedicine. The Journal of Physical Chemistry B 2006;110(14):7238-7248.

89. Daniel MC, Astruc D. Gold nanoparticles: assembly, supramolecular chemistry, quantum-size-related properties, and applications toward biology, catalysis, and nanotechnology. Chem Rev 2004 Jan;104(1):293-346.

90. Murphy CJ, Sau TK, Gole AM, Orendorff CJ, Gao J, Gou L, et al. Anisotropic metal nanoparticles: Synthesis, assembly, and optical applications. J Phys Chem B 2005 Jul 28;109(29):13857-13870.

91. Skrabalak SE, Chen J, Au L, Lu X, Li X, Xia Y. Gold Nanocages for Biomedical Applications. Advanced Materials 2007;19(20):3177-3184.

92. Hirsch LR, Gobin AM, Lowery AR, Tam F, Drezek RA, Halas NJ, et al. Metal nanoshells. Ann Biomed Eng 2006 Jan;34(1):15-22.

93. Connor EE, Mwamuka J, Gole A, Murphy CJ, Wyatt MD. Gold nanoparticles are taken up by human cells but do not cause acute cytotoxicity. Small 2005 Mar;1(3):325-327.

94. Thomas M, Klibanov AM. Conjugation to gold nanoparticles enhances polyethylenimine's transfer of plasmid DNA into mammalian cells. Proc Natl Acad Sci U S A 2003 Aug 5;100(16):9138-9143.

95. Kreibig U, Vollmer, M. Optical Properties of Metal Clusters. Berlin, Germany: Springer, 1995.

96. Landsman ML, Kwant G, Mook GA, Zijlstra WG. Light-absorbing properties, stability, and spectral stabilization of indocyanine green. Journal of Applied Physiology 1976 April 1, 1976;40(4):575-583.

97. El-Sayed IH, Huang X, El-Sayed MA. Surface Plasmon Resonance Scattering and Absorption of anti-EGFR Antibody Conjugated Gold Nanoparticles in Cancer Diagnostics: Applications in Oral Cancer. Nano Letters 2005;5(5):829-834.

98. Nerambourg N, Werts, Charlot M, Blanchard-Desce M. Quenching of Molecular Fluorescence on the Surface of Monolayer-Protected Gold Nanoparticles Investigated Using Place Exchange Equilibria. Langmuir 2007;23(10):5563-5570.

99. Dulkeith E, Ringler M, Klar TA, Feldmann J, MuÃ±oz Javier A, Parak WJ. Gold Nanoparticles Quench Fluorescence by Phase Induced Radiative Rate Suppression. Nano Letters 2005;5(4):585-589.

100. Gu T, Whitesell JK, Fox MA. Energy Transfer from a Surface-Bound Arene to the Gold Core in ω-Fluorenyl-Alkane-1-Thiolate Monolayer-Protected Gold Clusters. Chemistry of Materials 2003;15(6):1358-1366.

101. Nabika H, Deki S. Enhancing and Quenching Functions of Silver Nanoparticles on the Luminescent Properties of Europium Complex in the Solution Phase. The Journal of Physical Chemistry B 2003;107(35):9161-9164.

102. Campion A, Kambhampati P. Surface-enhanced Raman scattering. Chemical Society Reviews 1998 Jul;27(4):241-250.

103. Kneipp K, Kneipp H, Itzkan I, Dasari RR, Feld MS. Ultrasensitive chemical analysis by Raman spectroscopy. Chemical Reviews 1999 Oct;99(10):2957-+.

104. Nie SM, Emory SR. Probing single molecules and single nanoparticles by surface-enhanced Raman scattering. Science 1997 Feb;275(5303):1102-1106.

105. Kneipp K, Kneipp H, Itzkan I, Dasari RR, Feld MS. Surface-enhanced Raman scattering and biophysics. Journal of Physics-Condensed Matter 2002 May;14(18):R597-R624.

106. Qian XM, Nie SM. Single-molecule and single-nanoparticle SERS: from fundamental mechanisms to biomedical applications. Chemical Society Reviews 2008;37(5):912-920.

107. Cheng Y, C. Samia A, Meyers JD, Panagopoulos I, Fei B, Burda C. Highly Efficient Drug Delivery with Gold Nanoparticle Vectors for in Vivo Photodynamic Therapy of Cancer. Journal of the American Chemical Society 2008;130(32):10643-10647.

108. Zheng M, Davidson F, Huang X. Ethylene Glycol Monolayer Protected Nanoparticles for Eliminating Nonspecific Binding with Biological Moleculesâ€ Journal of the American Chemical Society 2003;125(26):7790-7791.

109. Yao H, Momozawa O, Hamatani T, Kimura K. Stepwise Size-Selective Extraction of Carboxylate-Modified Gold Nanoparticles from an Aqueous Suspension into Toluene with Tetraoctylammonium Cations. Chemistry of Materials 2001;13(12):4692-4697.

110. Hussain N, Singh B, Sakthivel T, Florence AT. Formulation and stability of surface-tethered DNA-gold-dendron nanoparticles. International Journal of Pharmaceutics 2003;254(1):27-31.

111. Templeton AC, Chen S, Gross SM, Murray RW. Water-Soluble, Isolable Gold Clusters Protected by Tiopronin and Coenzyme A Monolayers. Langmuir 1998;15(1):66-76.

112. Badia A, Singh S, Demers L, Cuccia L, Brown GR, Lennox RB. Self-Assembled Monolayers on Gold Nanoparticles. Chemistry – A European Journal 1996;2(3):359-363.

113. Brust M, Fink J, Bethell D, Schiffrin DJ, Kiely C. Synthesis and reactions of functionalised gold nanoparticles. Journal of the Chemical Society, Chemical Communications 1995(16):1655-1656.

114. Di Felice R, Selloni A. Adsorption modes of cysteine on Au(111): Thiolate, amino-thiolate, disulfide. The Journal of Chemical Physics 2004;120(10):4906-4914.

115. Owens III DE, Peppas NA. Opsonization, biodistribution, and pharmacokinetics of polymeric nanoparticles. International Journal of Pharmaceutics 2006;307(1):93-102.

116. Bain CD, Evall J, Whitesides GM. Formation of monolayers by the coadsorption of thiols on gold: variation in the head group, tail group, and solvent. Journal of the American Chemical Society 1989;111(18):7155-7164.

117. Collard DM, Fox MA. Use of electroactive thiols to study the formation and exchange of alkanethiol monolayers on gold. Langmuir 1991;7(6):1192-1197.

118. Hostetler MJ, Templeton AC, Murray RW. Dynamics of Place-Exchange Reactions on Monolayer-Protected Gold Cluster Molecules. Langmuir 1999;15(11):3782-3789.

119. Medley CD, Smith JE, Tang Z, Wu Y, Bamrungsap S, Tan W. Gold Nanoparticle-Based Colorimetric Assay for the Direct Detection of Cancerous Cells. Analytical Chemistry 2008;80(4):1067-1072.

120. Rosi NL, Mirkin CA. Nanostructures in biodiagnostics. Chemical Reviews 2005 Apr;105(4):1547-1562.

121. Cao YWC, Jin RC, Mirkin CA. Nanoparticles with Raman spectroscopic fingerprints for DNA and RNA detection. Science 2002 Aug;297(5586):1536-1540.

122. Farokhzad OC, Jon SY, Khadelmhosseini A, Tran TNT, LaVan DA, Langer R. Nanopartide-aptamer bioconjugates: A new approach for targeting prostate cancer cells. Cancer Research 2004 Nov;64(21):7668-7672.

123. Cheng Y, Samia AC, Meyers JD, Panagopoulos I, Fei BW, Burda C. Highly efficient drug delivery with gold nanoparticle vectors for in vivo photodynamic therapy of cancer. Journal of the American Chemical Society 2008 Aug;130(32):10643-10647.

124. Gibson JD, Khanal BP, Zubarev ER. Paclitaxel-functionalized gold nanoparticles. Journal of the American Chemical Society 2007 Sep;129(37):11653-11661.

125. Daniel MC, Astruc D. Gold nanoparticles: Assembly, supramolecular chemistry, quantum-size-related properties, and applications toward biology, catalysis, and nanotechnology. Chemical Reviews 2004 Jan;104(1):293-346.

126. Gewirtz DA. A critical evaluation of the mechanisms of action proposed for the antitumor effects of the anthracycline antibiotics Adriamycin and daunorubicin. Biochemical Pharmacology 1999 Apr;57(7):727-741.

127. Keizer HG, Pinedo HM, Schuurhuis GJ, Joenje H. DOXORUBICIN (ADRIAMYCIN) - A CRITICAL-REVIEW OF FREE RADICAL-DEPENDENT MECHANISMS OF CYTOTOXICITY. Pharmacology & Therapeutics 1990;47(2):219-231.

128. Young RC, Ozols RF, Myers CE. THE ANTHRACYCLINE ANTI-NEOPLASTIC DRUGS. New England Journal of Medicine 1981;305(3):139-153.

129. Fan HY, Dash AK. Effect of cross-linking on the in vitro release kinetics of doxorubicin from gelatin un-plants. International Journal of Pharmaceutics 2001 Feb;213(1-2):103-116.

130. Greenfield RS, Kaneko T, Daues A, Edson MA, Fitzgerald KA, Olech LJ, et al. EVALUATION INVITRO OF ADRIAMYCIN IMMUNOCONJUGATES SYNTHESIZED USING AN ACID-SENSITIVE HYDRAZONE LINKER. Cancer Research 1990 Oct;50(20):6600-6607.

131. Pong BK, Lee JY, Trout BL. First principles computational study for understanding the interactions between ssDNA and gold nanoparticles: Adsorption of methylamine on gold nanoparticulate surfaces. Langmuir 2005 Dec;21(25):11599-11603.

132. Love JC, Estroff LA, Kriebel JK, Nuzzo RG, Whitesides GM. Self-assembled monolayers of thiolates on metals as a form of nanotechnology. Chemical Reviews 2005 Apr;105(4):1103-1169.

133. Felice RD. Adsorption modes of cysteine on Au(111): Thiolate, amino-thiolate, disulfide. Journal of Chemical Physics 2004 March 2004;120(10):4906-4914.

134. Kaneko T, Willner D, Monkovic I, Knipe JO, Braslawsky GR, Greenfield RS, et al. NEW HYDRAZONE DERIVATIVES OF ADRIAMYCIN AND THEIR IMMUNOCONJUGATES - A CORRELATION BETWEEN ACID STABILITY AND CYTOTOXICITY. Bioconjugate Chemistry 1991 May-Jun;2(3):133-141.

135. Ipe BI, Thomas KG, Barazzouk S, Hotchandani S, Kamat PV. Photoinduced charge separation in a fluorophore-gold nanoassembly. Journal of Physical Chemistry B 2002 Jan;106(1):18-21.

136. Montalti M, Prodi L, Zaccheroni N, Battistini G. Modulation of the photophysical properties of gold nanoparticles by accurate control of the surface coverage. Langmuir 2004 Aug;20(18):7884-7886.

137. Hu J, Zhang J, Liu F, Kittredge K, Whitesell JK, Fox MA. Competitive photochemical reactivity in a self-assembled monolayer on a colloidal gold cluster. Journal of the American Chemical Society 2001 Feb;123(7):1464-1470.

138. Zhang J, Whitesell JK, Fox MA. Photoreactivity of self-assembled monolayers of azobenzene or stilbene derivatives capped on colloidal gold clusters. Chemistry of Materials 2001 Jul;13(7):2323-2331.

139. Anger P, Bharadwaj P, Novotny L. Enhancement and quenching of single-molecule fluorescence. Physical Review Letters 2006 Mar;96(11):113002.

140. Glomm WR. Functionalized gold nanoparticles for applications in bionanotechnology. Journal of Dispersion Science and Technology 2005;26(3):389-414.

141. Greenwald RB, Choe YH, McGuire J, Conover CD. Effective drug delivery by PEGylated drug conjugates. Advanced Drug Delivery Reviews 2003;55(2):217-250.

142. Liu Y, Shipton MK, Ryan J, Kaufman ED, Franzen S, Feldheim DL. Synthesis, Stability, and Cellular Internalization of Gold Nanoparticles Containing Mixed Peptide;Poly(ethylene glycol) Monolayers. Analytical Chemistry 2007;79(6):2221-2229.

143. Paciotti GF, Kingston DGI, Tamarkin L. Colloidal gold nanoparticles: A novel nanoparticle platform for developing multifunctional tumor-targeted drug delivery vectors. Drug Development Research 2006 Jan;67(1):47-54.

144. Marsh D, Bartucci R, Sportelli L. Lipid membranes with grafted polymers: physicochemical aspects. Biochimica Et Biophysica Acta-Biomembranes 2003 Sep;1615(1-2):33-59.

145. Schlenoff JB, Li M, Ly H. Stability and self-exchange in alkanethiol monolayers. Journal of the American Chemical Society 1995 Dec;117(50):12528-12536.

146. Wuelfing WP, Gross SM, Miles DT, Murray RW. Nanometer gold clusters protected by surface-bound monolayers of thiolated poly(ethylene glycol) polymer electrolyte. Journal of the American Chemical Society 1998 Dec;120(48):12696-12697.

147. Krug JT, Wang GD, Emory SR, Nie S. Efficient Raman Enhancement and Intermittent Light Emission Observed in Single Gold Nanocrystals. Journal of the American Chemical Society 1999;121(39):9208-9214.

148. Beljebbar A, Sockalingum GD, Angiboust JF, Manfait M. Comparative FT SERS, resonance Raman and SERRS studies of doxorubicin and its complex with DNA. Spectrochimica Acta Part a-Molecular and Biomolecular Spectroscopy 1995;51(12):2083-2090.

149. Nabiev IR, Morjani H, Manfait M. Selective analysis of antitumor drug interaction with living cancer cells as probed by surface-enhanced Raman spectroscopy. European Biophysics Journal 1991 May 1991;19(6):311-316.

150. Tsen M, Sun L. Surface-enhanced Raman scattering from functionalized self-assembled monolayers: Part 1. Distance dependence of enhanced Raman scattering from a terminal phenyl group. Analytica Chimica Acta 1995;307(2-3):333-340.

151. Ye Q, Fang JX, Sun L. Surface-enhanced Raman scattering from functionalized self-assembled monolayers .2. Distance dependence of enhanced Raman scattering from an azobenzene terminal group. Journal of Physical Chemistry B 1997;101(41):8221-8224.

152. Loren A, Eliasson C, Josefson M, Murty K, Kall M, Abrahamsson J, et al. Feasibility of quantitative determination of doxorubicin with surface-enhanced Raman spectroscopy. Journal of Raman Spectroscopy 2001 Nov;32(11):971-974.

153. Strekal N, German A, Gachko G, Maskevich A, Maskevich S. The study of the doxorubicin adsorbed onto chemically modified silver films by surface-enhanced spectroscopy. Journal of Molecular Structure 2001;563-564:183-191.

154. Yan Q, Priebe W, Chaires JB, Czernuszewicz RS. Interaction of doxorubicin and its derivatives with DNA: Elucidation by resonance Raman and surface-enhanced resonance Raman spectroscopy. Biospectroscopy 1997;3(4):307-316.

155. Sokolov K, Follen M, Aaron J, Pavlova I, Malpica A, Lotan R, et al. Real-time vital optical imaging of precancer using anti-epidermal growth factor receptor antibodies conjugated to gold nanoparticles. Cancer Research 2003;63(9):1999-2004.

156. Willner D, Trail PA, Hofstead SJ, King HD, Lasch SJ, Braslawsky GR, et al. (6-MALEIMIDOCAPROYL)HYDRAZONE OF DOXORUBICIN - A NEW DERIVATIVE FOR THE PREPARATION OF IMMUNOCONJUGATES OF DOXORUBICIN. Bioconjugate Chemistry 1993 Nov-Dec;4(6):521-527.

157. Ozeki T, Yuasa H, Kanaya Y. Control of medicine release from solid dispersion composed of the poly(ethylene oxide) carboxyvinylpolymer interpolymer complex by varying molecular weight of poly(ethylene oxide). Journal of Controlled Release 1999 Mar;58(1):87-95.

158. Costanzo PJ, Dan N, Lancaster KS, Lebrilla CB, Patten TE. Effect of changing polymer chain length on the target-mediated agglutination of polymer-grafted nanoparticles. Macromolecules 2008 Feb;41(4):1570-1576.

159. Kataoka K, Matsumoto T, Yokoyama M, Okano T, Sakurai Y, Fukushima S, et al. Doxorubicin-loaded poly(ethylene glycol)-poly(beta-benzyl-l-aspartate) copolymer micelles: their pharmaceutical characteristics and biological significance. 5th Symposium on Controlled Drug Delivery; 1998 Apr 01-03; Noordwijk Aan Zee, Netherlands; 1998. p. 143-153.

160. Gillies ER, Frechet JMJ. pH-responsive copolymer assemblies for controlled release of doxorubicin. Bioconjugate Chemistry 2005 Mar-Apr;16(2):361-368.

161. Jia Z, Wong L, Davis TP, Bulmus V. One-Pot Conversion of RAFT-Generated Multifunctional Block Copolymers of HPMA to Doxorubicin Conjugated Acid- and Reductant-Sensitive Crosslinked Micelles. Biomacromolecules 2008;9(11):3106-3113.

162. Daniel M-C, Astruc D. Gold Nanoparticles: Assembly, Supramolecular Chemistry, Quantum-Size-Related Properties, and Applications toward Biology, Catalysis, and Nanotechnology. Chemical Reviews 2003;104(1):293-346.

163. Dixit V, Van den Bossche J, Sherman DM, Thompson DH, Andres RP. Synthesis and grafting of thioctic acid-PEG-folate conjugates onto Au nanoparticles for selective targeting of folate receptor-positive tumor cells. Bioconjugate Chemistry 2006 May;17(3):603-609.

164. Mukherjee P, Bhattacharya R, Mukhopadhyay D. Gold Nanoparticles Bearing Functional Anti-Cancer Drug and Anti-Angiogenic Agent: A "2 in 1" System with Potential Application in Cancer Therapeutics. Journal of Biomedical Nanotechnology 2005 Jun;1(2):224-228.

165. Podsiadlo P, Sinani VA, Bahng JH, Kam NWS, Lee J, Kotov NA. Gold nanoparticles enhance the anti-leukemia action of a 6-mercaptopurine chemotherapeutic agent. Langmuir 2008 Jan;24(2):568-574.

166. Chen YH, Tsai CY, Huang PY, Chang MY, Cheng PC, Chou CH, et al. Methotrexate conjugated to gold nanoparticles inhibits tumor growth in a syngeneic lung tumor model. Molecular Pharmaceutics 2007 Sep-Oct;4(5):713-722.

167. Kang B, Mackey MA, El-Sayed MA. Nuclear targeting of gold nanoparticles in cancer cells induces DNA damage, causing cytokinesis arrest and apoptosis. J Am Chem Soc Feb 10;132(5):1517-1519.

168. Kaneko T, Willner D, Monkovic I, Knipe JO, Braslawsky GR, Greenfield RS, et al. New hydrazone derivatives of adriamycin and their immunoconjugates--a correlation between acid stability and cytotoxicity. Bioconjug Chem 1991 May-Jun;2(3):133-141.

169. Hucknall A, Rangarajan S, Chilkoti A. In Pursuit of Zero: Polymer Brushes that Resist the Adsorption of Proteins. Advanced Materials 2009;21(23):2441-2446.

170. Chan Y-HM, Schweiss R, Werner C, Grunze M. Electrokinetic Characterization of Oligo- and Poly(ethylene glycol)-Terminated Self-Assembled Monolayers on Gold and Glass Surfaces. Langmuir 2003;19(18):7380-7385.

171. Herrwerth S, Eck W, Reinhardt S, Grunze M. Factors that Determine the Protein Resistance of Oligoether Self-Assembled Monolayers âˆ’ Internal Hydrophilicity, Terminal Hydrophilicity, and Lateral Packing Density. Journal of the American Chemical Society 2003;125(31):9359-9366.

172. Heuberger M, Drobek T, Spencer ND. Interaction Forces and Morphology of a Protein-Resistant Poly(ethylene glycol) Layer. Biophysical Journal 2005;88(1):495-504.

173. Kreuzer HJr, Wang RLC, Grunze M. Hydroxide Ion Adsorption on Self-Assembled Monolayers. Journal of the American Chemical Society 2003;125(27):8384-8389.

174. Szleifer I. Polymers and proteins: interactions at interfaces. Current Opinion in Solid State and Materials Science 1997;2(3):337-344.

175. Jeon SI, Lee JH, Andrade JD, De Gennes PG. Protein--surface interactions in the presence of polyethylene oxide: I. Simplified theory. Journal of Colloid and Interface Science 1991;142(1):149-158.

176. Jain RK. Transport of Molecules, Particles, and Cells in Solid Tumors. Annual Review of Biomedical Engineering 1999;1(1):241-263.

177. Dreher MR, Chilkoti A. Toward a systems engineering approach to cancer drug delivery. J Natl Cancer Inst 2007 Jul 4;99(13):983-985.

178. Tang N, Du G, Wang N, Liu C, Hang H, Liang W. Improving Penetration in Tumors With Nanoassemblies of Phospholipids and Doxorubicin. Journal of the National Cancer Institute 2007 July 4, 2007;99(13):1004-1015.

179. Jain RKP, T. P. Lymphatics make the break. Science 2003;299(5604):209-210.

180. Padera TP, Kadambi A, di Tomaso E, Carrelra CM, Brown EB, Boucher Y, et al. Lymphatic Metastasis in the Absence of Functional Intratumor Lymphatics. Science 2002;296(5574):1883.

181. Swartz MA, Skobe M. Lymphatic function, lymphangiogenesis, and cancer metastasis. Microscopy Research and Technique 2001;55(2):92-99.

182. Jain RK, Baxter LT. Mechanisms of Heterogeneous Distribution of Monoclonal Antibodies and Other Macromolecules in Tumors: Significance of Elevated Interstitial Pressure. Cancer Research 1988 December 1, 1988;48(24 Part 1):7022-7032.

183. Pluen A, Boucher Y, Ramanujan S, McKee TD, Gohongi T, di Tomaso E, et al. Role of tumor-host interactions in interstitial diffusion of macromolecules: Cranial vs. subcutaneous tumors. Proceedings of the National Academy of Sciences of the United States of America 2001 April 10, 2001;98(8):4628-4633.

184. Kirpotin DB, Drummond DC, Shao Y, Shalaby MR, Hong K, Nielsen UB, et al. Antibody Targeting of Long-Circulating Lipidic Nanoparticles Does Not Increase Tumor Localization but Does Increase Internalization in Animal Models. Cancer Research 2006 July 1, 2006;66(13):6732-6740.

185. Iyer AK, Khaled G, Fang J, Maeda H. Exploiting the enhanced permeability and retention effect for tumor targeting. Drug Discovery Today 2006;11(17-18):812-818.

186. Tabata Y, Kawai T, Murakami Y, Ikada Y. Electric Charge Influence of Dextran Derivatives on their Tumor Accumulation After Intravenous Injection. Drug Delivery 1997;4(3):213-221.

187. Takakura Y, Atsumi R, Hashida M, Sezaki H. Development of a novel polymeric prodrug of mitomycin C, mitomycin C-dextran conjugate with anionic charge. II. Disposition and pharmacokinetics following intravenous and intramuscular administration. International Journal of Pharmaceutics 1987;37(1-2):145-154.

188. Michel CC, Curry FE. Microvascular Permeability. Physiological Reviews 1999 July 1, 1999;79(3):703-761.

189. Stroh M, Zimmer JP, Duda DG, Levchenko TS, Cohen KS, Brown EB, et al. Quantum dots spectrally distinguish multiple species within the tumor milieu in vivo. Nat Med 2005;11(6):678-682.

190. Kimura NT, Taniguchi Si, Aoki K, Baba T. Selective Localization and Growth of Bifidobacterium bifidum in Mouse Tumors following Intravenous Administration. Cancer Research 1980 June 1, 1980;40(6):2061-2068.

191. Dvorak AM, Feng D. The Vesiculo-Vacuolar Organelle (VVO): A New Endothelial Cell Permeability Organelle. Journal of Histochemistry & Cytochemistry 2001 April 1, 2001;49(4):419-431.

192. Charrois GJR, Allen TM. Rate of biodistribution of STEALTH® liposomes to tumor and skin: influence of liposome diameter and implications for toxicity and therapeutic activity. Biochimica et Biophysica Acta (BBA) - Biomembranes 2003;1609(1):102-108.

193. Charrois GJR, Allen TM. Drug release rate influences the pharmacokinetics, biodistribution, therapeutic activity, and toxicity of pegylated liposomal doxorubicin formulations in murine breast cancer. Biochimica et Biophysica Acta (BBA) - Biomembranes 2004;1663(1-2):167-177.

194. Pirollo KF, Chang EH. Does a targeting ligand influence nanoparticle tumor localization or uptake? Trends in Biotechnology 2008;26(10):552-558.

195. Choi CHJ, Alabi CA, Webster P, Davis ME. Mechanism of active targeting in solid tumors with transferrin-containing gold nanoparticles. Proceedings of the National Academy of Sciences 2010 January 19, 2010;107(3):1235-1240.

196. McNeeley KM, Annapragada A, Bellamkonda RV. Decreased circulation time offsets increased efficacy of PEGylated nanocarriers targeting folate receptors of glioma. Nanotechnology 2007;18(38):385101.

197. Goel R, Shah N, Visaria R, Paciotti GF, Bischof JC. Biodistribution of TNF-alpha-coated gold nanoparticles in an in vivo model system. Nanomedicine (Lond) 2009 Jun;4(4):401-410.

198. Chen Y-S, Hung Y-C, Liau I, Huang G. Assessment of the In Vivo Toxicity of Gold Nanoparticles. Nanoscale Research Letters 2009;4(8):858-864.

199. Cho WS, Cho M, Jeong J, Choi M, Cho HY, Han BS, et al. Acute toxicity and pharmacokinetics of 13 nm-sized PEG-coated gold nanoparticles. Toxicol Appl Pharmacol 2009 Apr 1;236(1):16-24.

200. Torchilin VP. Nanoparticulates as Drug Carriers. London: Imperial College Press, 2006.

201. Storm G, Belliot SO, Daemen T, Lasic DD. Surface modification of nanoparticles to oppose uptake by the mononuclear phagocyte system. Advanced Drug Delivery Reviews 1995;17(1):31-48.

202. Balasubramanian SK, Jittiwat J, Manikandan J, Ong C-N, Yu LE, Ong W-Y. Biodistribution of gold nanoparticles and gene expression changes in the liver and spleen after intravenous administration in rats. Biomaterials;31(8):2034-2042.

203. Bergen JM, von Recum HA, Goodman TT, Massey AP, Pun SH. Gold nanoparticles as a versatile platform for optimizing physicochemical parameters for targeted drug delivery. Macromol Biosci 2006 Jul 14;6(7):506-516.

204. Sadauskas E, Danscher G, Stoltenberg M, Vogel U, Larsen A, Wallin H. Protracted elimination of gold nanoparticles from mouse liver. Nanomedicine 2009 Jun;5(2):162-169.

205. Semmler-Behnke M, Kreyling WG, Lipka J, Fertsch S, Wenk A, Takenaka S, et al. Biodistribution of 1.4- and 18-nm Gold Particles in Rats. Small 2008;4(12):2108-2111.

206. Kira A, Kim H, Yasuda K. Contribution of Nanoscale Curvature to Number Density of Immobilized DNA on Gold Nanoparticles. Langmuir 2009;25(3):1285-1288.

207. Gabizon A, Horowitz AT, Goren D, Tzemach D, Shmeeda H, Zalipsky S. In Vivo Fate of Folate-Targeted Polyethylene-Glycol Liposomes in Tumor-Bearing Mice. Clinical Cancer Research 2003 December 15, 2003;9(17):6551-6559.

208. Smith RW, Leppard B, Barnett NL, Millward-Sadler GH, McCrae F, Cawley MID. Chrysiasis revisited: a clinical and pathological study. British Journal of Dermatology 1995;133(5):671-678.

209. Sonavane G, Tomoda K, Sano A, Ohshima H, Terada H, Makino K. In vitro permeation of gold nanoparticles through rat skin and rat intestine: Effect of particle size. Colloids and Surfaces B: Biointerfaces 2008;65(1):1-10.

210. Cho WS, Cho M, Jeong J, Choi M, Han BS, Shin HS, et al. Size-dependent tissue kinetics of PEG-coated gold nanoparticles. Toxicol Appl Pharmacol 2010 May 15;245(1):116-123.

211. Deng X, Jia G, Wang H, Sun H, Wang X, Yang S, et al. Translocation and fate of multi-walled carbon nanotubes in vivo. Carbon 2007;45(7):1419-1424.

212. Yang RSH, Chang LW, Wu J-P, Tsai M-H, Wang H-J, Kuo Y-C, et al. Persistent Tissue Kinetics and Redistribution of Nanoparticles, Quantum Dot 705, in Mice: ICP-MS Quantitative Assessment. Environ Health Perspect 2007;115(9).

213. Jain TK, Reddy MK, Morales MA, Leslie-Pelecky DL, Labhasetwar V. Biodistribution, Clearance, and Biocompatibility of Iron Oxide Magnetic Nanoparticles in Rats. Molecular Pharmaceutics 2008;5(2):316-327.

214. Lasagna-Reeves C, Gonzalez-Romero D, Barria MA, Olmedo I, Clos A, Sadagopa Ramanujam VM, et al. Bioaccumulation and toxicity of gold nanoparticles after repeated administration in mice. Biochemical and Biophysical Research Communications 2010;393(4):649-655.

215. Garnett MC, Kallinteri P. Nanomedicines and nanotoxicology: some physiological principles. Occupational Medicine 2006 August 2006;56(5):307-311.

216. Cedervall T, Lynch I, Foy M, Berggård T, Donnelly SC, Cagney G, et al. Detailed Identification of Plasma Proteins Adsorbed on Copolymer Nanoparticles. Angewandte Chemie International Edition 2007;46(30):5754-5756.

217. Longmire M, Choyke PL, Kobayashi H. Clearance properties of nano-sized particles and molecules as imaging agents: considerations and caveats. Nanomedicine 2008;3(5):703-717.

218. Guyton ACH, J.E. Textbook of Medical Physiology. 11TH ed. Philadelphia: Elsevier Saunders Publisher, 2006.

219. Renaud G, Hamilton RL, Havel RJ. Hepatic metabolism of colloidal gold-low-density lipoprotein complexes in the rat: Evidence for bulk excretion of lysosomal contents into bile. Hepatology 1989;9(3):380-392.

220. Hardonk MJ, Harms G, Koudstaal J. Zonal heterogeneity of rat hepatocytes in the in vivo uptake of 17 nm colloidal gold granules. Histochemistry and Cell Biology 1985;83(5):473-477.

221. Pan D, Pramanik M, Senpan A, Ghosh S, Wickline SA, Wang LV, et al. Near infrared photoacoustic detection of sentinel lymph nodes with gold nanobeacons. Biomaterials 2010 May;31(14):4088-4093.

222. Videira MA, Botelho MF, Santos AC, Gouveia LF, Pedroso de Lima JJ, Almeida AnJ. Lymphatic Uptake of Pulmonary Delivered Radiolabelled Solid Lipid Nanoparticles. Journal of Drug Targeting 2002;10(8):607-613.

223. Videira MA, Gano L, Santos C, Neves M, Almeida AJ. Lymphatic uptake of lipid nanoparticles following endotracheal administration. Journal of Microencapsulation 2006;23(8):855-862.

224. Iwai K, Maeda H, Konno T. Use of oily contrast medium for selective drug targeting to tumor: enhanced therapeutic effect and X-ray image. Cancer Res 1984 May;44(5):2115-2121.

225. Iwai K, Maeda H, Konno T, Matsumura Y, Yamashita R, Yamasaki K, et al. Tumor targeting by arterial administration of lipids: rabbit model with VX2 carcinoma in the liver. Anticancer Res 1987 May-Jun;7(3 Pt B):321-327.

226. www.doxil.com.

227. www.ClinicalTrials.gov.

228. Barenholz Y. Liposome application: problems and prospects. Current Opinion in Colloid & Interface Science 2001;6(1):66-77.

229. Gabizon A, Shmeeda H, Barenholz Y. Pharmacokinetics of Pegylated Liposomal Doxorubicin: Review of Animal and Human Studies. Clinical Pharmacokinetics 2003;42(5):419-436.

230. Plosker GL. Pegylated Liposomal Doxorubicin: A Review of its Use in the Treatment of Relapsed or Refractory Multiple Myeloma. Drugs 2008;68(17):2535-2551.

231. Petrelli F, Borgonovo K, Barni S. Targeted delivery for breast cancer therapy: the history of nanoparticle-albumin-bound paclitaxel. Expert Opinion on Pharmacotherapy 2010;11(8):1413-1432.

232. www.abraxane.com.

VITA

KATE Y.J. LEE

Kate Lee was born in Seoul, South Korea. Due to her dad's job, Kate Lee spent most of her childhood in Yangon, Myanmar, where she attended International School of Yangon. Later in her teens, she again moved with her family to Houston, Texas. She received her B.S. degree in Chemical Engineering at the University of Texas at Austin in 2004. After graduation, Kate joined a business consulting firm called Accenture and worked as an analyst for one year. Due to her passion in biomedical engineering, Kate decided to pursue her Ph.D. degree at Georgia Institute of Technology. She once visited Georgia Institute of Technology as an undergraduate for a summer research program and was impressed with the deparment. Apart from research, Kate loves to go to the gym where she is actively involved in cardio kickboxing, boxing, yoga, and boot camp classes. Kate enjoys singing and dancing. Kate also loves to travel and try different food and culture.